STRUCTURAL SYSTEMS

RESEARCH PROJECT

PRECAST SEISMIC STRUCTURAL SYSTEMS PRESSS-3: THE FIVE-STORY PRECAST TEST BUILDING VOL. 3-5: WALL DIRECTION RESPONSE

By

JAMES CONLEY
SRI SRITHARAN
M.J.N. PRIESTLEY

Department of Structural Engineering
University of California, San Diego
La Jolla, California 92093-0085

University of California, San Diego

Department of Structural Engineering

Structural Systems Research Project

Report No. SSRP- 99/19

FINAL

Precast Seismic Structural Systems PRESSS-3: The Five-Story Precast Test Building Vol. 3-5: Wall Direction Response

by

James Conley
Graduate Student Researcher

Sri Sritharan
Assistant Project Scientist

M.J.N. Priestley
Professor of Structural Engineering

July 2002

ACKNOWLEDGMENTS

ABSTRACT

Precast Seismic Structural Systems PRESSS-3: The Five-Story Precast Test Building Vol. 3-1: Wall Direction Response

Past precast concrete structural systems have exhibited poor seismic performance. In an effort to evaluate and improve this the Precast Seismic Structural System (PRESSS) Project was initiated ten years ago. As the culmination of this project a sixty-percent scaled five-story building was constructed and tested under pseudodynamic earthquake loads at UCSD. The building had four precast concrete structural frame systems for lateral-load resisting in one direction and a jointed precast panel structural wall system for the other. The wall panel connections consisted of unbonded post-tensioning bars and energy dissipating, U-shaped flexural plates. In order to predict the seismic response of the building a simple, inelastic, time-history analytical model was created. The model consisted of elastic frame elements and springs representing the panels and foundation, with non-linear inelastic springs representing the post-tensioning bars and U-plates. The agreement between prediction and experiment proved extremely close, showing that the simple model captured the force and displacement characteristics of the wall system. Only minimal damage in the wall direction occurred, after being taken to drift levels up to 2.65% and base shear levels 63% higher than the design level. The Direct Displacement-Based Design approach, in accordance with which the structure was designed, was further validated by this test. Residual drift levels after design level excitation were very low, 0.06% after sustaining a peak drift of 1.8%. The jointed wall system performed exceptionally, the result being a building at the "immediate occupancy" level after an event 50% higher than the design earthquake intensity.

TABLE OF CONTENTS

LIST OF FIGURES

LIST OF TABLES

LIST OF SYMBOLS

a	= depth of compressive stress block
A_e	= equivalent elastic area used for equivalent viscous damping calculations
a_g	= ground acceleration
A_h	= hysteretic area used for equivalent viscous damping calculations
b_c	= column width
b_w	= wall panel width
d_s	= distance from extreme compression fiber to centroid of steel
E	= modulus of elasticity
E_{pt}	= modulus of elasticity of post-tensioning
E_{ss}	= modulus of elasticity of stainless steel
f'_c	= concrete compressive strength
F_i	= floor force of the ith floor
G	= shear modulus
h_c	= depth of column
h_{fi}	= elevation of floor level i
h_{ni}	= elevation of node level i
I_g	= second moment of inertia of the gross concrete section
k_0	= initial stiffness
k_{bs}	= base spring stiffness
K_{eff}	= effective secant stiffness for DBD procedure
k_{eff}	= effective secant stiffness used for equivalent viscous damping calculations
k_m	= moment stiffness
k_p	= secondary stiffness as defined by Al-Bermani hysteresis rule
k_{pt}	= stiffness of post-tensioning
k_T	= tangent stiffness as defined by Al-Bermani hysteresis rule
k_u	= UFP stiffness
λ_{pt}	= unbonded length of post-tensioning

ℓ_{ub} = length of bent portion of UFP

ℓ_{u} = center-to-center distance between UFP flanges

M_c = moment resistance of column base

m_e = effective mass for DBD procedure

P = axial load

R = seismic force reduction factor for ductility

S_i = story shear of the ith floor

T = fundamental period of vibration

T_{eff} = effective period of vibration for DBD procedure

T_s = tension force in steel

V_b = base shear

V_c = column shear resistance

V_m = maximum/minimum base shear

V_u = yield shear force in UFP

$\ddot{x}$ = relative acceleration vector

$\dot{x}$ = relative velocity vector

x = relative displacement vector

x_{fi} = displacement at floor level i

x_{ni} = displacement at node level i

α = positive yield force scaling factor as defined by Al-Bermani hysteresis rule

β = negative yield force scaling factor as defined by Al-Bermani hysteresis rule

Δ = displacement

Δ_d = target displacement for DBD procedure

ε = strain

η = equivalent viscous damping

θ_d = design drift for DBD procedure

ξ = equivalent viscous damping

ϕ = diameter

σ = stress

σ_y = steel yield stress

1 INTRODUCTION

Precast concrete enjoys worldwide popularity in building construction due to material cost efficiency, fabrication quality, and erection speed. However, the poor performance of precast concrete in past earthquakes has mostly limited its use to non-lateral load resisting building systems. Where such systems are allowed they are constrained by limitations imposed on them that are not representative of the unique advantages that precast concrete can offer. This is due primarily to the widespread belief that a "strong" jointed structural system must exist, where inelastic actions and member ductility occur in areas away from the joint, emulating the behavior of a monolithic concrete system. This method forces damage to occur to the structure in order to save the lives of the occupants. While life safety is clearly the most important goal in a moderate to large intensity earthquake event, it is not clear that structural damage is necessary to achieve this.

The nature of precast concrete is to have separate components, such as beams and columns, brought together in a "jointed construction" configuration. Limiting the inelastic member deformations to the jointed region greatly reduces damage to the structural elements and concentrates the ductility demand in elements that can easily handle such demands. By using "jointed construction" many other advantages are also evident, and will be described herein. Recently current codes have begun to allow design that relies on these unique properties, but jointed systems can only be used if they are validated on a case-by-case basis. The incorporation of precast concrete into modern design code is due, in part, to the achievements of the *PRESSS* research program.

1.1 PRESSS Program

In an effort to further expand the understanding and improve the performance of precast concrete in seismic regions, the Precast Seismic Structural Systems (*PRESSS*) research program

(sponsored by the National Science Foundation, the Precast/Prestressed Concrete Institute, and the Precast/Prestressed Concrete Manufacturers Association of California) was initiated in 1990 (Priestley, 1991). Since the beginning of the *PRESSS* program, all of the research teams involved in the project have focused on two primary objectives:

- to develop comprehensive and rational design recommendations needed for a broader acceptance of precast concrete construction in different seismic zones;

- to develop new materials, concepts, and technologies for precast concrete in different seismic zones.

Phase I of the *PRESSS* research program focused on identifying and evaluating the most promising seismic precast concrete building systems (Nakaki and Englekirk, 1991). This phase included input from all spectra of the precast industry and precast related research. Phase II emphasized experimental and analytical studies of different ductile-connection precast systems and the development of seismic design procedures for precast buildings in various seismic zones (Priestley, 1996).

The concepts developed in Phase II are based on four generic force-displacement relationships (shown in Figure 1-1), each with different equivalent viscous damping characteristics, ξ, as described below.

- **Non-Linear Elastic (NLE) Connection Systems** are generally unbonded post-tensioned connection systems where cracking develops but stress in post-tensioning remains in the elastic range as illustrated in Figure 1-1 (b). $\xi \approx 10$ percent.

- **Tension-Compression Yield (TCY) Connection Systems** are generally medium strength steel connections where steel yields alternately in tension and compression, simulating monolithic concrete response as shown in Figure 1-1 (c). $\xi \approx 35$ percent.

2

- **Shear Yield (SY) Connection Systems** typically occur in vertical joint regions between adjacent precast panels in panel systems where the connection yields in inelastic shear response as illustrated in Figure 1-1 (c). $\xi \approx 25\text{-}35$ percent

- **Energy Dissipating/Coulomb Friction (CF) Connection Systems** are special damping devices typically involving friction sliding, where response is characterized as rigid-perfectly plastic. $\xi \approx 20\text{-}60$ percent as shown in Figure 1-1 (e).

Combinations of these generic behaviors can result in maximizing energy damping with self-centering characteristics as shown in Figure 1-1 (d) and (f) (Priestley, 1996).

This generic connection technology was incorporated into the investigation of precast wall panel system components by combining the NLE behavior of unbonded post-tensioning bars with the energy dissipating characteristics of the SY and CF devices as discussed subsequently.

1.1.1 Precast Wall Panel Systems

The high initial stiffness and lateral load capability of shear walls make them an excellent choice for seismic resisting systems in precast concrete buildings. Precast wall panel systems with unbonded post-tensioned tendons generally consist of more than one panel joined by both horizontal and/or vertical connections. Incorporating the dry jointed philosophy, the predominate behavior of the panels is idealized as rocking motion. The panel sections undergo a rigid body rotation as lateral drift occurs due to seismic loading. This rotation results in opening of a gap at the horizontal joint areas and in relative displacement between panels at the vertical joints. The connections across the joint regions determine the displacement of the structure; and by implementing the behavior characteristics generalized earlier, advantages such as self-centering capabilities and energy dissipation can be added to the system.

Research in the area of precast wall panel seismic response was evaluated as a part of the PRESSS Phase I program. An extensive research review was conducted by Kurama et al. (1996),

3
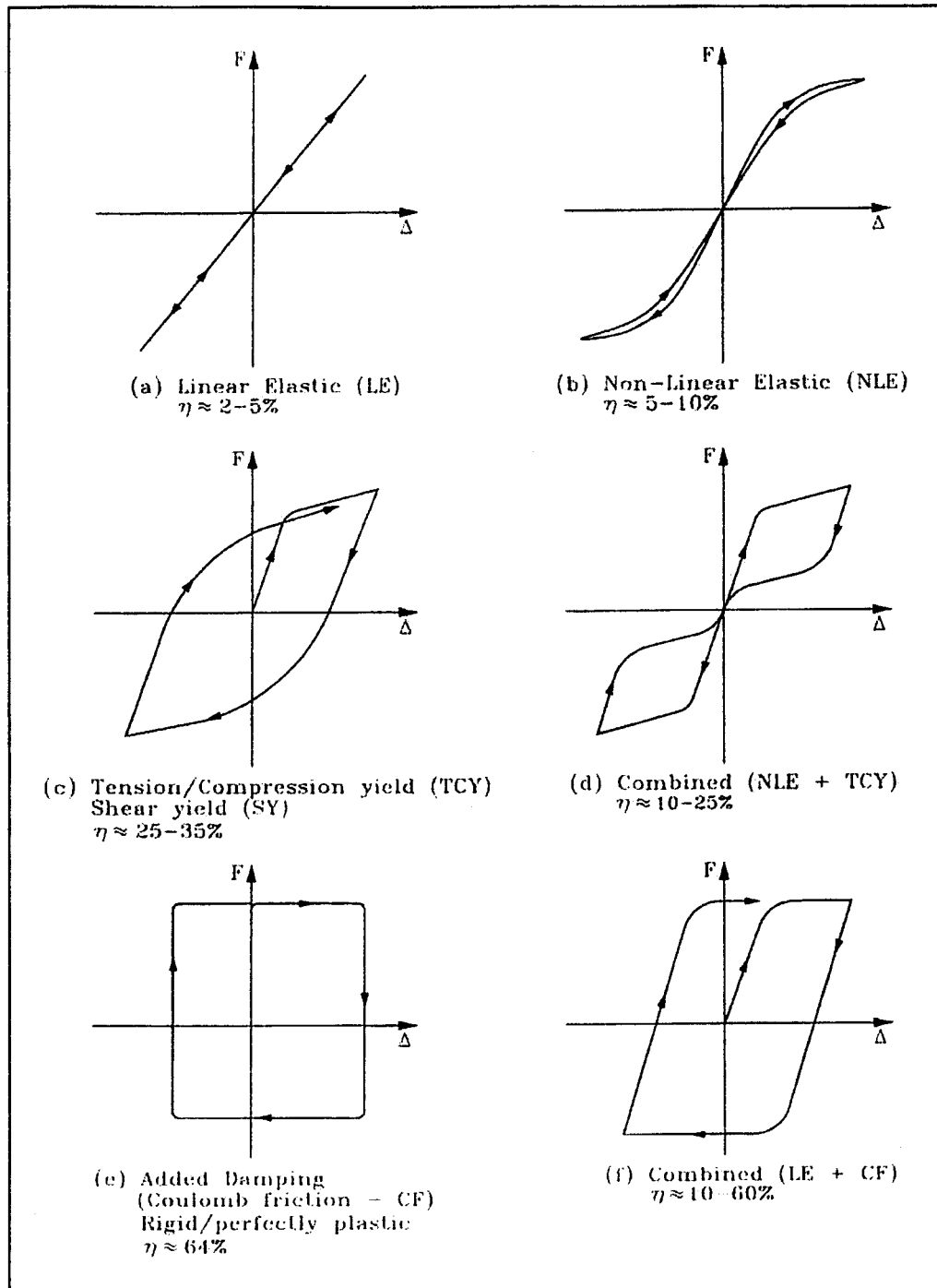
Figure 1-1 Hysteretic Characteristics for Generic PRESSS Connection Systems (Priestley, 1996)

which included work done by Pall et al. (1980), Muller (1986), and Schultz (1992) to name a few. From the developments in Phase I specific connection mechanisms were then tested during Phase II.

1.1.2 NIST Testing

As a part of the second phase of the *PRESSS* program, Shultz and Magaña performed testing of vertical and horizontal connection mechanisms in 1994 at the National Institute of Standards and Technology (NIST). The experimental program included seven vertical joint specimens which represented regions surrounding vertical joint connections in precast shear walls (shown in Figure 1-2) and four shear wall specimens for the study of horizontal joint connections (shown in Figure 1-3). The connections represented different combinations of the hysteretic ductile connection behavior suggested in Phase II. The vertical and horizontal specimens were tested in the NIST Tri-directional Testing Facility using cyclic drift histories that simulate seismic motions.

The vertical connection specimens were 2/3 scale and nominally the same except for the block-out region containing the anchor plates and connector. The connections that showed the best hysteretic behavior at large number of cycles would best be suited for use in Zone 4-earthquake design areas. The Vertical Joint Friction (VJF) and U-shaped Flexural Plate (UFP) specimens displayed an outstanding ability to resist seismic forces over a wide range of displacement. The VJF is an adaptation of the slotted, bolted friction connection proposed by Grigorian et al. (1992) for steel buildings. Kelly et al. (1972) proposed the UFP as an energy-dissipating flexible connector in which rolling bending action resists vertical shear force. The force displacement results for the two specimens are shown in Figure 1-4. The VJF connector utilizes Coulomb Friction hysteretic behavior characteristics, while the UFPs are associated with flexural yielding type behavior (similar to SY behavior).

Figure 1-2 Vertical Connection Specimen Tested at NIST (Priestley, 1996)
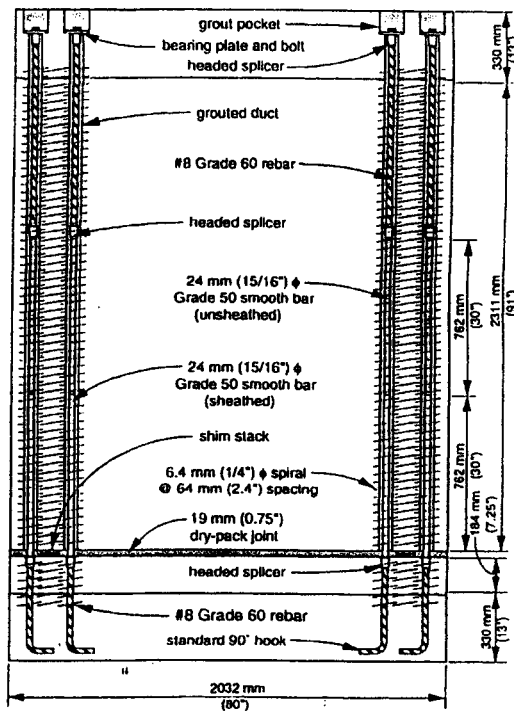
(a) DSB
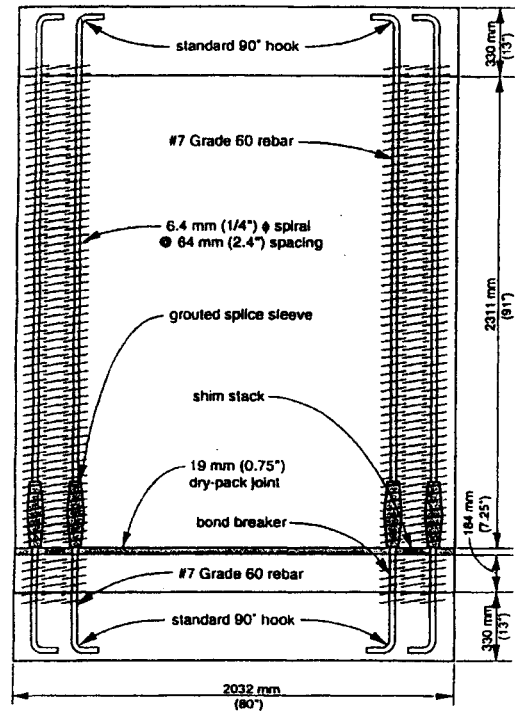
(b) GSS
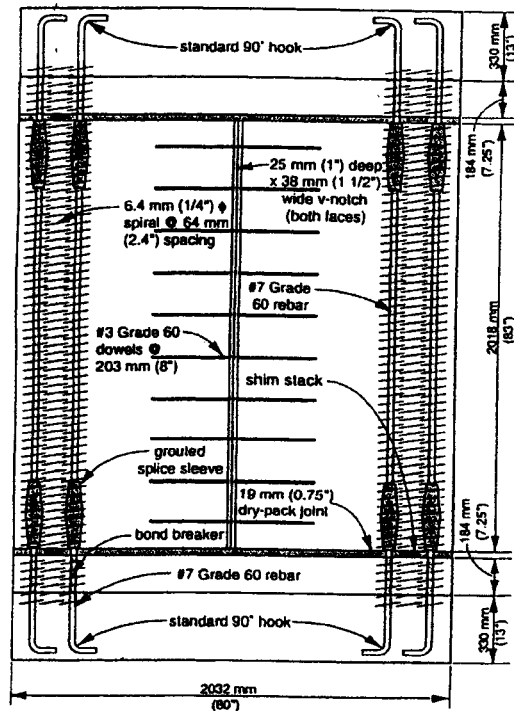
(c) PVJ
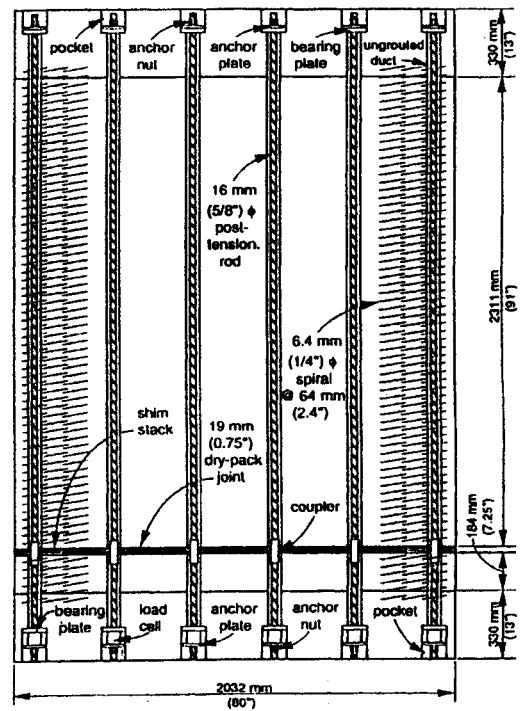
(d) PTT

Figure 1-3 Horizontal Connection Specimen Tested at NIST (Priestley, 1996)

7

LATERAL DISPLACEMENT (in.)

(a) Unit VJF

LATERAL DISPLACEMENT (in.)
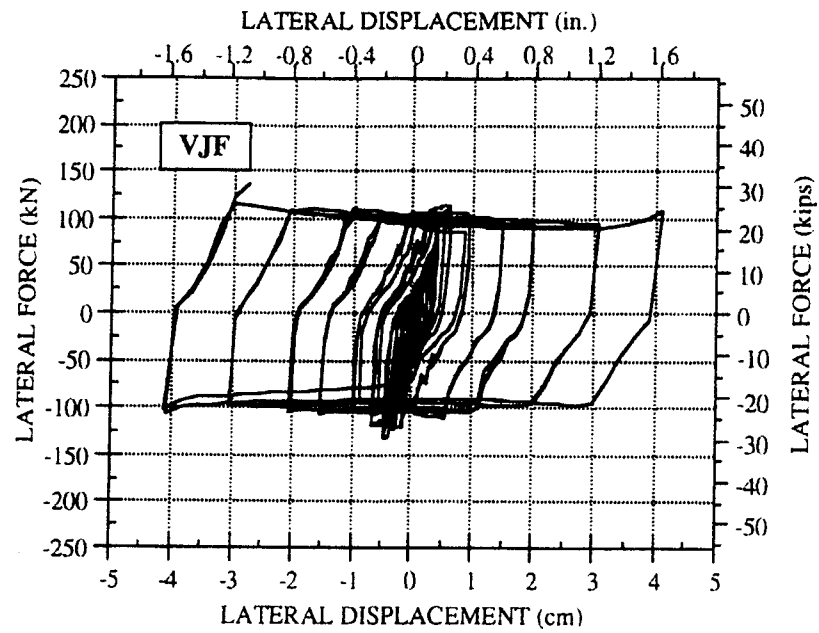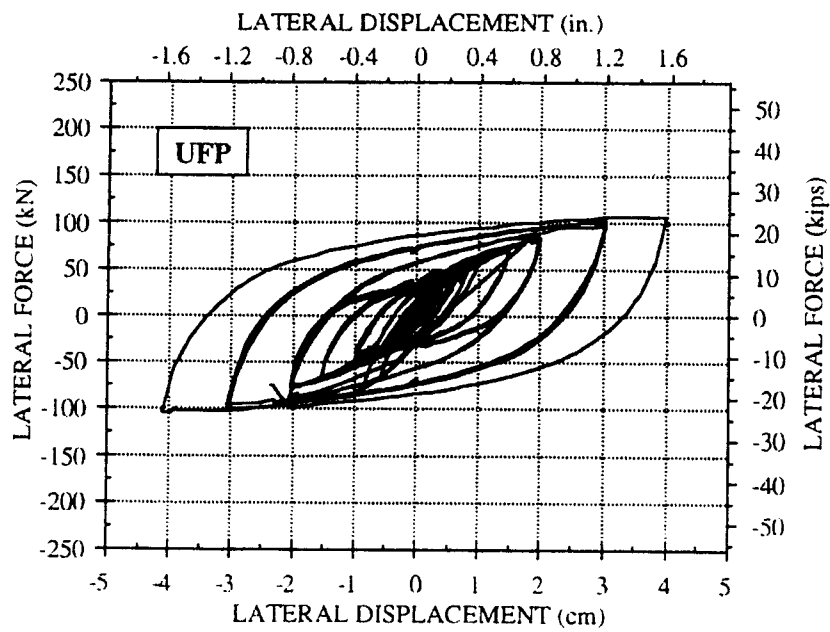
(b) Unit UFP

Figure 1-4 VJF and UFP Test Results (Priestley, 1996)

8

The horizontal joints consisted of four different types of connection mechanism illustrated in Figure 1-3. The different test specimens are briefly described below.

- **Grouted Splice Sleeve (GSS).** The connection is composed of vertical rebar spliced, using proprietary sleeves with the rebar debonded a specific length below the joint. The sleeves allow stress transfer across the joint, enabling the reinforcement to yield under lateral loading and plastic hinging to occur at the base of the panel representing TCY behavior.

- **Post-Tensioned Tendon (PTT).** Vertical reinforcement is provided in the form of high strength prestressing bars with standard couplers, unbonded along the height of the wall. Lateral load transfer occurs by flexure across the joint representing NLE behavior.

- **Precast Vertical Joint (PVJ).** GSS connections are used at the top and bottom with a vertical groove along the specimen centerline. Upon cracking of the vertical joint, sliding of the panels generates vertical shear resistance and energy dissipation in a CF type behavior.

- **Debonded Smooth Bar (DSB).** This connection detail maintains large deformation capacity by using debonded smooth bars. These bars are coupled to deformed reinforcing bars grouted into the wall ducts. This connection employs a TCY type behavior.

Results indicate that the PTT and GSS specimens performed the best, maintaining ductility through the test regime. The PTT connection is most suited for systems where hysteretic damping is not required at the vertical joints. For such systems the GSS connection is recommended.

With a basis for connection technology and a better understanding of the precast panel behavior, the NIST test set the stage for analytical modeling procedure to be developed as part of Phase II of the *PRESSS* program.

1.1.3 Lehigh Testing

The Phase II testing conducted at Lehigh University focused on the expected behavior, analytical modeling, and evaluation of lateral load behavior of unbonded post-tensioned precast

walls with only horizontal connections (Kurama et al., 1996). This section briefly summarizes the results from Lehigh investigations and parametric studies.

It was determined that the desired mode of deformation is gap opening in flexure along the connections. Shear slip along the horizontal connections is not desired and should be prevented by proper design and proportioning of the wall. As a result of the unbonding, large cyclic lateral displacements can be achieved while the bars remain linear-elastic, keeping their initial prestress levels. As a result of the gap opening, large compressive strains develop in the concrete along the horizontal connections, particularly between the base panel and the foundation. Spiral reinforcement is necessary at the base panel to prevent the concrete from crushing prematurely.

An analytical model for unbonded precast walls based on the fiber beam-column element in DRAIN-2DX was crated to evaluate lateral load behavior. Figure 1-5 shows an illustration of the Lehigh analytical model. Since shear slip along the horizontal connections can be prevented and shear deformations in the wall panels reduced by unbonded post-tensioning, the analytical model concentrates on gap opening along the horizontal connections and the axial-flexural behavior of the wall panels. Concrete is modeled using fiber elements and the unbonded post-tensioning modeled by truss elements.

The fiber wall model can provide simple yet accurate and realistic representations of the lateral load behavior of the wall panels described. The fiber model can be used to perform static nonlinear lateral load analysis and nonlinear time history dynamic analysis of the walls. The fiber wall model was successfully used to predict the behavior of multistory post-tensioned precast walls tested by Muller (1986). However, these walls did not have unbonded post-

10

DRAIN-2DX Model of a 6-Story Precast Wall with Debonded Post-Tensioning
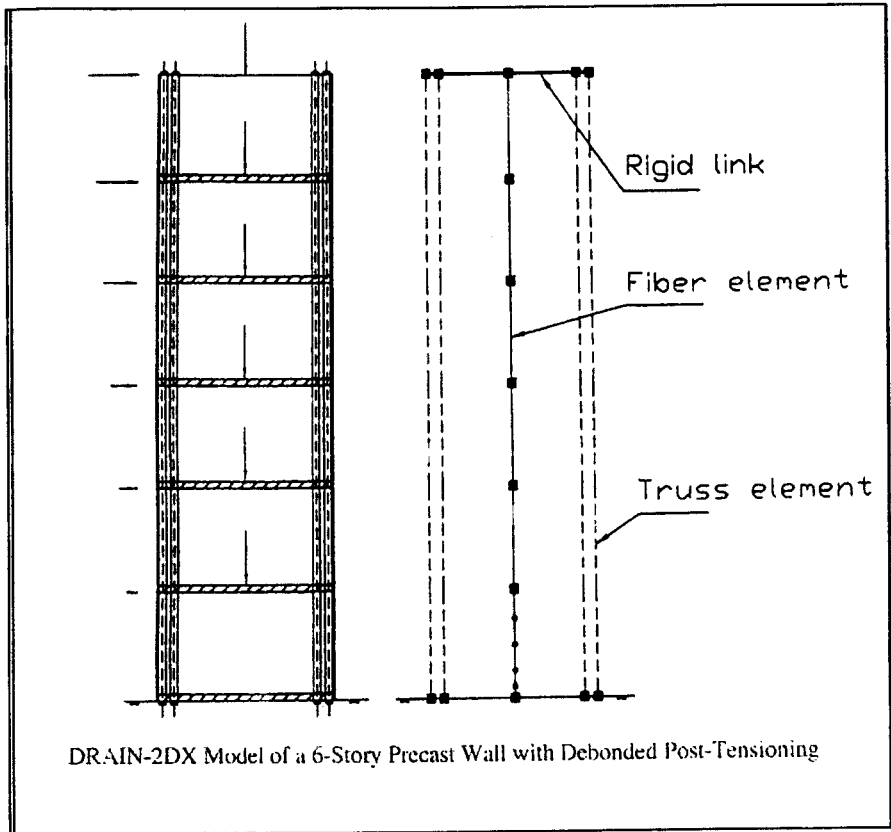
Figure 1-5 Lehigh Fiber Wall Model (Priestley, 1996)

tensioning; therefore, tests of *unbonded* post-tensioned multistory precast walls were needed to fully verify the fiber wall model.

The rigid wall model, which describes the nonlinear rocking motion of a rigid block on a rigid foundation, can be used to determine simple behavior characteristics of the wall panels, including the effects of axial load, prestress, and flexural reinforcement.

The results from the Lehigh and NIST investigations helped expand the understanding of precast panel lateral load cyclic behavior. This set the stage for all the component tests to be validated by a super-assemblage test -- the third phase of the *PRESSS* program.

1.2 Research Scope

The third phase of the *PRESSS* program comprises the design, erection and testing of a five-story precast concrete building using dry jointed connections, as well as the finalizing of detailed design recommendations to be implemented into the appropriate building codes. As the key element of the final phase of the *PRESSS* project, a 60 percent scale five-story precast concrete building was constructed and tested under simulated seismic loading at the UCSD Charles Lee Powell Structural Laboratory. The tests were carried out between June and September 1999. The test building implemented the NLE and TCY generic behaviors in one direction of testing (frame system), while using a derivative of the connection mechanisms and unbonded post-tensioning systems investigated by NIST and Lehigh in the other direction (wall system). The wall system of the *PRESSS* test building considers the behavior of the jointed unbonded post-tensioned panel system, with PT bars and GSS couplers providing the horizontal joint connections. An appropriate level of hysteretic damping is also added by implementing UFPs in the vertical joint region.

The focus of the theoretical work done at UCSD for the wall direction of testing was to prepare an analytical model that could be used for predicting the behavior of the *PRESSS* building during actual testing circumstances. The model was developed based on wall geometry, basic

12

material properties, and connector and foundation characteristics. As a further objective the model was developed so that any typical design firm could use it as a basis to reproduce similar building models with minimal effort and still be able to provide accurate estimations of building force and displacement characteristics. With these objectives in mind an analytical model for the precast panel seismic resisting system was created.

Analytical predictions would be validated by comparisons with the results from the *PRESSS* super-assemblage testing for both overall force-displacement characteristics and certain individual component details.

1.3   Report Layout

A brief description of the current code provisions and research performed under previous phases of the *PRESSS* program has been discussed, in particular those issues related to the wall direction of testing on the building, namely the precast wall panels.

Chapter 2 will present overall and specific details of the *PRESSS* test building, including material descriptions, relevant design aspects, instrumentation details, and a description of testing procedures used.

Chapter 3 discusses issues related to the theoretical modeling of the test building. It includes an overview of the modeling objectives for the project and then examines in detail the assumptions made and steps taken to create the analytical model. Viscous damping characteristics of the test structure will be evaluated along with a discussion of the test predictions.

Chapter 4 presents the full wall-direction experimental results of the five-story building in an overall and specific comparison of the test structure with the analytical model predictions. Observations of the resisting and non-resisting components of the test structure at the varied levels of input will also be described.

Finally, conclusions from this report will be established and will include a brief description of overall wall performance and some additional improvements suggested for the analytical model. Design and analytical modeling recommendations will be presented along with a discussion of the impact on the future of seismic design due to the results of the *PRESSS* five-story building test.

2 PRESSS TEST BUILDING

The final stage of the *PRESSS* Project was to design, build, and test a five-story structure using the concepts developed and tested in previous *PRESSS* phases. A detailed design report of the *PRESSS* Test Building is being completed (Stanton et al., in press), therefore only a brief summary of the structural features relevant to this report shall be presented here. The design of the test building itself is based on two different prototypes, each 100 ft. x 200 ft. in plan, with story heights of 12 ft. 6 in. (Figure 2-1). The lateral load resistance is provided by a combination of frames in the longitudinal direction and shear walls in the transverse direction. The flooring used for each prototype was selected based on the typical flooring systems available for precast concrete and on previous investigations of earlier *PRESSS* phases. In the first configuration, shown in Figure 2-1(a), pretopped double tees span between beams at the prototype center line and beams at the perimeter. Figure 2-1(b) shows the other configuration, with topped hollow core planks spanning between beams. Due to space limitations at the Powell Lab, a 60 percent scaled version of the prototype was created. The effects of this scaling on different quantities of importance in the test structure are shown in Table 2-1.

Table 2-1 Scale Factor Adjustments

Quantity	Prototype	Model
Length	L	$0.6L$
Mass	m	0.6^3m
Time	T	$0.6t$
Stress	σ	σ
Velocity	V	V
Acceleration	A	$A/0.6$
Force	F	0.6^2F
Moment	M	0.6^3M
Damping	C	0.6^2C
Period	T	$0.6T$

(a) PRESSS Prototype Building Double-Tee Configuration

(b) PRESSS Prototype Building Hollow Core Configuration
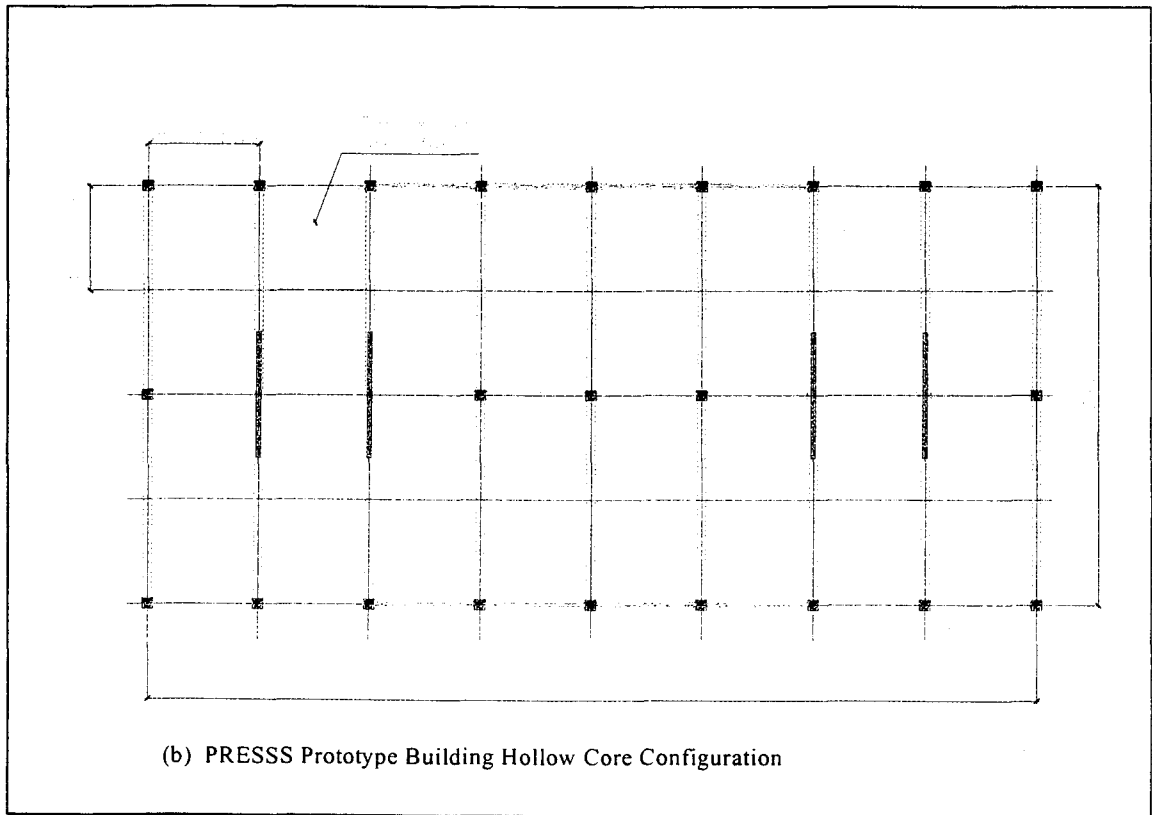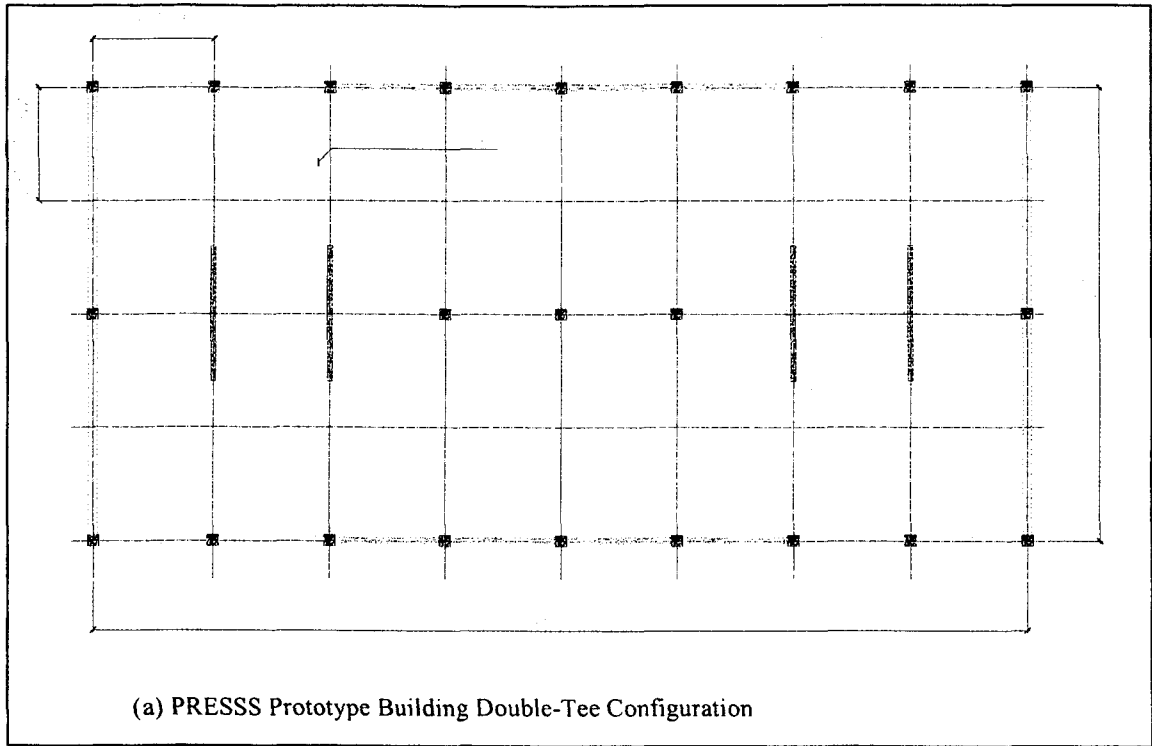
Figure 2-1 PRESSS Prototype Buildings

16

The test building is shown in Figure 2-2, with15 ft. two-bay frames making up the perimeter. The first three levels implemented a pretopped double tee floor configuration, spanning between seismic frames and connected to each panel, as detailed in Section 2.2.4. The top two levels used six-inch hollow core planks and actuator connection panels spanning between the gravity frames and the structural wall and connected to one another, as well as the seismic frames, with a two-inch cast-in-place topping. A plan view of the top two levels is shown below the photo in Figure 2-2. Connection details of the hollow core planks to the structural wall are described in Section 2.2.4. Two different precast frames, one with prestressed beams and the other using mild reinforcing steel connections, provided lateral resistance of the building in one direction of response. A central structural wall made of jointed precast panel sections provided lateral resistance in the perpendicular direction. Non-seismic gravity frames without moment connections between columns and beams ran parallel to the structural wall.

The seismic frames were comprised of four different beam-to-column connection details as shown in Figure 2-3. The prestressed frame used a hybrid connection with single bay beams and multistory columns on the first three levels. The top two levels of this frame were comprised of two bay prestressed beams with single story columns. The non-prestressed frame used connections providing moment resistance through TCY systems (TCY denotes tension/compression yielding, as noted in 1.1). The first three levels used the TCY Gap connection, where beams were clamped to the columns by unbonded post-tensioning threaded bars reacting through grout pads at the bottom of the beam. The top two floors of this frame provided moment capacity by the TCY connection using mild steel reinforcing bars grouted into corrugated ducts. The TCY connection approximates the behavior of conventional reinforced concrete connections with equal top and bottom reinforcing steel. Further discussion of the frame connection systems can be found elsewhere (Pampanin et al., in press).

17
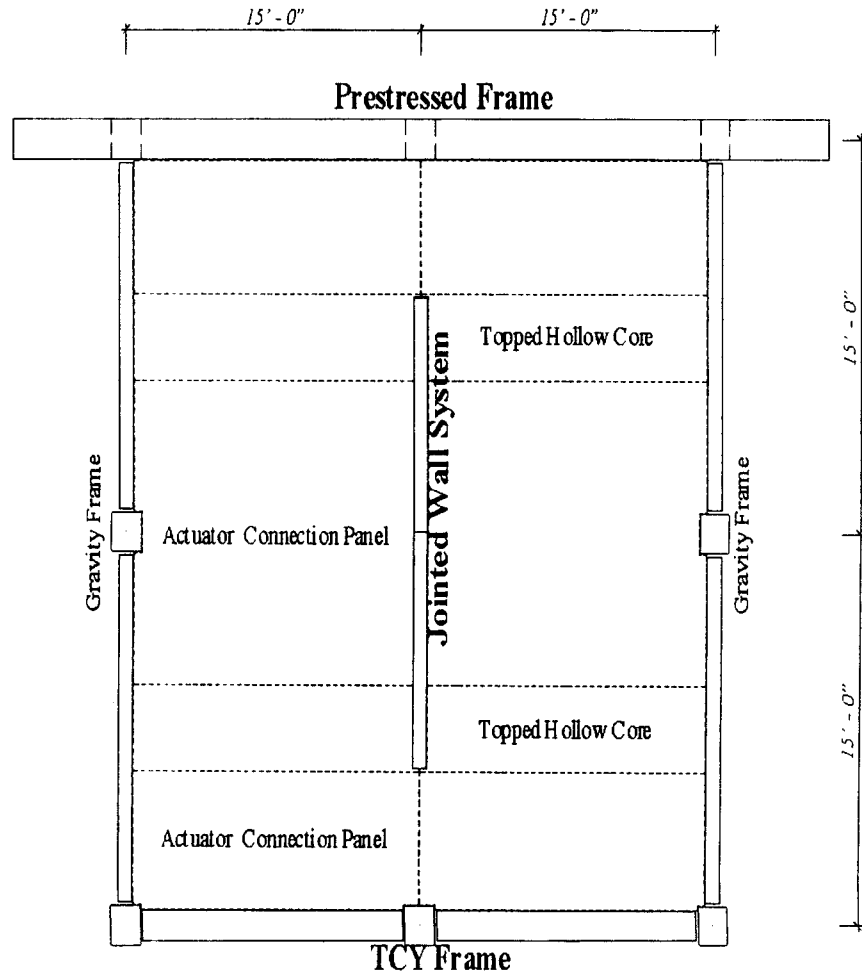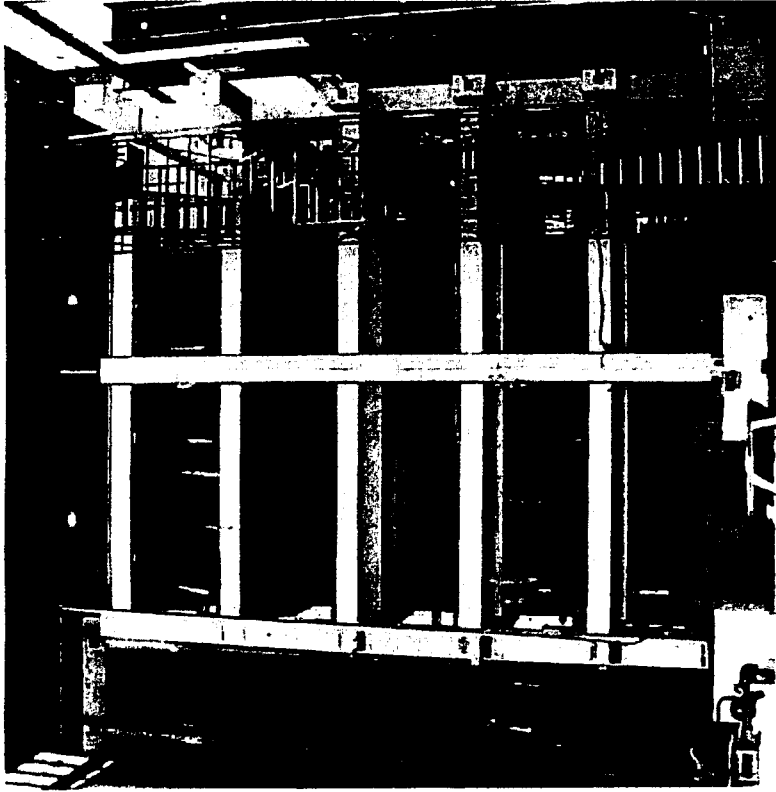
Figure 2-2 Test Building and Plan

Prestressed Frame

15' - 0"   15' - 0"

Gravity Frame

Jointed Wall System

Topped Hollow Core

Actuator Connection Panel

Topped Hollow Core

Actuator Connection Panel

Gravity Frame

15' - 0"

15' - 0"

TCY Frame

18
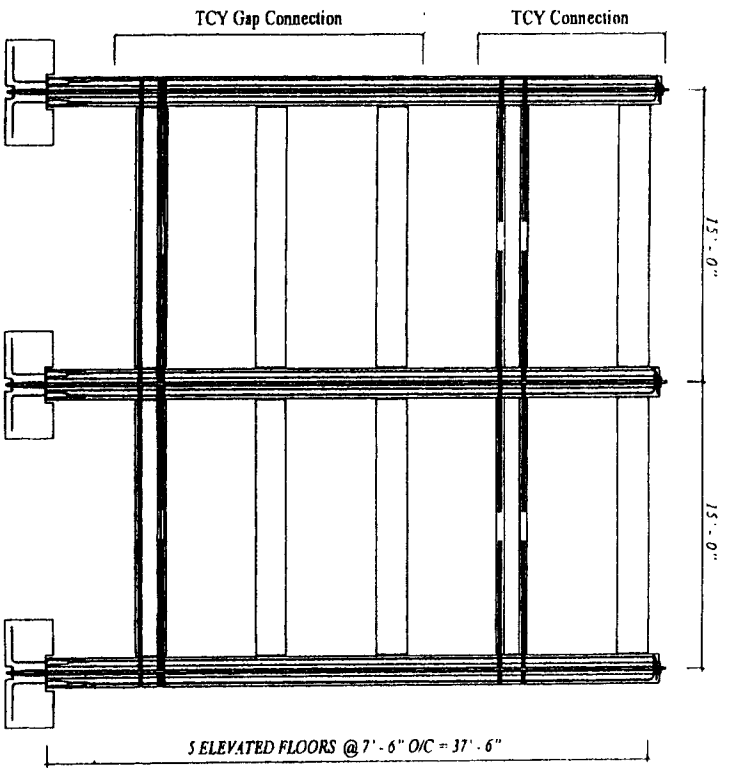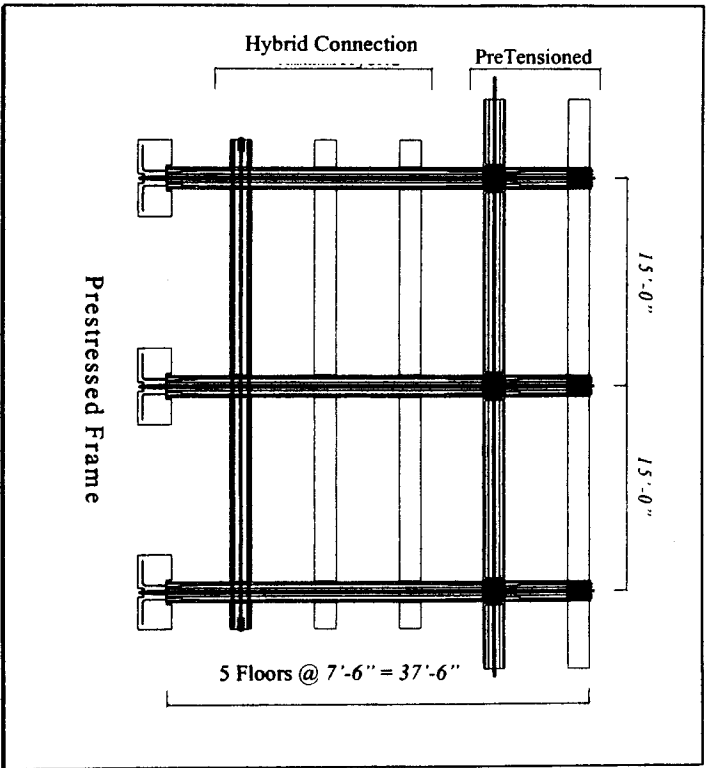
Figure 2-3 Frame Elevation Detail

TCY Frame

TCY Gap Connection   TCY Connection

15'-0"

15'-0"

5 ELEVATED FLOORS @ 7'-6" O/C = 37'-6"

Prestressed Frame

Hybrid Connection   PreTensioned

15'-0"

15'-0"

5 Floors @ 7'-6" = 37'-6"

The structural wall consisted of four precast panels two-and-a-half stories in height as shown

in Figure 2-4. The GSS connection system, developed in Phase II of the *PRESSS* project,

provided the connection across the horizontal joint between panels at mid-height of the structure.

Unbonded post-tensioning threaded bars ran down the center of each wall panel connecting the

panels to the foundation. Stainless-steel, energy-dissipating, U-shaped flexural plates, welded to

imbedded plates in the adjacent panels, provided the connection across the vertical joint

extending down the center of the wall system. In addition to furnishing energy dissipation, these

plates provide increased lateral resistance due to shear coupling between the two structural walls.

Construction of the *PRESSS* Test Building occurred over a two-week period inside the

UCSD Powell Structural Research Laboratory. It should be noted that the erection speed of the

PRESSS test building, even within the space limitations of the Powell Laboratory, was

remarkable. The shorter construction period results in faster building occupation for the owner.

This represents one of the advantages of precast structures from a profitability standpoint. A

report detailing the various aspects of the construction process will be released at a later date

(Nakaki et al., in press).

2.1 Test Building Materials

Samples of materials used in the construction of the test building were tested at the UCSD

laboratories in order to determine their actual properties. Concrete cylinder specimens were

delivered to the laboratories with the columns, beams and panels from each of the supporting

precast companies. The cylinders were tested according to ASTM standards for their

compression strength before post-tensioning, on the day of post-tensioning, and on the test day.

Similar compression tests were also performed for the hollow core topping concrete and the

foundation concrete. Results for the cylinder tests are shown in Table 2-2. Fiber-reinforced and

non-fiber-reinforced high strength grout was used in the horizontal joints and rebar coupling
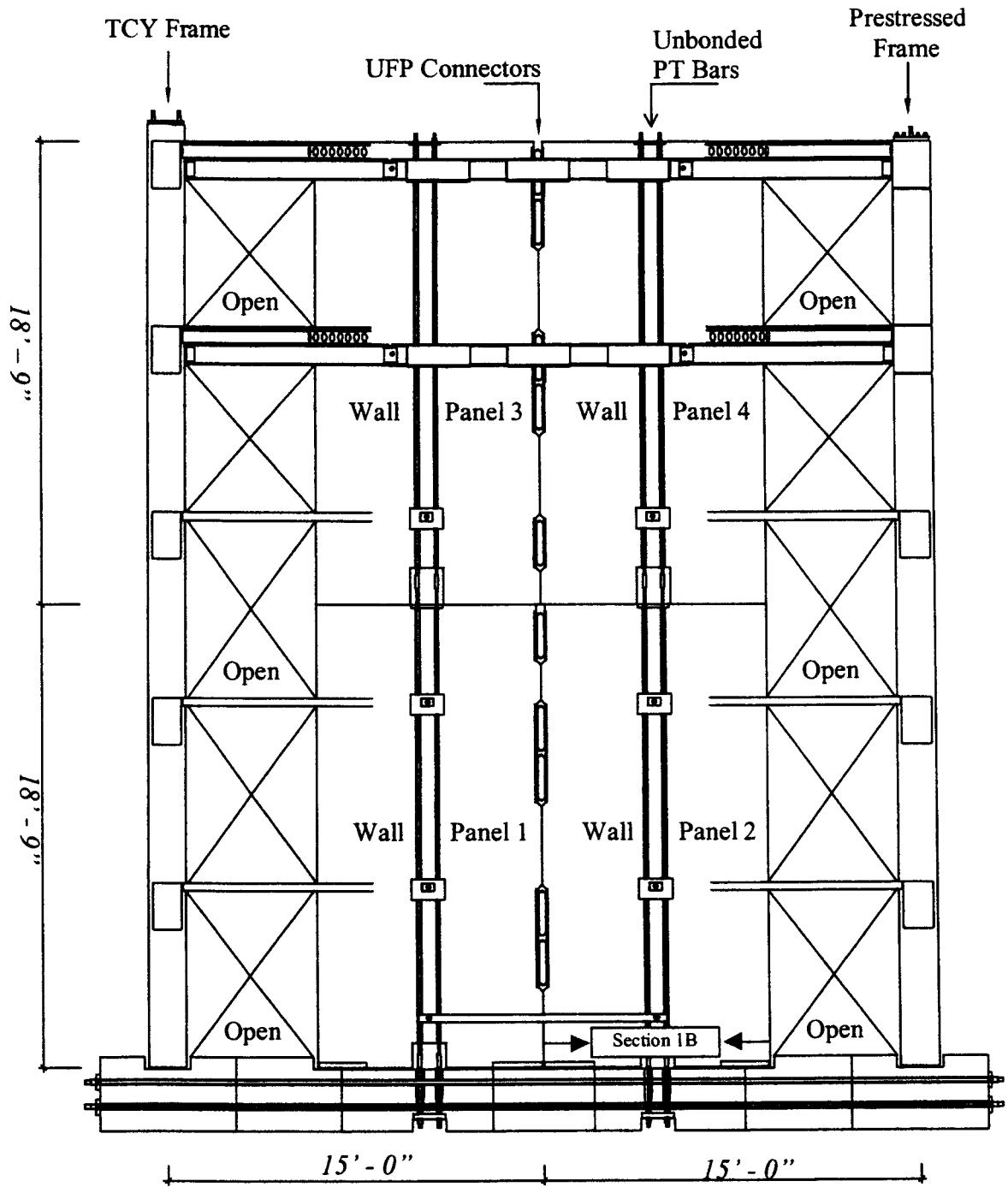
Figure 2-4 Wall Elevation Detail

21

devices in the wall system, respectively. The 3 in. x 3 in. x 3 in. grout cubes were tested for their

one, seven, and twenty eight day strengths according to ASTM standards for grout, with an

additional test representative of the strength during testing. Table 2-3 shows the resulting values

from the grout tests.

Table 2-2 Concrete Cylinder Compressive Strengths

Specimen	Pre date	Pre-PT Results	PT date	PT Results	DOT 1 date	DOT 1 Results
Gravity Column C4					8/19/99	6.60 +/- 0.21 ksi
Gravity Column C5					8/19/99	8.31 +/- 1.52 ksi
Gravity Beam GB-10R			7/6/99	6.44 +/- 0.1 ksi		
Gravity Beam GB-10			7/6/99	6.37 +/- 0.02 ksi	8/18/99	6.39 ksi
Gravity Beam GB-9R			7/6/99	6.73 +/- 0.01 ksi		
Gravity Beam GB-9					8/18/99	7.24 +/- 0.22 ksi
Gravity Beam GB-8R					8/18/99	7.96 +/- 0.31 ksi
Gravity Beam GB-7, 7R, 8					8/18/99	6.78 +/- 0.01 ksi
Gravity Beam GB-2R, 4R, 6R	6/23/99	8.27 +/- 0.13 ksi	7/6/99	8.39 ksi	8/19/99	7.85 +/- 1.19 ksi
Gravity Beam GB-2,4,6 Double Tee DT-6R			7/12/99	8.15 ksi	8/19/99	8.12 +/- 0.67 ksi
Gravity Beam GB-1, 3, 5			7/12/99	7.50 ksi	8/19/99	7.83 +/- 0.20 ksi
Gravity Beam GB-1R, 3R, 5R			7/12/99	8.31 ksi	8/19/99	8.38 +/- 0.52 ksi
Wall Panel W-1	6/23/99	6.99 +/- 0.16 ksi	7/6/99	6.97 ksi	8/16/99	7.31 +/- 0.67 ksi
Wall Panel W-1R	6/23/99	7.51 +/- 0.02 ksi	7/6/99	7.67 ksi	8/16/99	7.96 +/- 0.13 ksi
Wall Panel W-2	6/23/99	8.17 +/- 0.24 ksi	7/6/99	8.58 ksi	8/16/99	9.14 +/- 0.11 ksi
Wall Panel W-2R	6/23/99	8.66 +/- 0.12 ksi	7/6/99	8.94 ksi	8/16/99	9.52 +/- 0.19 ksi

Specimen	cast	7-DAY	28-DAY	DOT date	DOT
5th Floor Topping	7/2/99	*3.10 +/- 0.10	3.77 +/- 0.00 ksi	8/20/99	4.19 +/- 0.04 ksi
4th Floor Topping	7/2/99	*3.25 +/- 0.14	4.16 +/- 0.15 ksi	8/20/99	4.47 +/- 0.07 ksi
Footings	4/5/99	3.32 +/- 0.03 ksi	4.64 +/- 0.14 ksi		

* 5th and 4th floor 7-Day specimen were tested as a 10-Day.

In order to obtain the most accurate values of the material properties for the post-

tensioning bars, tensile tests were performed on bar samples from the same batch of the PT bars

to be used in the test building. Figure 2-5 shows the stress-strain curves for the one-inch diameter

bars tested. This resulted in an average elastic modulus of 29,000 ksi and an average yield stress

value of 153 ksi.
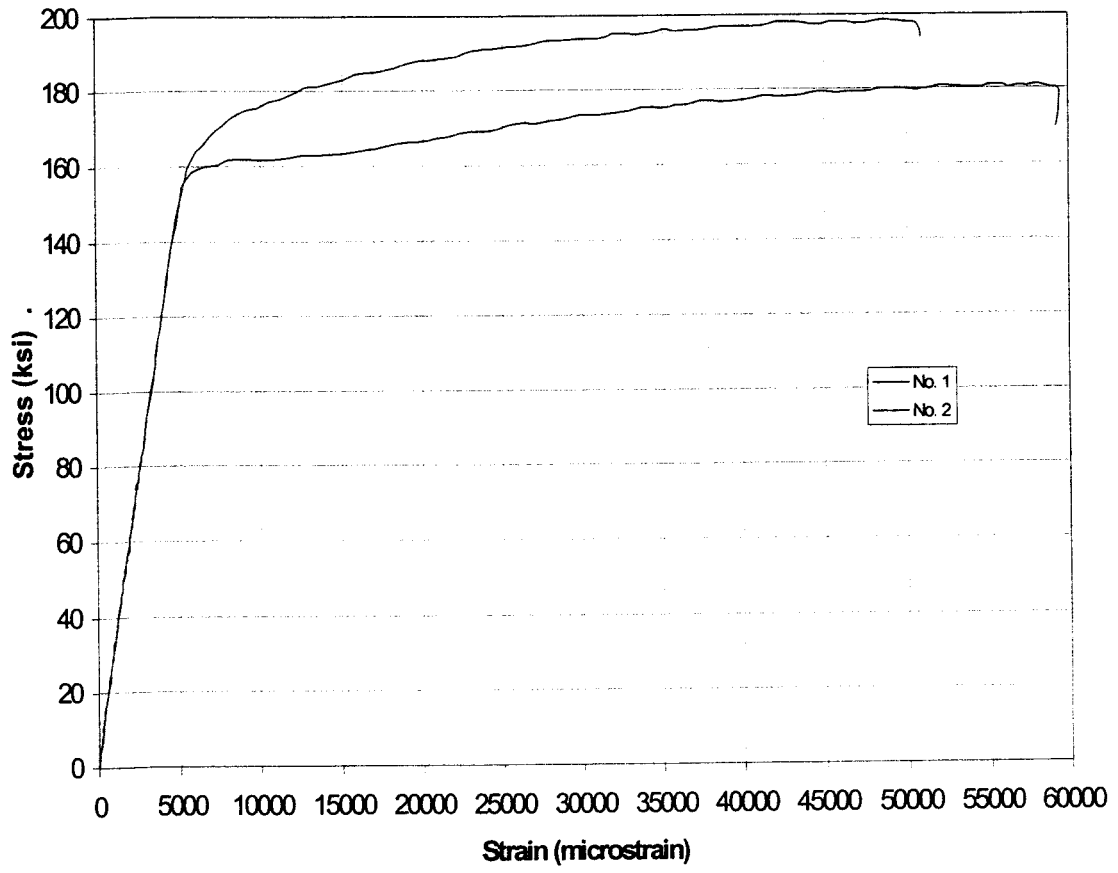
Figure 2-5 PT Bar Stress-Strain Curves

Table 2-3 Grout Cube Compressive Strength

Description	Cast	1-DAY	7-DAY	28-DAY	DOT date	DOT
6/2/99	6/2/99	3.75 ksi	7.33 +/- 0.02 ksi	7.9 ksi	8/18/99	9.08 +/- 0.29 ksi
NMB	6/3/99	4 ksi	7.90 +/- 0.32 ksi	8.43 ksi	9/2/99	8.79 +/- 0.22 ksi
W2RW	6/10/99	7.13 ksi	9.96 +/- 0.09 ksi	****8.91 ksi	8/18/99	11.02 +/- 2.04 ksi
BG-1	6/14/99	4.89 ksi	7.47 +/- 0.54 ksi	7.27 ksi	9/2/99	9.21 +/- 0.12 ksi
HC-seal	6/9/99		.42 +/- 0.00 ksi	**.72 ksi	9/2/99	1.06 +/- 0.01 ksi
BG-2	6/15/99	5.57 ksi	7.56 +/- 0.22 ksi	8.68 ksi	9/2/99	7.74 +/- 0.40 ksi
BG-3	6/16/99	5.65 ksi	8.33 +/- 0.63 ksi	8.55 ksi	9/2/99	9.26 +/- 0.04 ksi
BG-4	6/17/99	5.28 ksi	7.31 +/- 0.44 ksi	8.82 ksi	8/18/99	9.47 +/- 0.43 ksi
6/21/99	6/21/99	4.10 ksi	5.84 +/- 0.07 ksi	6.99 ksi	9/2/99	8.27 +/- 0.71 ksi
6/22/99	6/22/99	4.26 ksi	6.41 +/- 0.19 ksi	7.64 ksi	9/2/99	7.46 +/- 0.15 ksi
6/23/99	6/23/99	5.15 ksi	7.54 +/- 0.49 ksi	7.72 ksi	9/2/99	9.27 +/- 0.19 ksi
NMB-PC	6/25/99	***5.04 ksi	6.32 +/- 0.07 ksi	8.57 ksi	9/2/99	8.77 +/- 0.24 ksi
TCY-Gap	6/30/99	5.03 ksi	*7.58 +/- 0.13 ksi	8.52 ksi	9/2/99	8.39 +/- 0.14 ksi
8/20/99	8/20/99	3.82 ksi	5.77 +/- 0.24 ksi	6.89 ksi	9/2/99	6.08 +/- 0.67 ksi

* TCY-Gap 7-Day is a 6-Day.

** HC-Seal 28-Day is a 27-Day.

*** NMB-PC reusult is a 14-Day tested as a 17-Day. It is NOT a 1-Day test.

**** NMB 28-Day is a 32-Day

2.2 Relevant Design Aspects

Only brief design and construction details will be noted in this report as they relate to components in the analytical model of the wall lateral load resisting system. Although not specifically related to the analytical model, a description of the Displacement Based Design procedure is also included due to its importance in the building design.

2.2.1 PRESSS Building Design Procedure

Force Based Design procedures have been shown to have significant drawbacks for design of ductile precast systems (Priestley, 1998). Specifically, Force Based Design relies on elastic structural properties to determine elastic base shear which is reduced by an R factor related to the systems ductility assuming an emulation of monolithic concrete behavior. This procedure limits the advantages of precast systems because energy dissipation characteristics and concepts of yield displacement differ considerably from the elasto-plastic behavior assumed in Force

Based Design (Priestley, 1996). Therefore, the results of a Force Based Design procedure do not capture the true behavior of the jointed precast system.

For this reason, the prototype and test buildings were designed using a more consistent Direct Displacement Based Design (DBD) procedure (Priestley, 1996), in which the design is based on an inelastic target displacement and effective stiffness. The target structural displacement is determined from an allowable inter-story drift permitted by design codes while the effective stiffness is approximated to the secant stiffness of the building corresponding to its expected fundamental mode of response. Use of both the elastic stiffness for determining structural displacements and arbitrary reduction factors, as in Force Based Design, are completely eliminated by this approach (Nakaki et al., 1999).

The building was designed using an earthquake level compatible with the UBC 1997 Zone 4 acceleration response spectrum with intermediate soil type Sc (UBC, 1997), while achieving a maximum target drift of 2 percent. Displacement spectra from Appendix G of the SEAOC Bluebook (PBSE-SEAOC, 1998) were used due to a lack of displacement spectra requirements in the UBC.

Assuming a design drift of 2 percent, the DBD procedure shown in Figure 2-6 was carried out. The floor displacements were found using equation 2-6 (a). Then the target displacement, Δ_d, is found (2-6 (b)). Assuming an equivalent viscous damping coefficient of $\xi =$ 20 percent, the effective period, T_{eff}, is found using the design displacement response spectra or equation 2-6 (c). The effective mass, m_e, is found from the floor displacement, floor mass, and target displacement (2-6 (d)). Finally, the effective stiffness is found (2.6(e)) and used to calculate a design base shear.

The prototype building consisted of four shear walls resisting lateral loads. The mass per floor associated with each wall in the prototype was 1625 kips. This correlates to a value of 351 kips per floor in the *PRESSS* Test Building. Actual model weight per floor was less because of

25

Design Drift θ_d

$\Delta_i = \theta_d \cdot h_i$ (a)

Design target displacement Δ_d

$$\Delta_d = \frac{\sum_{i=1}^{n} m_i \cdot \Delta_i^2}{\sum_{i=1}^{n} m_i \cdot \Delta_i}$$ (b)

Estimate of damping ξ

Effective period T_{eff}

$$T_{eff} = \frac{T_{5p}}{\Delta_{5p}} \cdot \frac{\Delta_d}{\sqrt{\left(\frac{7}{2+\xi}\right)}}$$ (c)

$\xi\ 5\%$

$\xi\ 15\%$

$\xi\ 20\%$

T_{5p}

Δ_d

T_{eff}

Displacement

Period

$$m_e = \frac{\sum_{i=1}^{n} m_i \cdot \Delta_i}{\Delta_d}$$ (d)

Effective secant stiffness K_{eff}

$$K_{eff} = 4\pi^2 \cdot \frac{m_e}{T_{eff}^2}$$ (e)

Base Shear $V_b = K_{eff}\Delta_d$
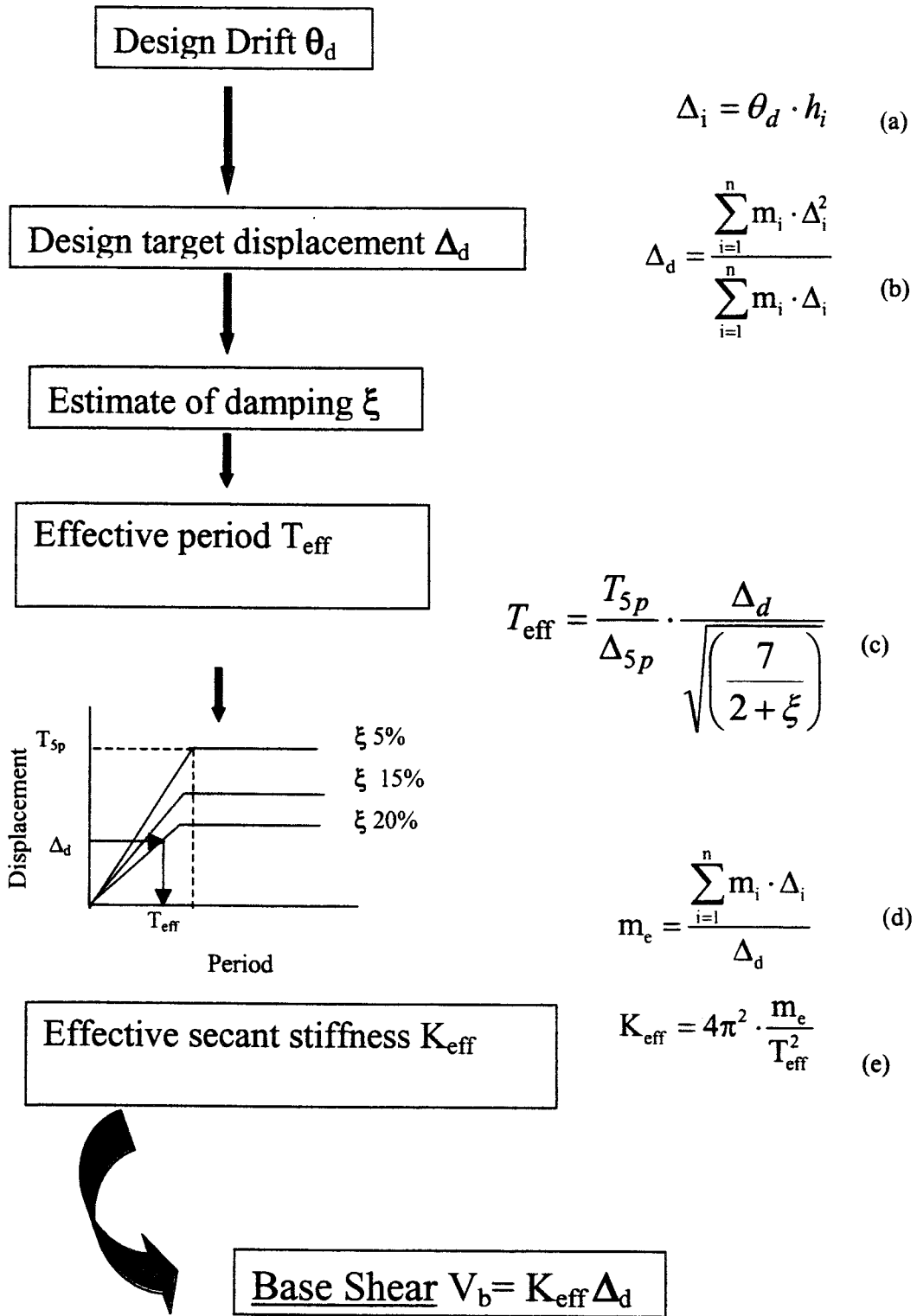
Figure 2-6 DBD Procedure

26

scale effects (Table 2-1) and a reduced tributary floor area, necessitated by the test-hall dimension limitations. It should be noted that the model is not aware of this mass, therefore the mass was input into the pseudodynamic control program as discussed subsequently.

2.2.2 Wall Details

The precast panels were designed to resist lateral seismic loads by the clamping force of the post-tensioning bar and additionally by shear coupling of the UFPs. Energy dissipation is provided through the yielding of the stainless steel U-plates and by rocking of the wall system. The wall panels were significantly reinforced to ensure that they remain elastic during the testing, except at the foundation interface. An adequate amount of confinement reinforcing was provided in order to sustain the high compression strains during maximum displacements. Figure 2-7 shows section cut from Figure 2-4 of a plan view of the reinforcement detailing at the base of the panel. The open space in the center of the wall was the blockout for the post-tension bar couplers

The panels rested on a rigid foundation, which was post-tensioned to the laboratory strong floor using inch and a quarter diameter high strength thread bars. The panels were set on shims in the blocked out portion of the foundation during erection. The panel base was then grouted to the foundation with high strength fiber reinforced grout to provide continuity and shear slip resistance of the wall system (Figure 2-8).

The post-tensioning bars provided further connection to the foundation. Four one-inch diameter unbonded Dywidag coupled thread bars ran down the centerline of the panels. The bars were coupled in two locations, just above the foundation and at the horizontal joint between panels (see Figure 2-4). The bars were bolted to anchor plates imbedded in the foundation as shown in Figure 2-9. The nuts were welded to the imbedded plate because access to the nuts was not available after the foundation had been cast. These post-tensioning bars were designed to

27
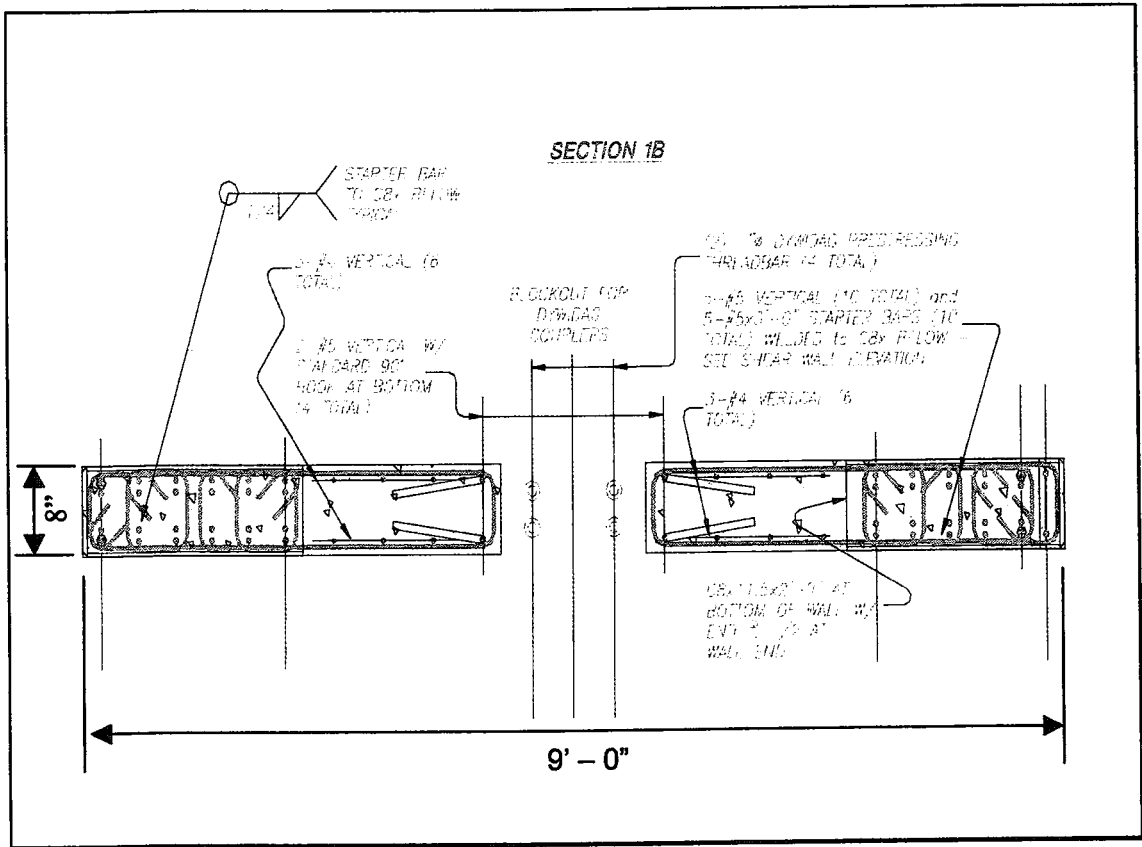
Figure 2-7 Wall Plan Drawing

Figure 2-8 Panel Base Detail
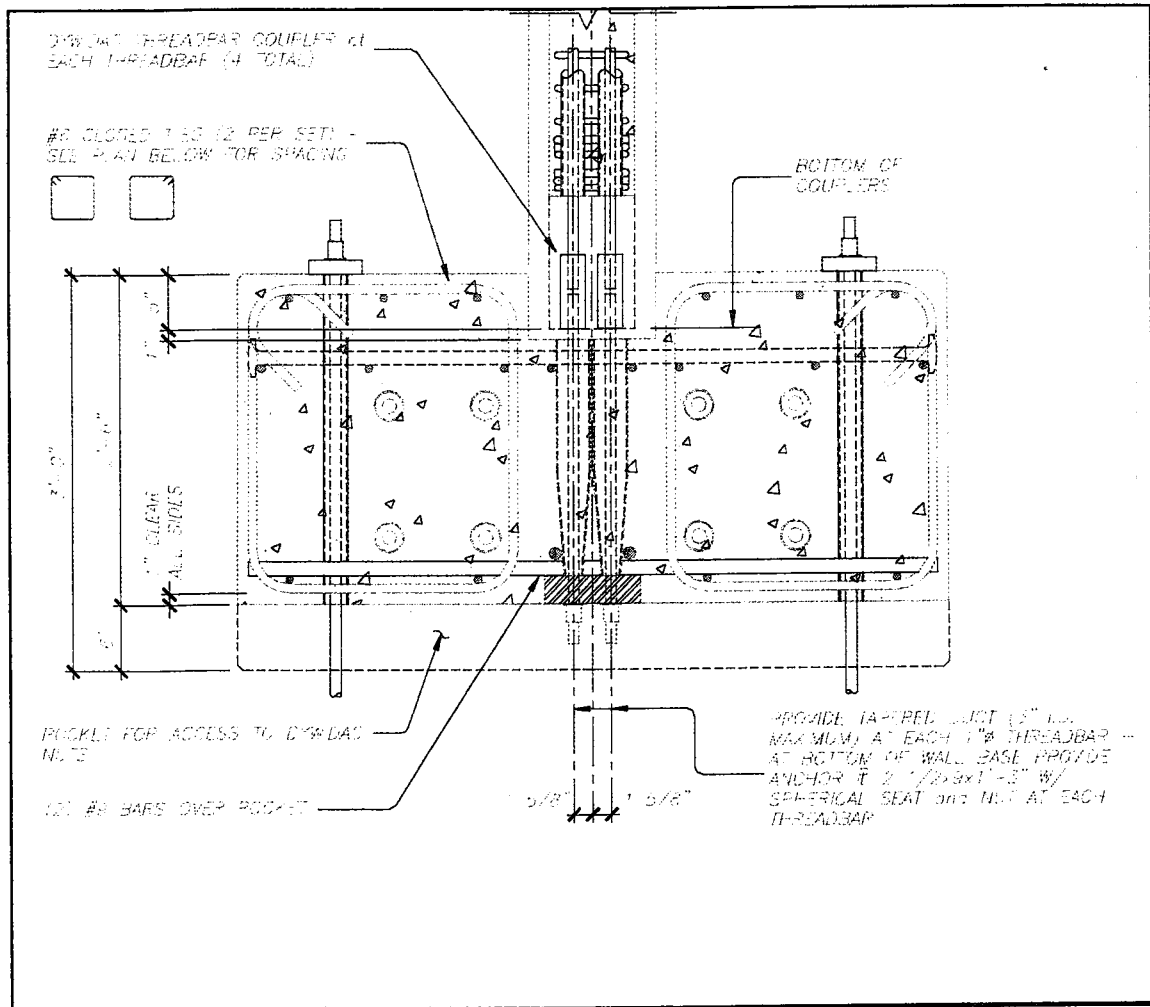
Figure 2-9 PT Connection Detail

remain elastic up to the design level drift of 2 percent. In this manner the PT bars served as a re-centering device after the earthquake and provided a component of the lateral resistance as the wall displaced. Each bar was post-tensioned to a force of 41 kips after erection of the test building.

2.2.3   U-Plate Details

Stainless steel U-shaped flexure plates (UFP) served to provide additional lateral resistance to the wall system by shear coupling along the vertical joint between the wall panels. The plates provided hysteretic damping as they yielded in flexure in relation to the relative vertical displacement between wall panels. These vertical connection components were chosen base on the NIST Phase II results discussed in 1.1.2. The UFP were welded to imbedded plates in the adjacent walls as shown in Figure 2-10. When the building displaced, the UFP rolled against the imbedded plates causing flexural yielding to occur. The UFP and weld geometry was such that adequate room was available for this displacement. This action provided increased resistance to the applied lateral load.

2.2.4   Flooring Connection to Wall

The lateral load was transferred from the flooring systems to the wall resisting system through specially designed connections. The first three levels used a double tee floor configuration, with the double tees spanning from one seismic frame to the other. In order to limit the deformations of the double tee between the connection at the frame and the connection to the wall as the panels lift off and rock, a connection was required that allowed load to be transferred in the horizontal direction, but not in the vertical direction. To achieve this, the connection shown in Figure 2-11 was designed.
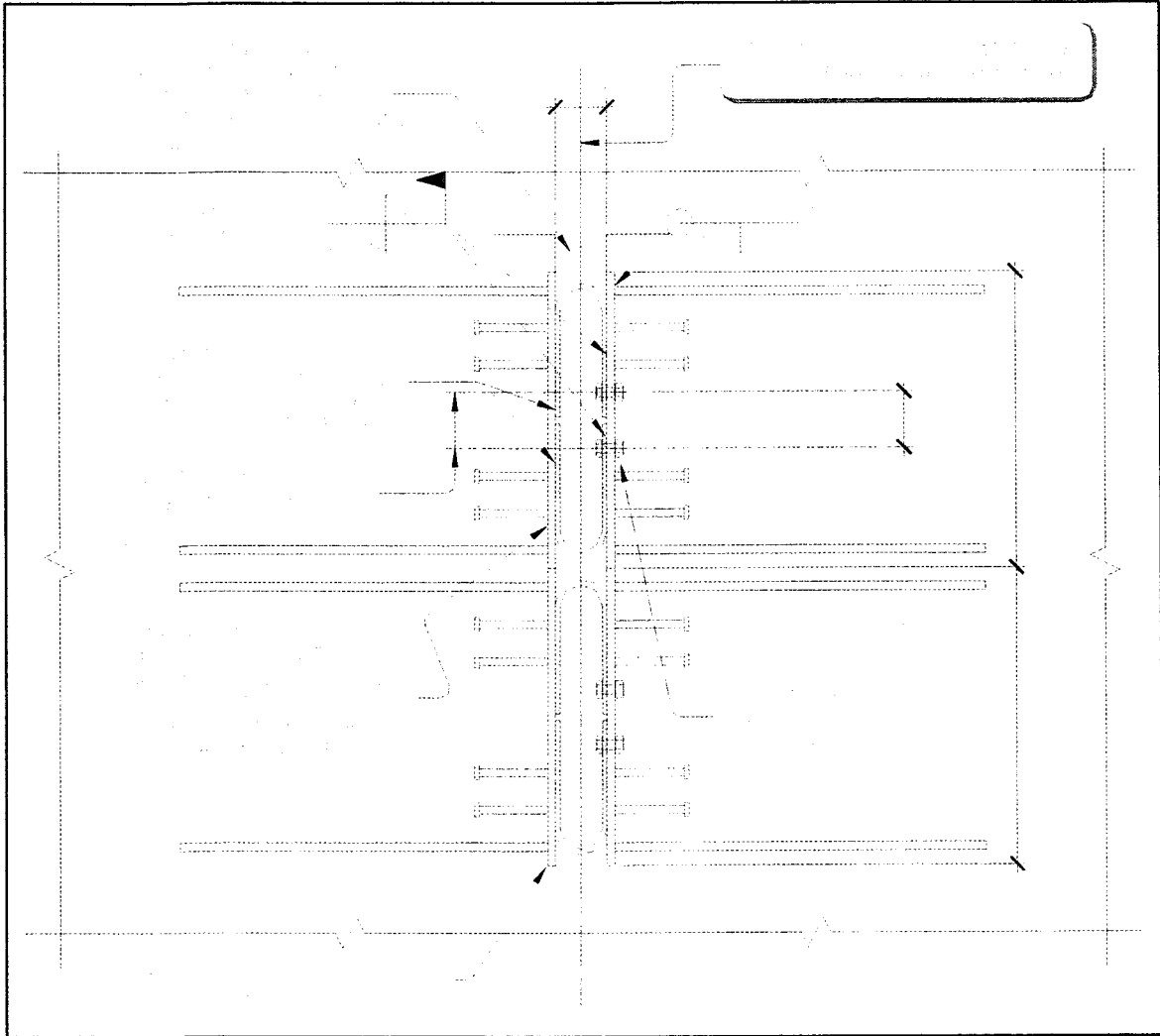
Figure 2-10 UFP Connection Detail

32
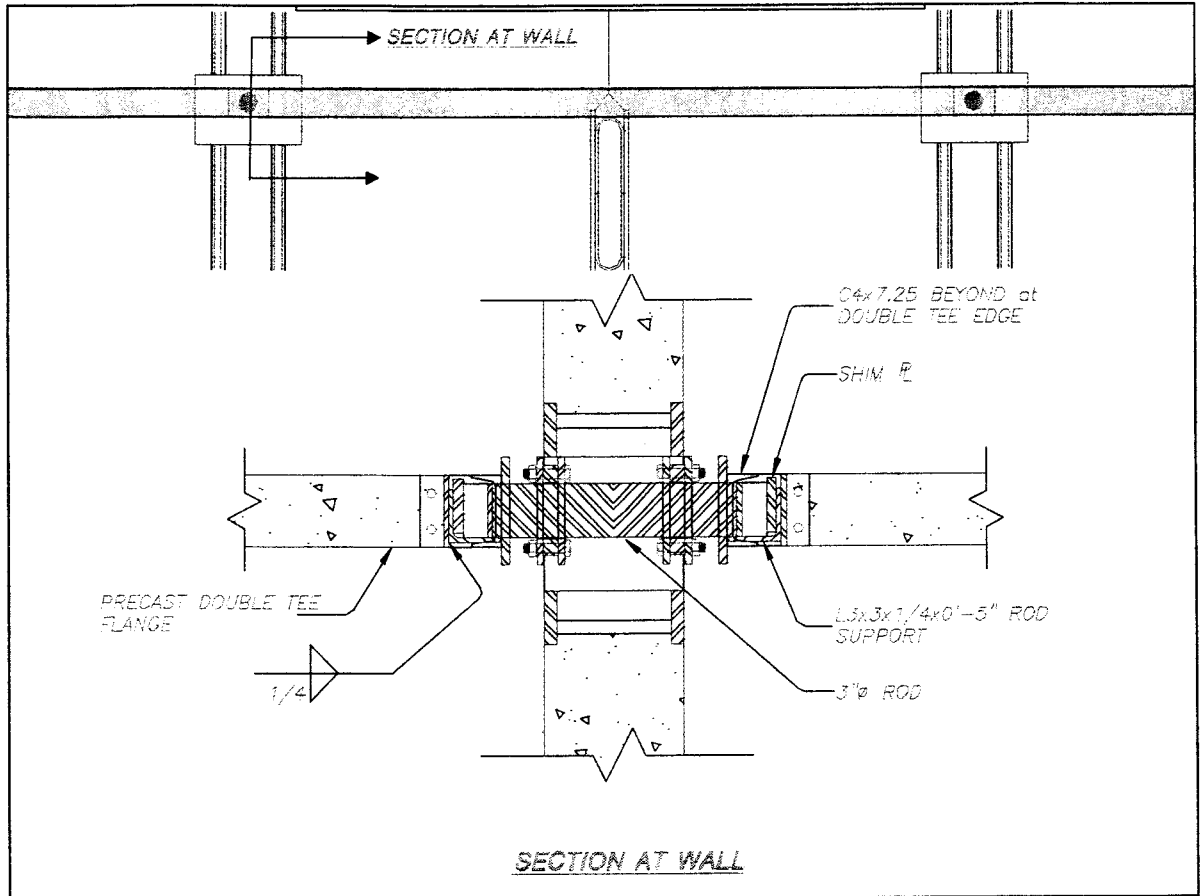
Figure 2-11 Double Tee to Wall Detail

The three-inch diameter steel rod was connected to the double tee flanges and beared on a plate system in the panel. The plate system was made up of an imbedded plate with a rectangular opening, with the steel rod going through two additional plates that were clamped to the imbedded plate. The rod was then free to travel along bearing pads vertically within the opening and bear on the imbedded plate allowing for lateral load transfer.

The transfer mechanism was simplified on the top two levels in the sense that the configuration of the hollow core panels allows for a larger relative displacement between the floor system at the frame and at the wall connection to occur. The hollow core planks and actuator connection panels (ACP) spanned between the wall and the gravity frame, bearing on a channel section at the wall and L-beams on the frame. The channel sections were bolted to the wall panel as shown in Figure 2-12. The bolts were then grouted to ensure bearing transfer of the lateral load from the channel section. After erection, plates were welded to the channel flanges and to imbedded plates in the ACPs. The lateral load was transferred from the ACPs to the wall panels though these welds. Wall lifting at the channel/wall connection was accommodated by yielding of the floor insitu topping at panel-to-panel connections.

2.3   Instrumentation and Data Recording

Primary data recorded during seismic simulation identified actuator forces and displacements, as well as displacements of the floor on either side of the wall panels. Instrumentation used to determine the floor and wall panel displacements consisted of Heidenhain devices measuring floor displacements and string potentiometers recording wall displacements. Potentiometers were also used to record displacements at locations at the wall base, top, vertical joint, horizontal joint, and gravity column base.

SECTION AT WALL

SECTION AT WALL

2" THICK CAST-IN-PLACE
TOPPING SLAB OVER 6"
PRECAST PLANKS PER PLAN

PRECAST CONCRETE SHEAR
WALL PANEL

℄ 1/2 TO MC10x
WEB

℄ 1/2 TO MC10x
TOP FLANGE - BACK-
UP PLATES REQUIRED

℄ 1/4 TO
℄ 5/8 IN PLANK

℄ 1/4 TO ℄ 1/2
at BOTTOM EDGE

℄ 1/2 TO MC10x
BOTTOM FLANGE
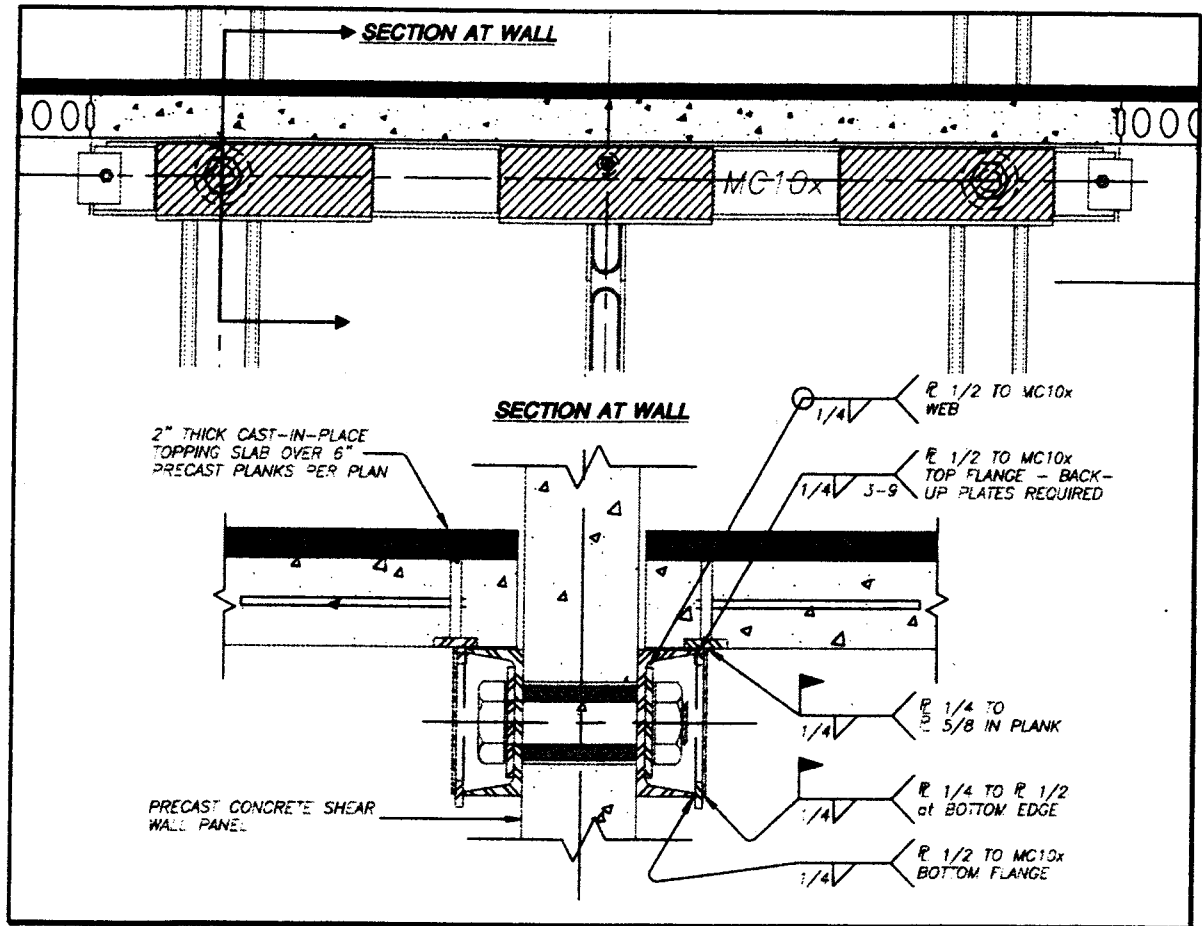
Figure 2-12 Hollow Core to Wall Detail

35

A large number of electrical resistance strain gages were placed on reinforcing bars in numerous locations. The locations of those gages of particular interest to this report are noted in Chapter 4.

In addition to electronic instrumentation, photographers recorded the condition of the building, after marking cracks with felt pens. To facilitate crack detection the entire building was painted with a white undercoat prior to testing. Time-lapse video recording, using three cameras, was made at all the critical loading stages.

2.4 Testing

The lateral forces and displacements were applied to the building using two actuators moving to equal displacements at each floor level. Each actuator was connected to the floor by actuator extensions and a triangulated connection mechanism, ensuring equal forces were applied at each of the two floor connection points per actuator. The connection system, shown in Figure 2-13, enabled the lateral load to be applied at the floor level, as would be the case for an actual earthquake, and allowed relative horizontal displacement between the connection points to occur. However, the setup imposed relatively small but additional vertical loads to the floor system that would not occur in a real earthquake, as a consequence of their location above the floor.

Earthquake records were chosen to test the structure based on levels corresponding to 33, 50, 100, and 150 percent of the design level earthquake. Figure 2-14 shows the four different input accelerograms used in the testing. These records were scaled in frequency and amplitude to match the design spectrum for the scaled test building. Of the four initial acceleration records chosen for the *PRESSS* test (Sritharan et al., 1999), only EQ-I and EQ-II were used, while EQ-IV was replaced by increasing the EQ-III accelerations fifty percent. The EQ-III record was modified with a low-pass filter to reduce the high frequency content introduced by use of the
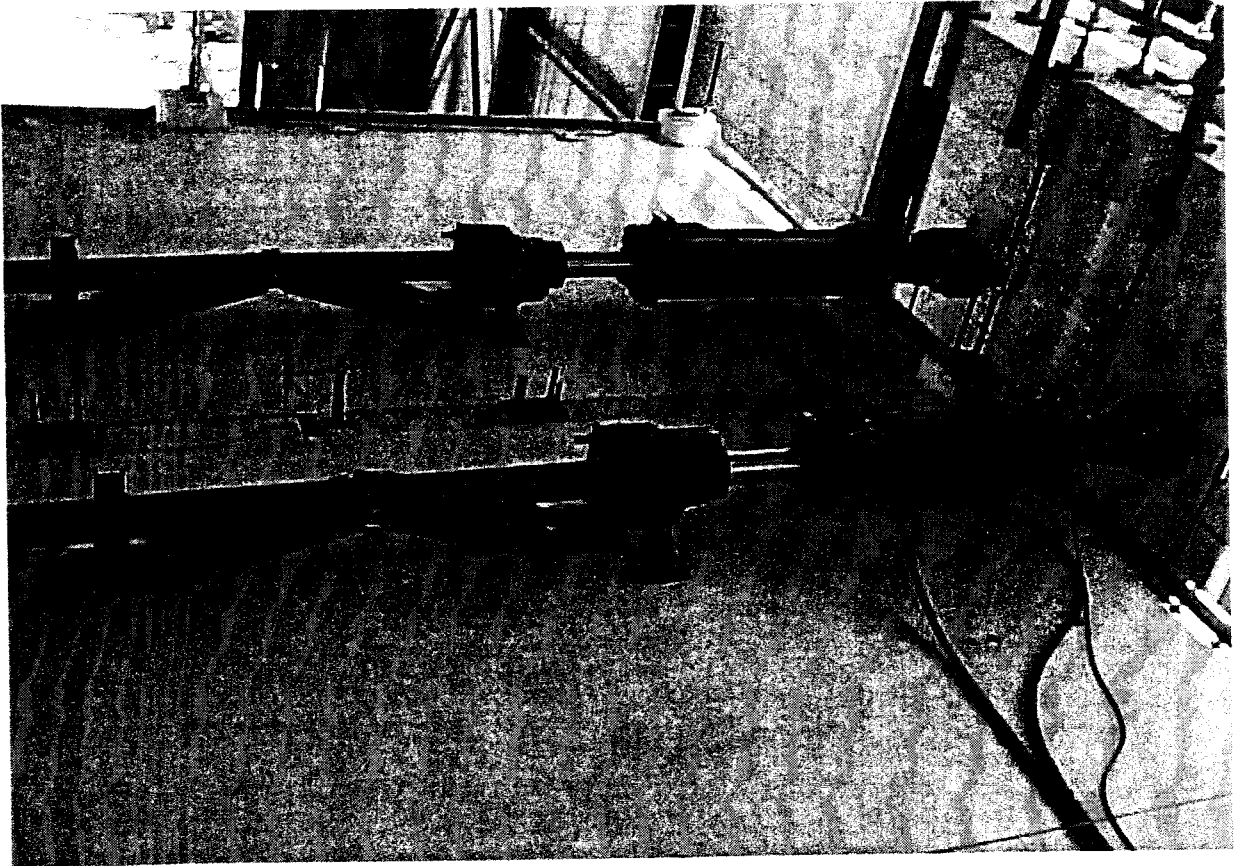
Figure 2-13 Actuator Extensions
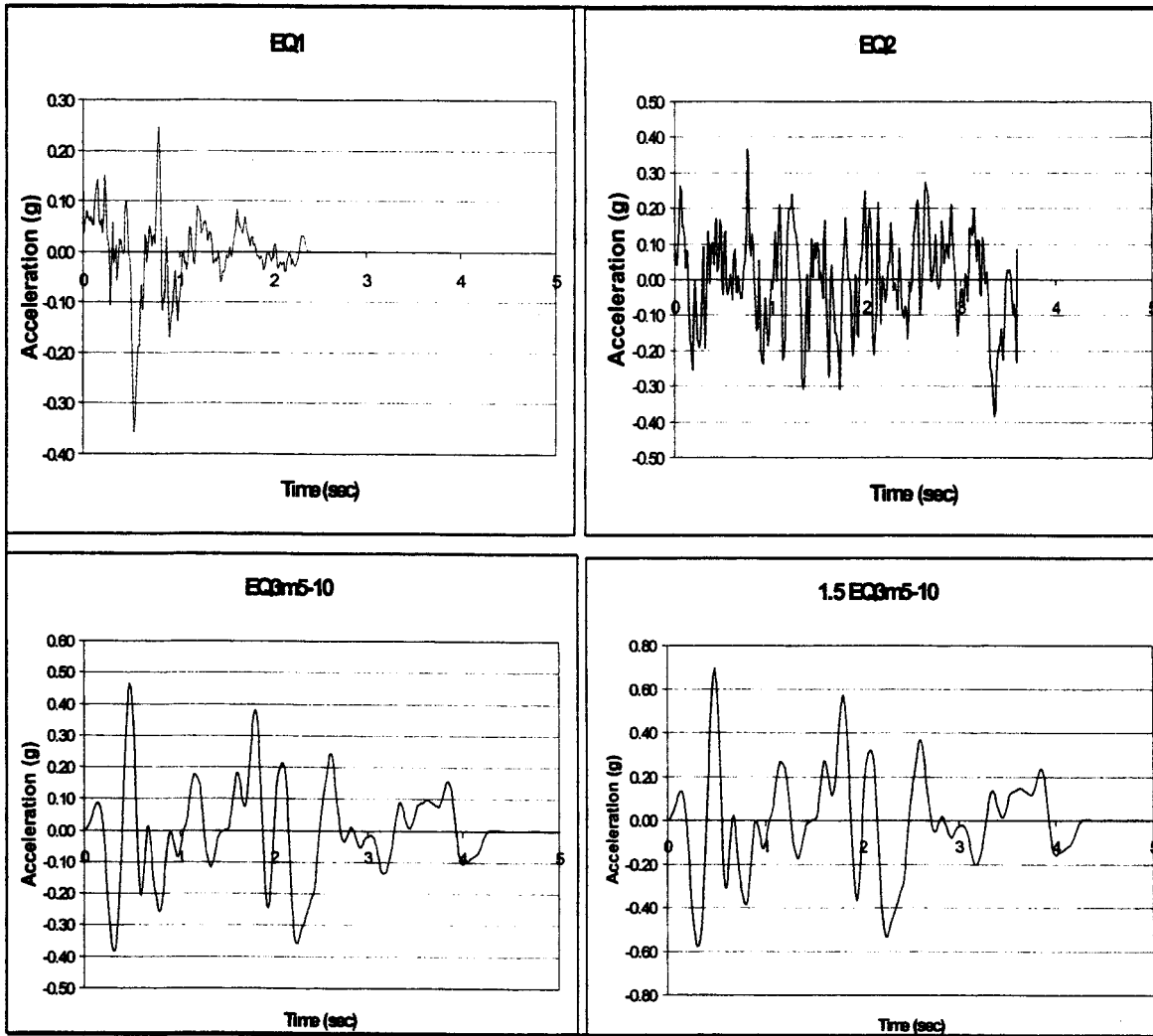
Figure 2-14 Acceleration Records

38

SHAPE program (Earth Mechanics, 1998) to create the acceleration record used for the test (Pampanin et al., in press). The reasons for modifying the record will be discussed subsequently.

The principle method of testing the building was pseudodynamic testing, the concept of which is presented in Figure 2-15. The computer program controlling the actuator input contained a simple five-degrees-of-freedom model of the building that was subjected to inelastic time-history analysis under the aforementioned acceleration records.

The response of the control model was governed by d'Alembert's equation of motion

$$[M]\ddot{x} + [C]\dot{x} + [K]x = -[M]a_g \qquad (2.1)$$

where [M], [C], and [K] are the mass, damping and stiffness matrices; and $\ddot{x}, \dot{x}$ and x are the relative acceleration, velocity and displacement vectors; and a_g is ground acceleration. The mass matrix was not the actual mass of the test structure, but the scaled quantity of the prototype mass in the wall direction of loading, as previously mentioned. Since viscous damping can not be directly modeled in the test, a damping matrix was input to the control model. A value of 2.5 percent critical damping was used to create this matrix. The initial stiffness matrix was calculated from the results of a flexibility test performed on the test structure, which will be described subsequently.

D'Alembert's equation was solved for each time step and the calculated displacement vector at the end of each time step was imposed on the test structure by the actuators. The measured restoring force vector required to apply these displacements represents the nonlinear stiffness terms [K]x; upon the next time step this updated stiffness matrix, [K], was used to determine the subsequent displacement vector. In this manner, as the stiffness of the actual structure is modified by inelastic action, or strength degradation, the control analytical procedure recognizes the change in stiffness and modifies the structural response accordingly. During this
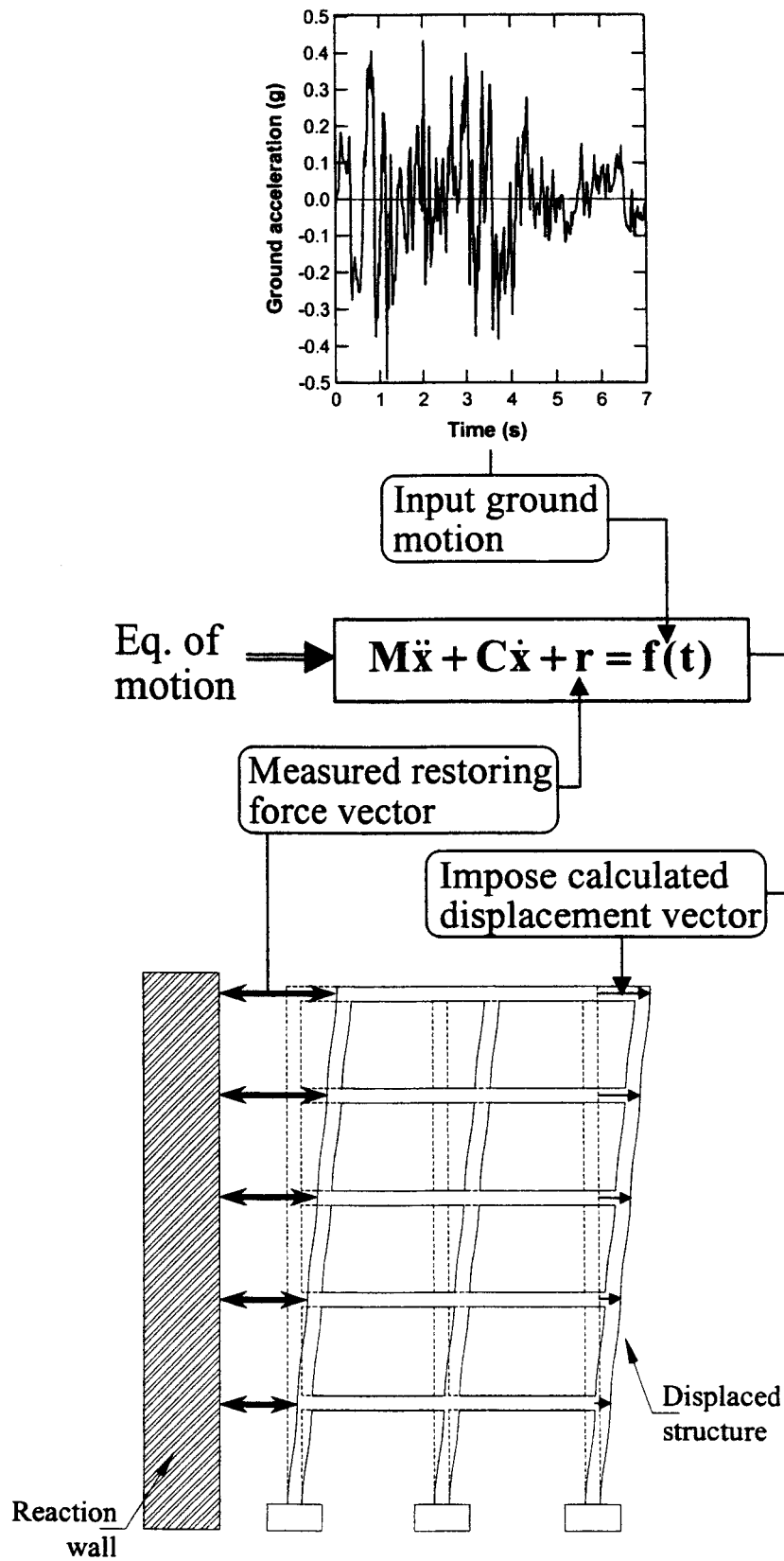
Figure 2-15 Pseudodynamic Testing Procedure

process, displacements defining the structural response were directly measured on the structure, whereas the command displacements were applied and monitored by internal transducers in the actuators. A discrepancy between external command and internal displacements, mostly due to flexibility in the load path, was corrected by iteratively multiplying the vector of displacement errors by the initial stiffness matrix until a predetermined tolerance was met. Further information of pseudodynamic testing can be found elsewhere (Igarashi, 1994).

The other two test procedures carried out on the *PRESSS* building were flexibility tests and inverse triangular (IT) load tests. Since the initial input to the building was based on an initial estimate of elastic stiffness, flexibility tests were periodically conducted at different stages of the test sequence to account for degradation of the test structure in previous tests. In the flexibility tests, actuator forces were applied sequentially and independently to the five floor levels. Using the resultant forces and displacements, the flexibility matrix was determined; and after inverting and smoothing, the stiffness matrix used to begin the pseudodynamic test was defined.

The IT test involved cyclic loading of the test structure using an inverse triangular force pattern to push to the maximum displacement achieved in the previous pseudodynamic test. This test procedure is done for three reasons, as noted below.

- The IT test exercises the test building to the same peak displacement in both directions of displacement (positive and negative), while the pseudodynamic test reaches a peak in only one direction.

- Multiple cycles at peak displacements are achieved, allowing equivalent viscous damping to be evaluated at different levels of drift. As a consequence of the time taken to actually apply the record (approximately 20 minutes per second of earthquake record) only one cycle at peak displacement occurs during pseudodynamic testing.

- When the peak displacement is reached the test can be paused and the building investigated. It is at this point that pictures of the structure were taken and damage descriptions were recorded.

The three loading types were repeated for each type of earthquake input used to test the building. Descriptions of the tests performed for the wall direction are noted in Table 2-4.

Initial testing at the design level EQ-3 had to be aborted after 0.6 seconds of scaled earthquake record, because of unacceptably high floor force levels. Before resuming testing, the earthquake record was filtered to reduce the severity of higher mode effects. Figure 2-16 (a) shows a comparison between the SEAOC PBSE Ad-Hoc Committee recommended design code spectrum (PBSE, 1998) and the EQ-3 level acceleration response spectra from non-scaled test records at 5 percent damping.

Table 2-4 Wall Direction Testing

Description	Test #	Duration (pseudo-time)	Δ-Max (in)**	Base Shear (kips)**
IT 0	023		0.15	71.4
0.25 EQ1	025	2.952	0.20	80.5
0.5 EQ1	032	3.972	0.41	142.3
1.0 EQ1	033	3.972	1.22	315.3
IT 1	034*		1.25	186.6
	036		1.25	174.3
1.0 EQ1	038	3.0	1.70	286.4
-1.0 EQ1	039	3.972	1.78	292.6
1.0 EQ2	040	5.304	3.00	294.7
IT 2	041*		3.00	221.3
-1.0 EQ2	046	5.208	2.84	299.4
1.0 EQ3	047	0.6	2.10	302.5
1.0 EQ3mod	049	0.6	2.07	214.5
1.0 EQ3mod2	050	0.606	1.94	260.9
1.0 EQ3m5-10	051	5.772	8.31	321.5
IT 3	052		8.31	278.2
	053		2.00	217.9
	054		8.31	278.2
-1.5 EQ3m5-10	055*	5.688	11.6	464.9

*-Flexibility Test Performed   **-Absolute Value

The original accelerogram was modified with a low-pass filter at a specified frequency with a taper value of a given percentage. A filter is, in the frequency domain, a function that multiplies the amplitude of each frequency content of the accelerogram by 0 or 1. A low-pass filter maintains the frequency content at a fixed value of frequency (Hz). Since a sudden change of 0 to 1 in this function will introduce undesired artificial effects to the signal (accelerogram), the taper operation is necessary to smooth the decay of this function from 1 to 0. For example, with a low-pass filter at 5 Hz, the 5.1 Hz content will not be cut off completely, but reduced a bit and this effect will be more significant on the higher frequencies (5.2, 5.3, etc....) (Sritharan et al., in press).

The first modification attempt was with a low-pass at 2Hz, 10 percent taper. This was too penalizing, reducing too much of the original signal as shown by the EQ3m2-10 acceleration spectra in Figure 2-16 (a). The EQ3m5-5 record spectrum matched reasonably well and was used for the 1.0 EQ3mod test noted in Table 2-4. Unacceptably high floor forces were still present, so the 1.0 EQ3mod2 test was run using the same record, but changing the control model to 5 percent assumed structural damping in the first mode. This test was also unsuccessful, so the record was further modified to EQ3m5-10. This modification matched the design spectrum reasonably well, and allowed a successful test to be run. Further references to EQ-3 or the design level earthquake in this report are representative of the EQ3m5-10 record.

The result of the modification is that EQ3m510 is much less important (in terms of peak ground acceleration) than before and is no longer compatible with the SEAOC 1998 Blue Book design spectra corresponding to EQ-III. More importantly, since the long periods were not effected by the modification, the compatibility with the displacement spectra was still good. The code and record displacement spectra are shown in Figure 2-16 (b). This is of greater importance to this test because the DBD procedure makes use of displacement spectra in its calculations.
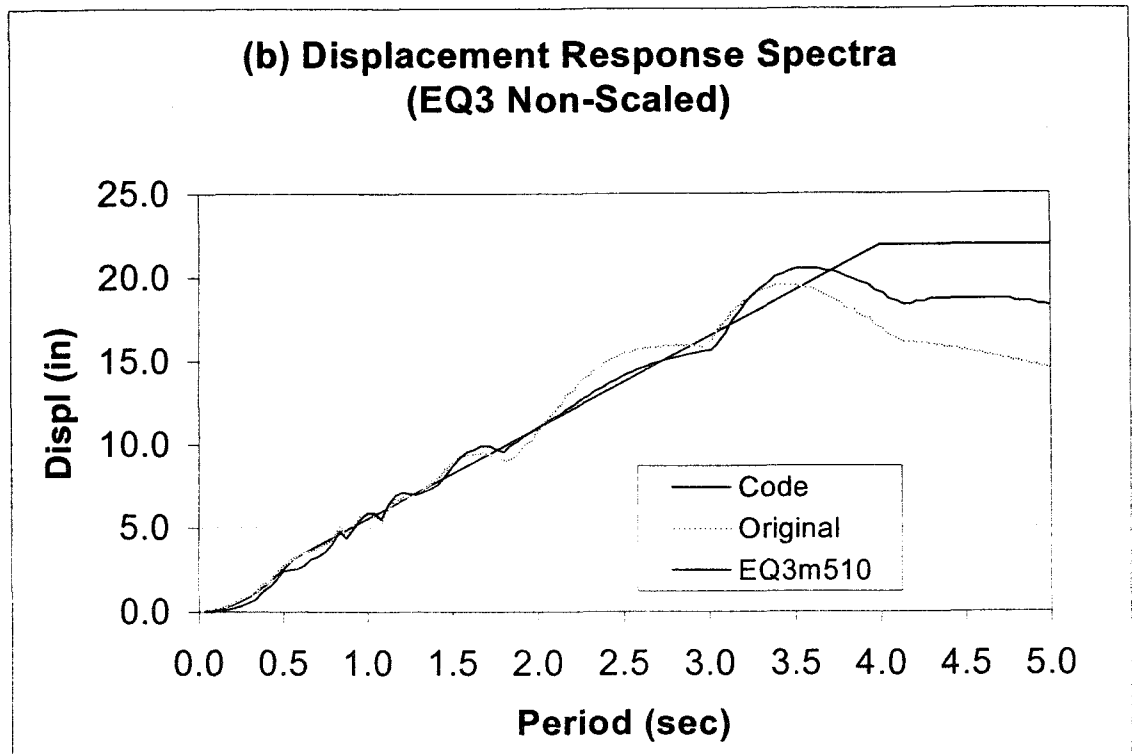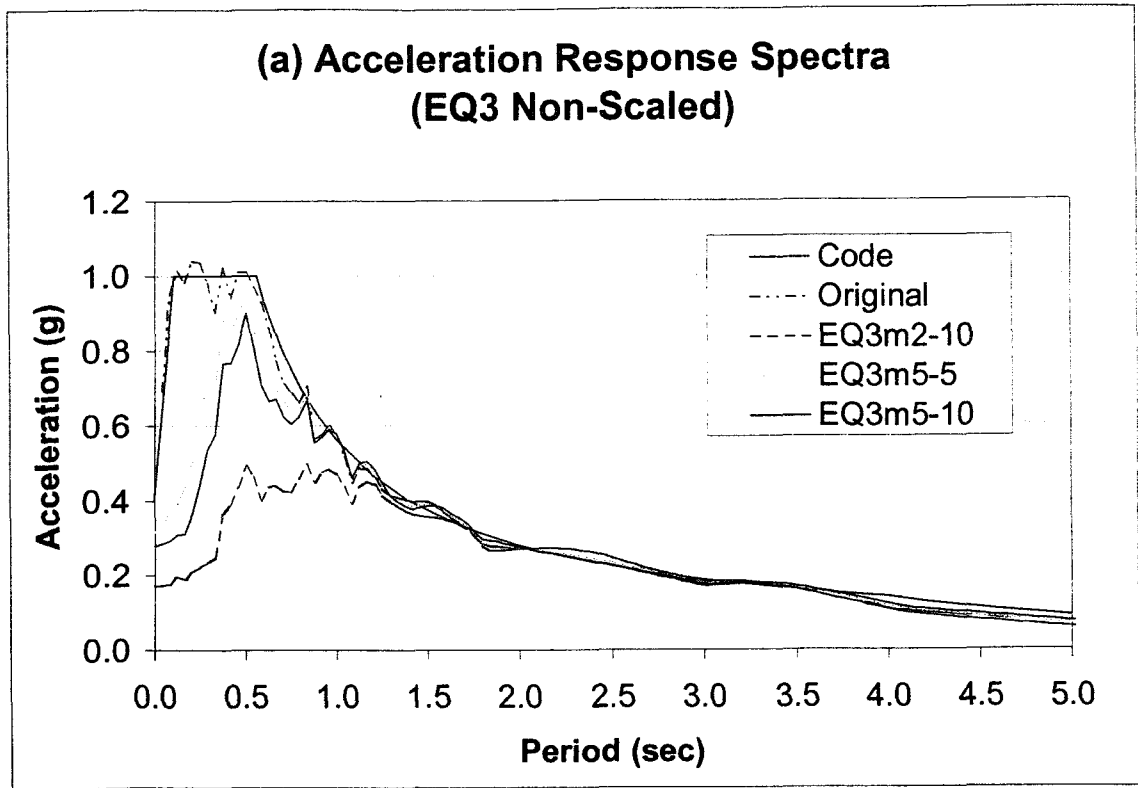
Figure 2-16 Input Record Response Spectra Comparisons

44

Having a working analytical model to predict building behavior was of great value for these tests. Results from the analytical model showed that filtering would not affect the peak displacements or base shear forces, which were primarily influenced by the first (inelastic) and second modes of response. Therefore, the testing could resume keeping with original objectives of the *PRESSS* Phase III Project.

3 THEORETICAL MODELING

3.1 Overview

The proposed plan for the *PRESSS* Phase III Project stated that analytical studies would be completed for the precast panel section of the project. A research team separate from those involved with the super-assemblage testing and building design would undertake this task. The plan was slightly changed in that two sets of theoretical model studies were conducted for the Five-Story Building. Lehigh University completed the main work associated with the analytical studies for Phase III. However, for testing purposes an analytical model was also prepared by the researchers at UCSD. This chapter includes a brief description of the Lehigh studies, which are currently ongoing, and a complete description and presentation of UCSD's analytical predictions.

3.1.1 Lehigh Fiber Element Model

As the main contributor of the analytical research group, Lehigh University took the designs prepared for the Five-Story Building and created a fiber element model, shown in Figure 3-1. The model, developed in Phase I of the *PRESSS* program, was subjected to inelastic time-history using the DRAIN family of computer codes. Although the Lehigh fiber element was a much more complicated model, results of the analysis did not differ more than 10-15 percent from the UCSD analyses. The researchers at Lehigh will report separately on their experiment/prediction comparisons at a later date (Sause et al., 2001).

3.1.2 UCSD Analytical Model

The focus of the theoretical work done at UCSD was to prepare an analytical model using the Ruaumoko program (Carr, 1998) that could predict the behavior of the *PRESSS* Building during actual testing circumstances. The model was purposely designed to be equivalent to a

truss element
(PT bar)

truss element
(in-plane behavior of
floor system)

simple link element
(vertical connector)

fiber element
(wall panel)

master node

slaved node

segment end
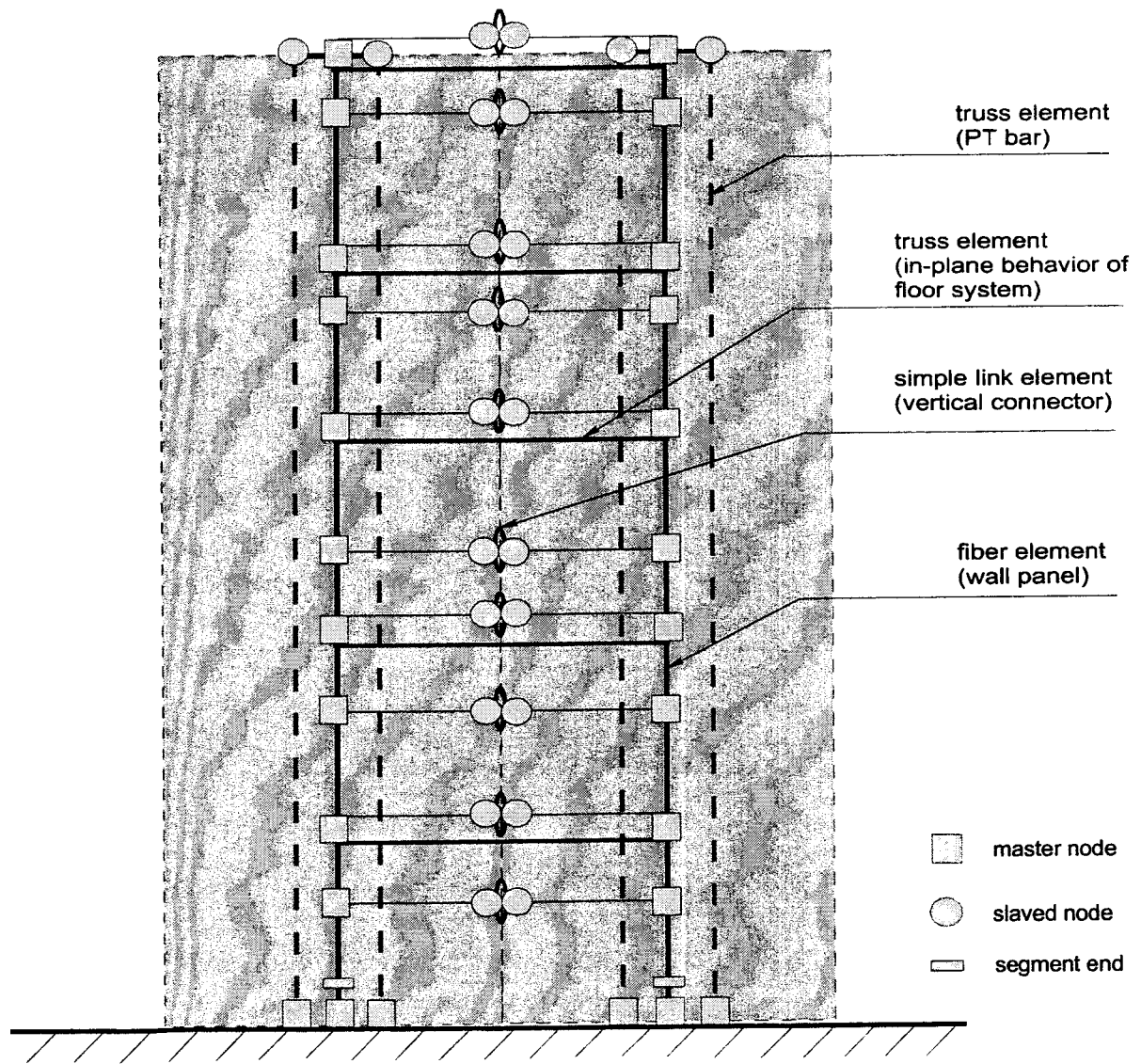
Figure 3-1 Lehigh Fiber Element Model (Sause, 2001)

simple program that would capture the general building behavior characteristics for a number of different earthquake input motions. The idea was to produce a model that any typical design firm could reproduce with minimal effort, yet still be able to provide an accurate prediction for force and displacement characteristics. With these objectives in mind the model for the precast panel seismic resisting system was created.

3.2   Model Description

The concept of the wall system model is fairly straightforward. It consisted of elastic frame elements representing the wall panels and rigid-links connected to spring elements that represented the other components of the system. Since the panels by design should perform elastically, gross uncracked section properties were used for those elements. The spring elements used selected hysteretic characteristics to model the behavior of the UFPs, PT Bars, and foundation. The horizontal joint located midway between the first and second level was assumed to be a rigid one. This meant that the two panels stacked on top of each other acted as a single wall. An additional column was placed to the right of the wall system model with floor displacements slaved to those of the wall to account for the added resistance of the seismic frame and gravity frame columns. Figure 3-2 shows the model. An example of the Ruaumoko data file used to run the model is located in the Appendix.

Each wall was modeled as five elements with nodes starting at the base and spaced vertically, as shown in Figure 3-2, in order to account for the location of the generalized mass at each floor. These nodal points are at the same level as the floor elevations. The analytical model assumed rigid diaphragm behavior for the floors, therefore the nodes for the walls and gravity column were constrained to displace equally in the X-direction at each floor level.

90.0"

$I_{gross} = 839808\ in^4$

90.0"

$I = 0.7\ \Sigma\ I_{gross\ col}$

90.0"

● Lumped
Nodal Mass

90.0"

90.0"

[A]   [B]   Rigid Link

Gravity Weight
& PT Forces

90.0"

Base Rigid Link

[C]   [D]
PT Spring   Compression
Only Spring

49.6"   53.0"   53.0"   49.6"   8"   8"
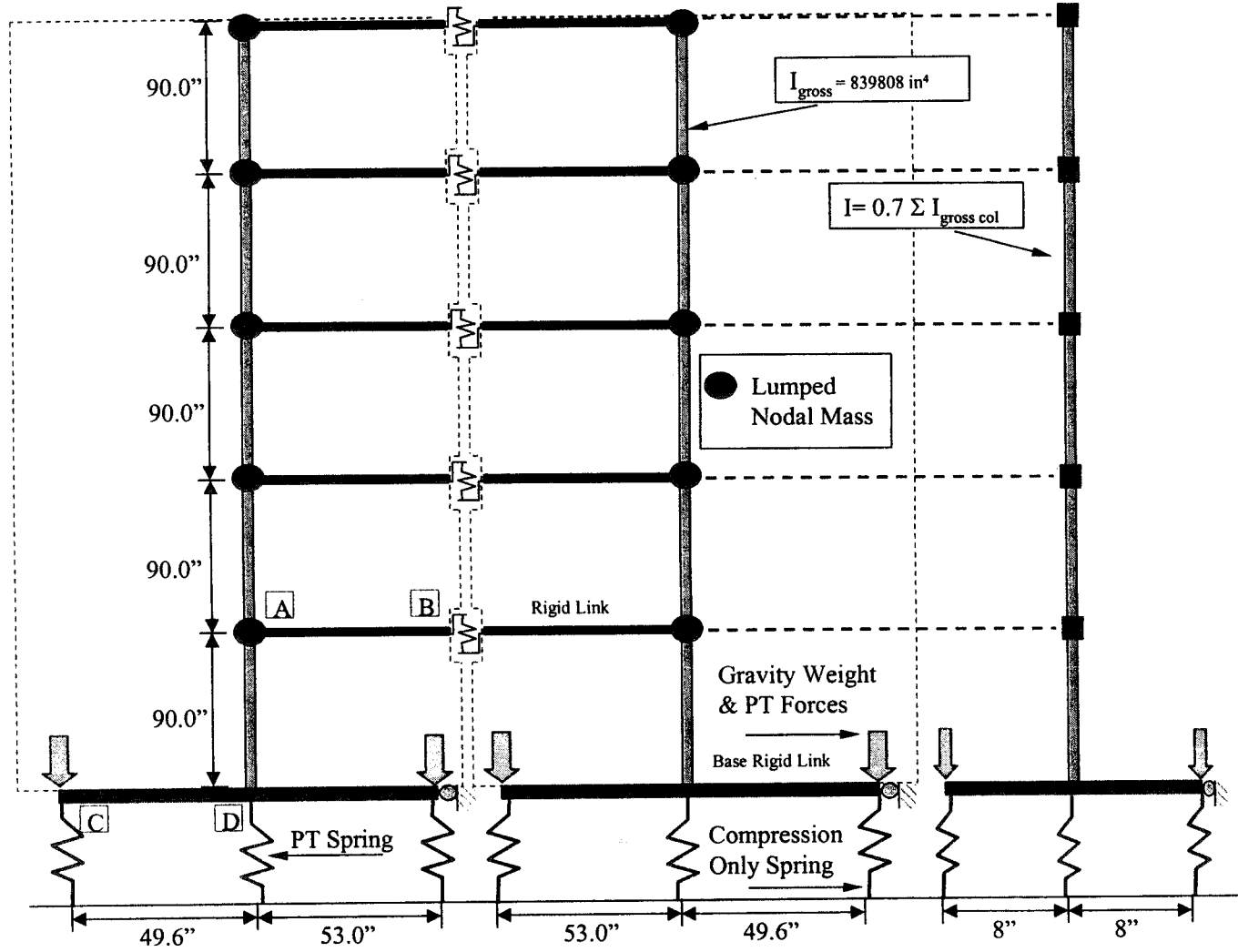
Figure 3-2 Ruaumoko Model

From each wall node a rigid-link extends inward to the centerline of the model where the vertical joint between the two walls exists in the test building. The rigid-links were modeled by taking the properties of the largest elements in the model (wall members) and increasing them by a magnitude of one hundred. Larger values than this were found to cause problems in the numerical calculations done by the Ruaumoko program, causing the program to crash. The rigid links had an offset of 0.01 in. to allow for vertical springs representing the UFPs. Specific details on the UFP springs are noted in Section 3.3.2.

The post-tensioning (PT) springs in the prototype act to provide a clamping force to the foundation as well as increased lateral resistance as the wall system rotates. They also serve as self-centering devices for the building. These were modeled as springs attached to the base of the wall elements and gravity column and fixed at the base. The PT-Spring element properties are described in Section 3.3.2.

The base nodes of the wall elements had rigid-links extending horizontally 49.6" from centerline toward the exterior of the panel and 53" toward the interior. The base node of the gravity column had rigid-links extending 8" outward horizontally. The location of these nodes corresponds to the calculated center of compression of the wall panel section and gravity column at a drift ratio of two percent. This is assuming a rectangular stress distribution at the toe of the panel. The right side base node was constrained from moving in the X direction on each wall and the gravity column. Therefore all the base nodes were constrained as a result of the rigid link element connecting them. This is congruent to the design assumption that no shear slipping will occur at the base of the wall. The concrete foundation was modeled with compression-only springs extending from the toe nodes and fixed on one end.

The mass of the structure is input in the form of weights and internally converted by the program to mass units by dividing the weights by the acceleration of gravity (Carr, 1998). As previously mentioned, the floor mass was related to the prototype and differed from the mass in the frame direction. The assumed masses in the wall direction at each floor level were lumped at

50

node locations along the wall frame elements closest to the respective floor levels one through five. Each of the aforementioned nodes had a value of 175.5 kips lumped nodal weight acting in the X direction.

Lumped nodal masses and member weights do not contribute to the self-weight of the model in terms of the static load. It was therefore necessary to model the self-weight of the wall panels as an external load applied in the "Loads" section of the Ruaumoko data file. The load was calculated as the weight of the wall panels, in addition to a tributary area corresponding to the panel connection detail on the fourth and fifth floors. This weight was distributed as a point load on the end nodes of the wall base as shown in Figure 3-2. The initial prestress load in the post-tensioning bars was also applied in this fashion as will be further clarified in Section 3.3.2. The total value for the resulting static load in the Y direction was 120.88 kips at the exterior and 113.12 kips at the interior wall base nodes.

The sum of the gravity and prestress loads for each column was also distributed as point loads on the gravity column base nodes as shown in Figure 3-2. The value at each node was assumed to be 600.9 kips. This value takes into account the added moment resistance due to the anchor bolts in the gravity frame columns by including the yield tensile force in the gravity column nodal load. This force is calculated based on two of the 60 ksi anchor bolts at yield per gravity frame column. A breakdown of each of the column loads is shown in Table 3-1.

Table 3-1 Column Vertical Loads

Column	C-1	C-2	C-3	C-4	C-5	C-6	C-7	C-8
Gravity Load*	74.0	111.1	74.0	47.5	47.5	66.8	109.4	66.8
PT Force*	50.0	34.5	50.0	114.8	114.8	50.0	34.5	50.0
Bolt Force*				53.1	53.1			
Sum*	124.0	145.6	124.0	215.4	215.4	116.8	143.9	116.8

* kips

The analytical model used Rayleigh damping of 2.5 percent in the first mode and 5 percent in the second mode. This corresponded to the 2.5 percent damping used for the control algorithm.

These forces and masses, combined with the individual element characteristics, helped to fulfill the objective of the analysis -- to create a simple, accurate model of the wall resisting system.

3.3   Characteristics of Elements

This section will detail how the model member properties were determined for each of the elements in the Ruaumoko analytical model. The material properties were taken directly from the specifications as noted previously in Chapter 2. No account for over-strength was assumed, although Ruaumoko is capable of taking over-strength into account.

The Ruaumoko program is a non-linear, time-history analysis tool, which allows the user to input non-linear hysteretic characteristics for different elements. There are thirty-six possible hysteresis rules to choose from. Each element requires input for its elastic characteristics, as well as certain stiffness degradation parameters based on the hysteresis desired. This allows the program to evaluate the non-linear aspects of the wall system, which begin occurring as soon as decompression of the wall starts. The ability of Ruaumoko to specify these hysteretic rules allows the user a wide range of freedom for creating an analytical model. Other time-history programs, such as DRAIN 2D, common in today's structural design office, could also be used to model this type of building. The procedure should be similar, with simple changes made to allow for the specifics of the design problem at hand. Certainly other design programs have frame and spring members such as the elements described here.

3.3.1 Frame Elements

3.3.1.1 Wall Members

The wall members are designed to remain elastic throughout the seismic event; therefore, they were modeled using a simple frame element with linear elastic characteristics. The frame element was a one component (Giberson) Beam member with the member built into the joint. There were no initial loads applied and no strength degradation properties. No damage indices were computed for this element. The moment of inertia was taken based on the uncracked properties of the wall. The cross-sectional area, moment of inertia, shear area, and other properties for the wall element are shown in Table 3-2.

Table 3-2 Wall Member Properties

Property	Ruaumoko Symbol	Value
Elastic (Young's) Modulus	E	$5.2 * 10^3$ ksi
Shear Modulus	G	$2.2 * 10^3$ ksi
Cross-sectional Area	A	864 in^2
Effective Shear Area	AS	736 in^2
Moment of Inertia	I	$839,808 \text{ in}^4$

3.3.1.2 Rigid Links

The rigid links were initially a problem in the model. Their properties were first set at levels much higher than those required to make them perform as "rigid" elements. This changed the geometric stiffness matrix significantly, causing the Ruaumoko program to fail during its iterations and crash. Upon a suggestion form Dr. Benzoni, the parameters of the rigid link elements were set such that they were approximately 100 times as stiff as the stiffest element in the model (the wall members). This corrected the problem. The Ruaumoko model results show that this level of stiffness for the rigid link members is acceptable. The properties used for the rigid link elements are shown in Table 3-3. The effective shear area of the rigid link element is set at 0 in^2 so that shear deformations are not taken into account.

53

Table 3-3 Rigid Link Member Properties

Property	Ruaumoko Symbol	Value
Elastic (Young's) Modulus	E	$5.2 * 10^5$ ksi
Shear Modulus	G	$2.2 * 10^5$ ksi
Cross-sectional Area	A	$86,400$ in^2
Effective Shear Area	AS	0 in^2
Moment of Inertia	I	$8.39 * 10^7$ in^4

The rigid link elements serve two purposes in the Ruaumoko model. First they connect the UFP springs to the wall elements in the correct geometric fashion. Second they connect the compression-only base springs to the base of the wall in the correct geometric fashion.

The wall rigid links extend from the wall element nodes, inward, to the center of the two walls where the joint is located. To simplify the model instead of having links extend to the location of each UFP plate, the links and UFP's were generalized per floor. In other words, where each level in the prototype has four U-shaped flexural plates contributing to the lateral resistance of each floor, the model has one UFP spring. The equivalent properties of these four springs combined are lumped into the single UFP spring per floor. This is further described in the Section 3.3.2. The base rigid links run outward from the base node of the walls and extend to the idealized center of compression for the walls. This is also the location of the compression-only base spring elements.

3.3.1.3 Gravity Column Members

The gravity column in the analytical model represents the influences from all of the columns in the test super assemblage. Since the columns were expected to undergo minimal cracking during the seismic event, the cracked section moment of inertia was used for the member. This value was 0.7 times the sum of the gross section properties for all the columns. The area was also taken as 0.7 times the sum of the column areas. The gravity column frame element was a one component (Giberson) Beam member with the member built into the joint. There were no initial

54

loads applied and no strength degradation properties. No damage indices were computed for this element. The moment of inertia was taken based on the cracked properties of the columns as described previously. The cross-sectional area, moment of inertia, shear area, and other properties for the wall element are shown in Table 3-4.

Table 3-4 Gravity Column Member Properties

Property	Ruaumoko Symbol	Value
Elastic (Young's) Modulus	E	$5.4 * 10^3$ ksi
Shear Modulus	G	$2.4 * 10^3$ ksi
Cross-sectional Area	A	1814 in^2
Effective Shear Area	AS	1814 in^2
Moment of Inertia	I	49,000 in^4

3.3.2 Spring Elements

3.3.2.1 Base Springs

The base springs were a bit less complicated of an endeavor in that the stiffness characteristics of the concrete were known. The challenge was to come up with a hysteretic rule that would allow for the gap opening characteristics of the wall system. The solution was to use Bi-linear elastic hysteresis. This rule is similar to the Bi-linear hysteresis with the exception that element force displacement characteristics load and unload elastically up and down the same path. This means that no hysteretic energy is dissipated in the element. In this manner the base spring element can provide the resistance of the concrete when the wall is in contact with the foundation and, by setting the yield surface at a minimal value, have no resistance when the gap opening occurs.

These elements extend vertically from the end of the base rigid links to three inches below that point. This value was chosen because it is the force value that is important and not necessarily the foundation displacement characteristics for this part of the analytical model. The

55

base spring element has no interactions between the X, Y, and theta Z components. No strength

degradation or damage indices were computed. The base spring is a zero weight element. Spring

stiffness properties are shown in Table 3-5. The base spring had yield values in the local X-

direction of +0.1 kips and –800 kips, giving it practically zero tensile resistance (0.1 kips is given

for numerical calculation reasons), making it essentially a compression-only spring. The stiffness

was determined by assuming a concrete deflection of 0.02 inches (0.05 cm) for a force of 200

kips (890 kN) with a yield compressive force of 800 kips (3560 kN) which was higher than the

maximum feasible, to ensure elastic response in compression. The force displacement

characteristics of the base spring were described previously.

The gravity column base springs were identical to the wall base springs, with a higher

compressive yield force, 6400 kips (28480 kN), to account for the higher external point load

representing the sum of gravity and post-tension forces for the columns.

Table 3-5 Compression-Only Base Spring Properties

Property	Ruaumoko Symbol	Value
Spring stiffness in the local X-direction	KX	10000.0 kip/in
Spring stiffness in the local Y-direction	KY	0.1 kip/in
Rotational stiffness of the member section	GJ	0.1 kip in/rad
Bi-Linear factor for spring forces	RF	0.0
Bi-Linear factor for rotation	RT	0.0

3.3.2.2   Post-Tensioning Springs

The post-tensioning bars in the test building were modeled as springs in the analytical

model. The spring provided stiffness in the vertical direction, with near zero stiffness in the

horizontal and rotational directions. The stiffness values in the horizontal and rotational

directions, as noted in Table 3-6, were required for computational reasons. The bars provide the

clamping force to the wall foundation giving shear and overturning moment resistance to the wall

system. Properties for these elements were based on the post-tensioning bar material and

geometric properties as mentioned in Chapter 2. The PT springs went from the base node of the wall frame elements and ran vertically to a point three inches from the base of the wall. The Dywidag bars were post-tensioned to a force of 41 kips for each bar. This resulted in a force of 164 kips per wall. The force of the PT was input as a nodal load placed at the extremities of the base rigid links. The post-tensioning effect in the element was modeled by giving the PT spring a pre-load force of this same amount in the local X-direction. These pre-load forces are internal and affect only the initial deformation of the member. They have no contribution to forces acting on the structure. This represented the lower bound of compressive force in the PT Bars.

Table 3-6 Wall PT Spring Properties

Property	Ruaumoko Symbol	Value
Spring stiffness in the local X-direction	KX	197 kip/in
Spring stiffness in the local Y-direction	KY	0.1 kip/in
Rotational stiffness of the member section	GJ	0.1 kip in/rad
Bi-Linear factor for spring forces	RF	0.02
Bi-Linear factor for rotation	RT	0

The Ruaumoko program allows for a number of element member properties to be defined for spring elements. There were no interactions between the X, Y, and theta Z components. A Bi-linear inelastic hysteresis rule was chosen to model the basic behavior of the PT steel. No strength degradation or damage indices were computed. The PT spring's objective is to model the behavior of the post-tensioned bars; therefore it is a zero weight element. Spring stiffness properties are shown in Table 3-6. The wall PT spring had yield values of +/- 375.0 kips.

The seismic and gravity columns used 1 ¼"post-tensioned Dywidag bars, two per column. This was represented by a single spring in the analytical model. The spring was identical to the wall PT spring, except for the stiffness in the local x-direction. The value for KX was 154 kips/in. A higher initial post tension force (498.6 kips) and yield force (+/- 3004 kips) was used to be representative of the multiple columns modeled as one.

3.3.2.3 U-Plate Springs

The most complex element of this analytical model is modeling of the springs for the UFP behavior. These U-plate springs were placed at the end of wall rigid links, extending inward from the wall elements (see Figure 3-2). These rigid links are offset 0.01 inches to allow for the springs. The springs are located at approximately each floor level, so they are representative of the behavior of the UFP's and are not exactly at the same location as the UFPs in the test building. The nodes at the ends of the UFP's were constrained to each other in the X-direction so that only the vertical effect of the UFP plate was taken into account.

In order to capture a greater understanding of how the UFP performs during testing, a component test was carried out. Extra plates made of the same materials and geometry were used in the test setup with the exception that the plate reduced in width from 7 inches to 3 inches to fit with the constraints of the testing machine. A flat plate was placed between tube steel welded into a large U shape as shown in Figure 3-3. This unit was then tested using the MTS testing machine at UCSD. The resulting force-displacement values are shown by the solid line in Figure 3-4; this gave an idea of the force displacement characteristics of the actual plates in the *PRESSS* building. Upon increased cyclic displacements of the U-plates significant work hardening effects

Figure 3-3 UFP Test Setup on MTS Machine
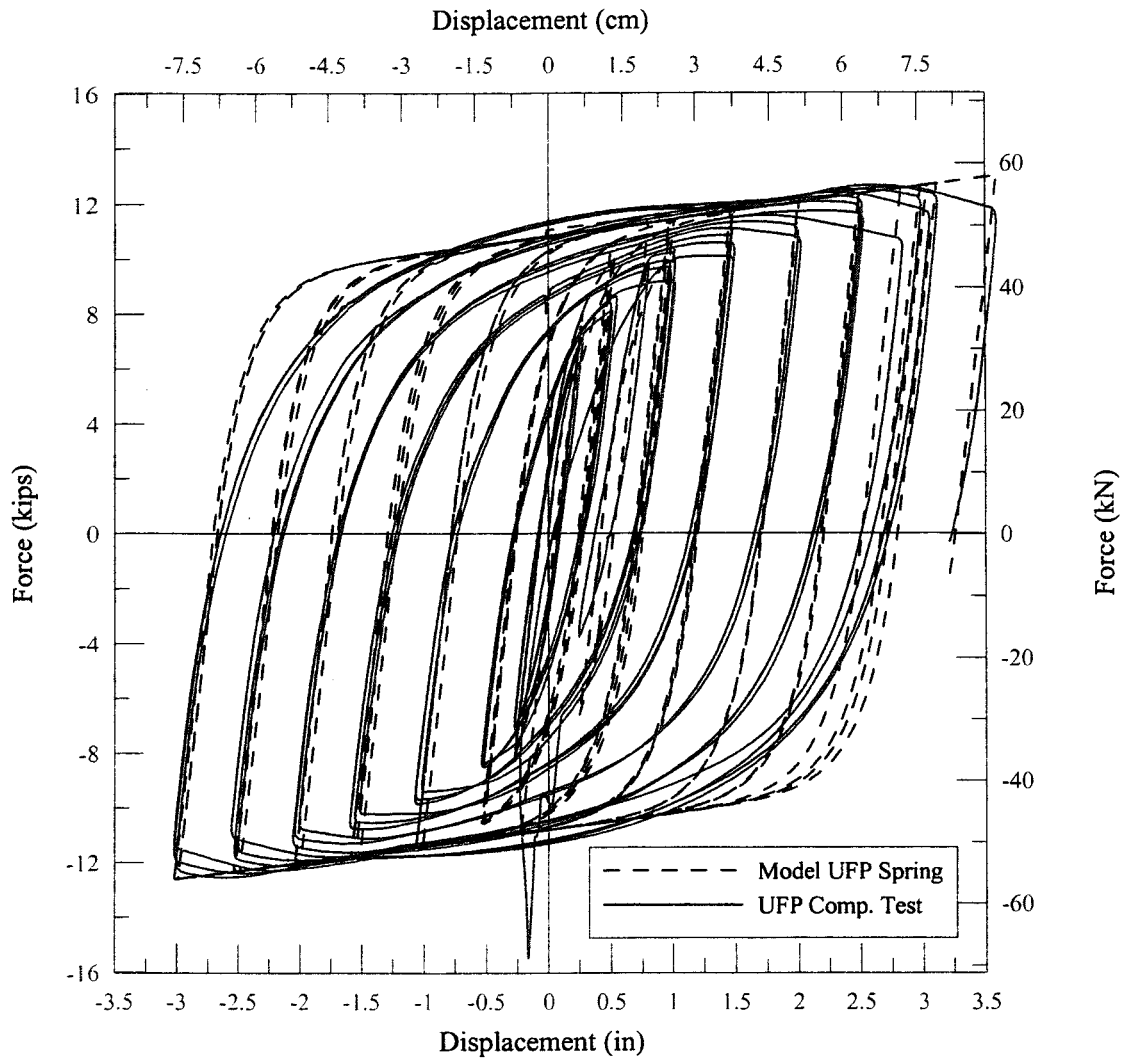
Figure 3-4 UFP Analytical and Component Test Comparison

are noticeable. Such effects are difficult to simulate in modeling the test structure when it undergoes a more random cyclic behavior such as the earthquake record used in testing of the super-assemblage. These results were then used to determine which hysteresis rule to be used in the model. The U-plate springs are modeled so that they capture close to the same force displacement characteristics as the UFPs.

The hysteresis model available in Ruaumoko that best compares to the component test is Al-Bermani Bounding surface hysteresis. This rule allows for Bauschinger effects in steel members by using bounding surfaces to create the hysteresis curve. The hysteretic characteristics of the Al-Bermani model are shown in Figure 3-5. The curve starts out with an initial stiffness, k_0, up until the force intersects the boundary line F_2 that corresponds to a percentage of the yield force, αF_y^+. The stiffness value then changes to k_T, where

$$k_T = k_0\left(1 - \left(\frac{F - F_2}{F_1 - F_2}\right)(1 - p)\right)$$

(3.1)

F is the force along this line and F_1 is the second boundary line that corresponds to the stiffness

$$k_p = pk_0$$

(3.2)

Upon a reversal in the incremental displacement the curve picks up the initial stiffness k_0, until a similar boundary is passed on the negative side corresponding to βF_y^-. Then k_T and k_p are picked up in a similar manner to the positive side of the hysteretic force.

The displacements from the UFP component test were then used to create a hysteretic plot following the Al-Bermani characteristics of the UFP spring to be used in the model. The following values were determined from this effort:

$$k_0 = 40 \text{ kip/in}$$

$$k_p = 0.6 \text{ kip/in}$$

$$F_y = 11 \text{ kips}$$
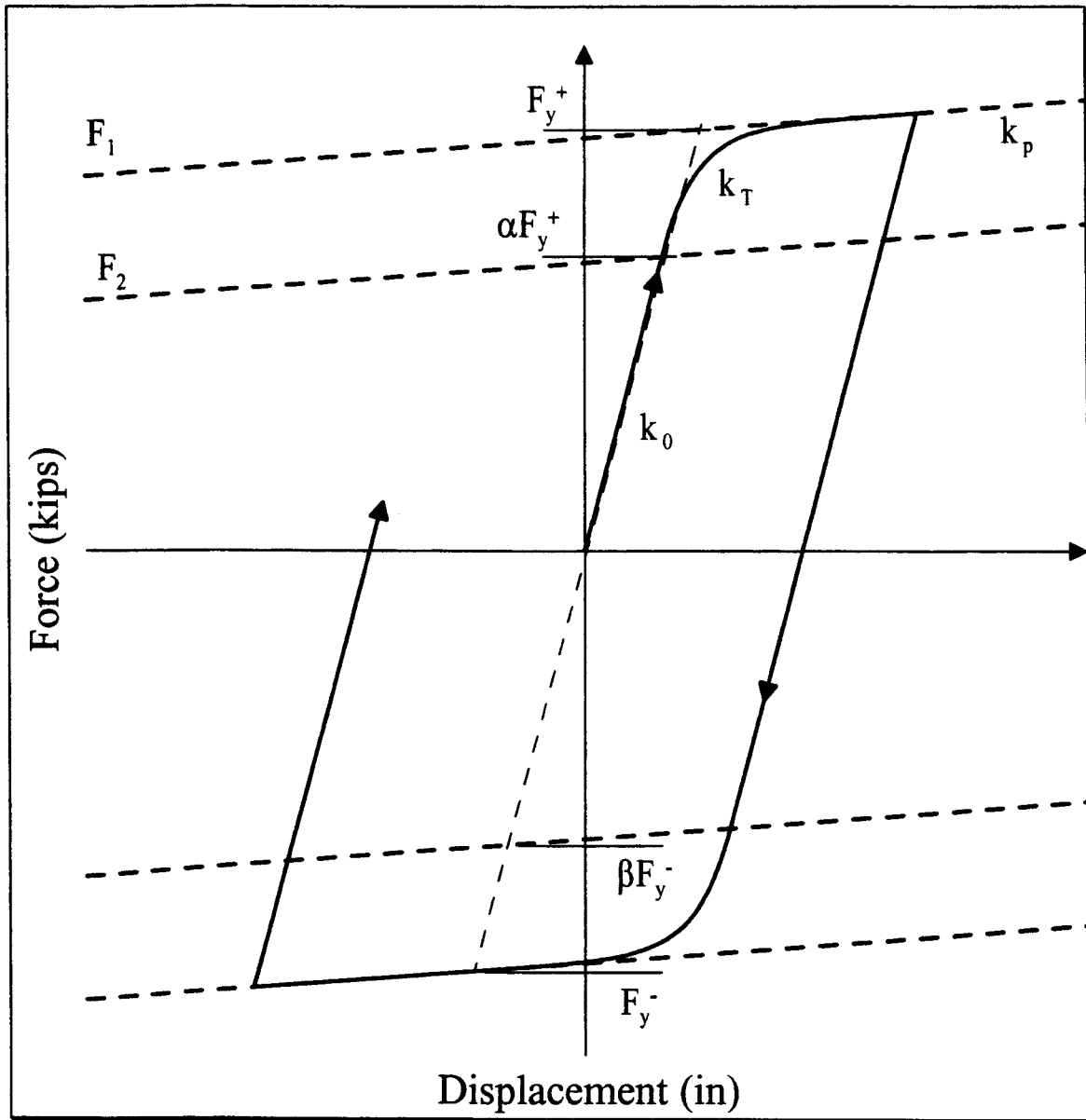
Figure 3-5 Al-Bermani Hysteretic Behavior

Figure 3-4 shows a hysteresis comparison of the model UFP spring with the aforementioned stiffness and yield values to the results of the UFP component test. It can be seen that the behavior correlates reasonably well and is suitable for the purposes of the analytical model.

The final step in determining the UFP spring behavior in the analytical model relative to the test building was to incorporate the scaling effects of the component test. The initial stiffness and yield values for the UFP spring hysteresis were scaled up by the ratio

$$\frac{\sum\limits_{1}^{m} A_b}{\sum\limits_{1}^{n} A_c} = \frac{14}{3} \qquad (3.3)$$

where A_b is the cross sectional area of the UFP in the test building, m is the number of UFPs per floor level, A_c is the cross sectional area of the UFP in the component test, and n is the number of UFPs in the test setup. The resulting element properties were used in the model UFP springs as shown in Table 3-6. In the element there were no interactions between the X, Y, and theta Z components. No strength degradation or damage indices were computed. The U-plate spring is a zero weight element. Spring stiffness properties are shown in Table 3-6. The U-plate spring had yield values in the local X-direction of +/- 51.3 kips which corresponds to the yield shear force of the UFPs per floor.

Table 3-7 UFP Spring Properties

Property	Ruaumoko Symbol	Value
Spring stiffness in the local X-direction	KX	186.6 kip/in
Spring stiffness in the local Y-direction	KY	0.1 kip/in
Rotational stiffness of the member section	GJ	0.1 kip in/rad
Bi-Linear factor for spring forces	RF	0.015
Bi-Linear factor for rotation	RT	0
Positive ALFA longitudinal direction	ALFAa	0.001
Negative BETA longitudinal direction	BETAa	0.001

3.4 Pushover Results

A pushover analysis was run using the Ruaumoko program to further evaluate the force-displacement relationships of the model. In the pushover analysis a load pattern is input to the program based on the displacement profile of the test building determined from the DBD procedure. This profile, shown in Table 3-8, was normalized to the top displacement and then input as the load distribution for the pushover. The pushover is a valuable resource for examining the model because it slowly increments the lateral load profile allowing various mechanisms in the model to be noted. Values of wall lift-off, UFP yield, and PT yield are labeled in Figure 3-6, where a base moment-displacement relationship for the pushover is shown.

It is of interest to note the influence of the additional column representing the seismic frame and gravity frame columns. A pushover analysis was also run using the same model without the gravity column. The results show a significant increase in resistance comes from the gravity and seismic columns. The analytical model shows an increase of approximately 23% in base overturning moment resistance due to the gravity column.
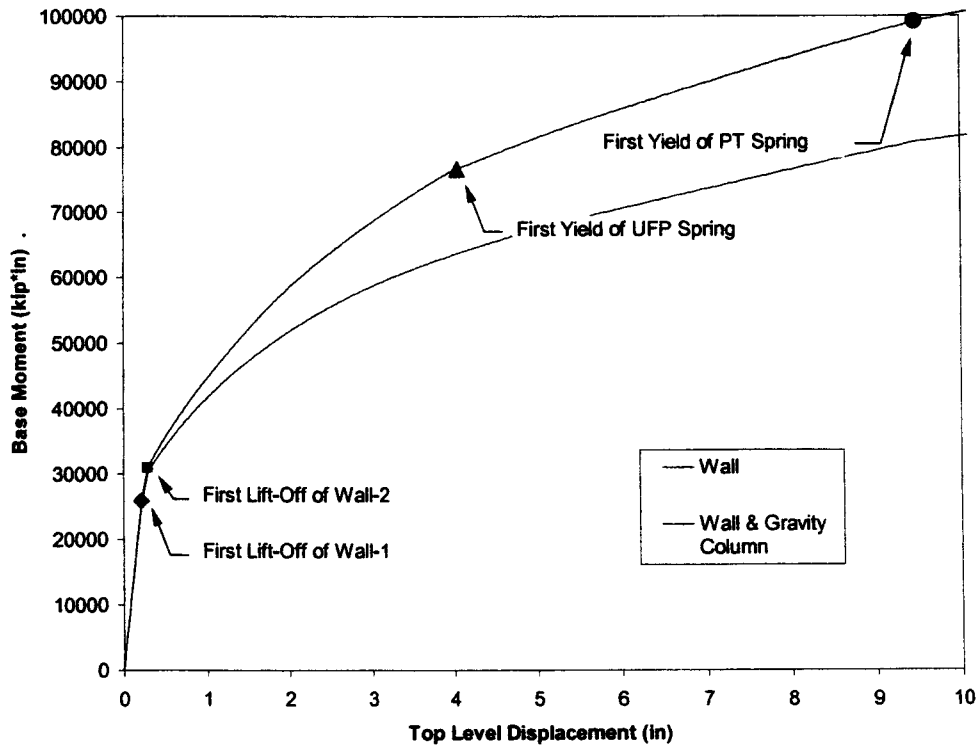
Figure 3-6 Pushover Comparison

Table 3-8 DBD Displacement Profile

Floor Level	DBD Displacement	Normalized Displacement
5	8.015732	1
4	6.224397	0.776523
3	4.464558	0.556974
2	2.771648	0.345776
1	1.1811	0.147348

3.5   Energy Considerations

It is of value to view the energy time history for the Ruaumoko model to validate the time

step used in the analysis. Furthermore, an evaluation of the energy absorbed by the UFP springs

65

in the model is also of interest. The energy absorbed by the UFP springs can be calculated by integrating the force-displacement hysteresis loop plots of the UFP spring elements. Since relative displacements along the vertical joint between panels are the same, and the UFP spring properties are the same up the height of the model, the hysteresis plot for the first level was assumed to be representative of subsequent levels. Multiplying the results of the first level integrated hysteresis loop by the number of UFP springs in the model gave an estimation of the total energy dissipated by the U plates.

Figure 3-7 (a) and (b) show the energy time histories at the EQ-3 and 1.5 EQ-3 input levels. The total of kinetic, damping and strain energy (labeled Sum in Figure 3-7) of the model matches the input energy quite well for both models. This validates that the time step for the analysis is sufficient. The time history of the energy dissipated by the UFP springs is also plotted. It is evident from this figure that both runs show that a good amount of energy is dissipated by the UFPs. It should be noted that the plots for the UFP energy dissipation overestimate actual energy absorbed. This is because the Al-Bermani hysteresis rule has a "fatter" loop compared to the UFP component test (see Figure 3-4). The level of energy dissipated correlates with the extra damping provided by the flexural yielding behavior of the U-plates.

3.6   Equivalent Viscous Damping Calculations

The equivalent viscous damping for the wall system was assumed to be 20 percent in the initial DBD procedures. To verify this equivalent viscous damping was calculated using results form the Inverse Triangular Load tests conducted on the *PRESSS* building. The biased base shear vs. top level displacement hysteresis loops for two different IT-3 tests (52 and 54) were used in order to get the most accurate value for the wall direction viscous damping. The Inverse Triangular (IT) load tests give the results of one complete load-displacement hysteresis loop.

66

(a) Energy Time History EQ-3
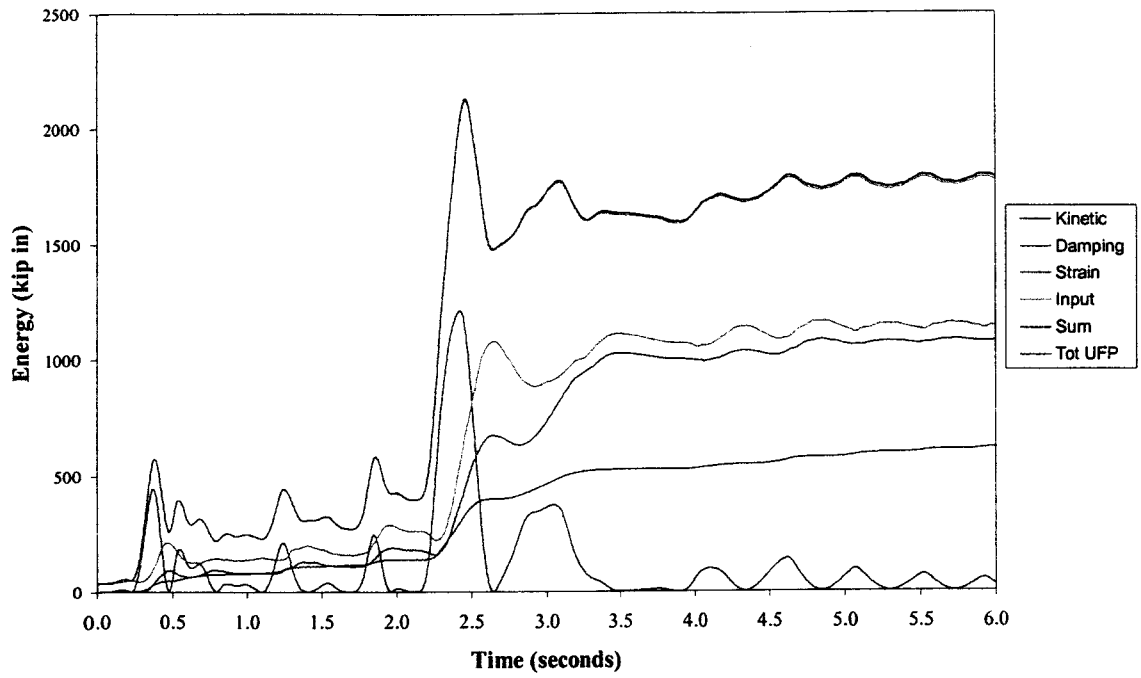
(b) Energy Time History 1.5 EQ-3
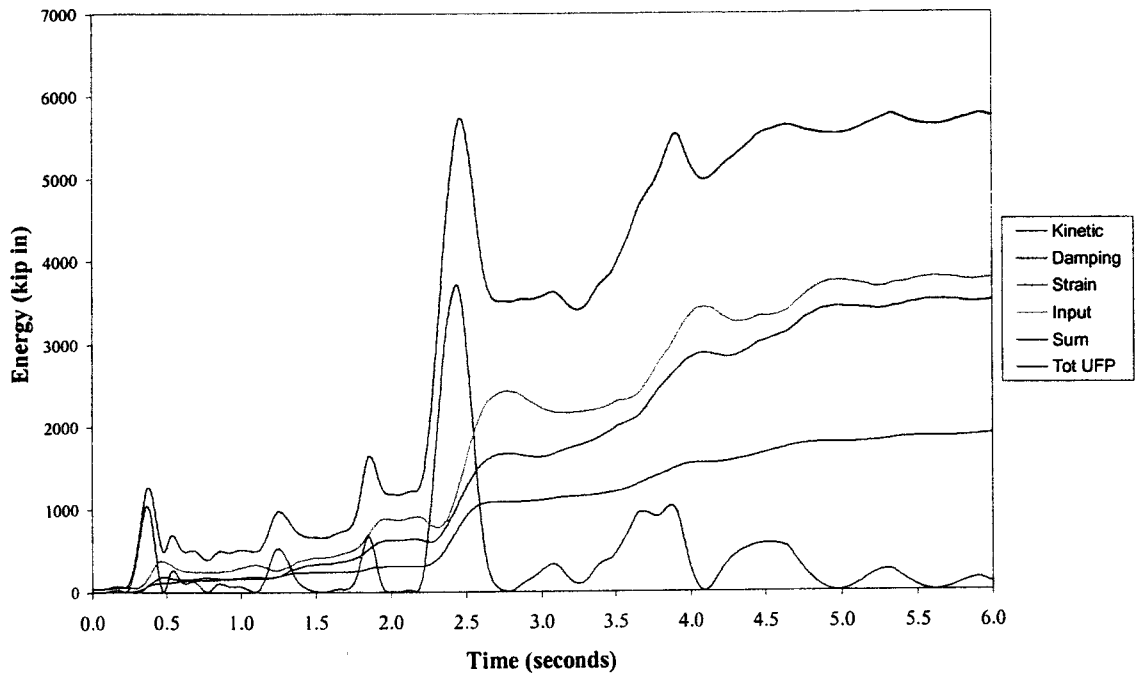
Figure 3-7 Energy Time Histories

67

From the IT test results one can find the hysteretic damping, or energy loss per cycle, represented by the area A_h in Figure 3-8. Then the equivalent elastic strain energy, A_e, is found. This is the energy that would be stored in an equivalent linear elastic system under static conditions with effective stiffness

$$k_{\textit{eff}} = \frac{V_m}{\Delta_m} = \frac{\frac{1}{2}\left(|V_{max}| + |V_{min}|\right)}{\frac{1}{2}\left(|\Delta_{max}| + |\Delta_{min}|\right)} \tag{3.4}$$

The equivalent viscous damping ratio can then be calculated

$$\xi_{eq} = \frac{A_h}{4\pi A_e} \tag{3.5}$$

For IT-3 (test 54), in order to "smooth out" the curve, values were added to make a full loop. This is shown by the Interp. Data curve in Figure 3-8. Without this data a gap that would not be representative of a true full cycle hysteretic loop would occur. The hysteretic loop for IT-3 (test 52) was more complete because the building was brought to a full cycle hysteretic loop and could be evaluated without using interpolated data.

The values of equivalent viscous damping were 15.78% and 15.57% for tests IT-3 (test 52) and IT-3 (test 54), respectively. When added to the assumed elastic damping of 5 percent, this indicates very close agreement with the 20 percent assumed for design.

3.7 Predictions

This simple model enabled realistic estimates of the force displacement response to be obtained prior to testing. Prior to each earthquake record being imposed on the test building, the in-elastic time-history analysis was run on the analytical model by inputting the earthquake record, which was to be subsequently used. The gravity column was not part of the original analytical model used during the testing program. The results from the model without the column influence were accurate enough for testing purposes, capturing approximately 80% of the resistance of the model including the gravity column as shown by comparison of the pushover

curves of the two models (Figure 3-6). In order to obtain a more accurate representation of the superstructure, addition of the gravity column to the analytical model was made after the testing program was completed. Prediction results described in subsequent chapters were obtained from the analytical model including the gravity column.

The results from these analyses will be presented in Chapter 4, where it will be most valuable to view a comparison of the model predictions to the results of the actual test building.
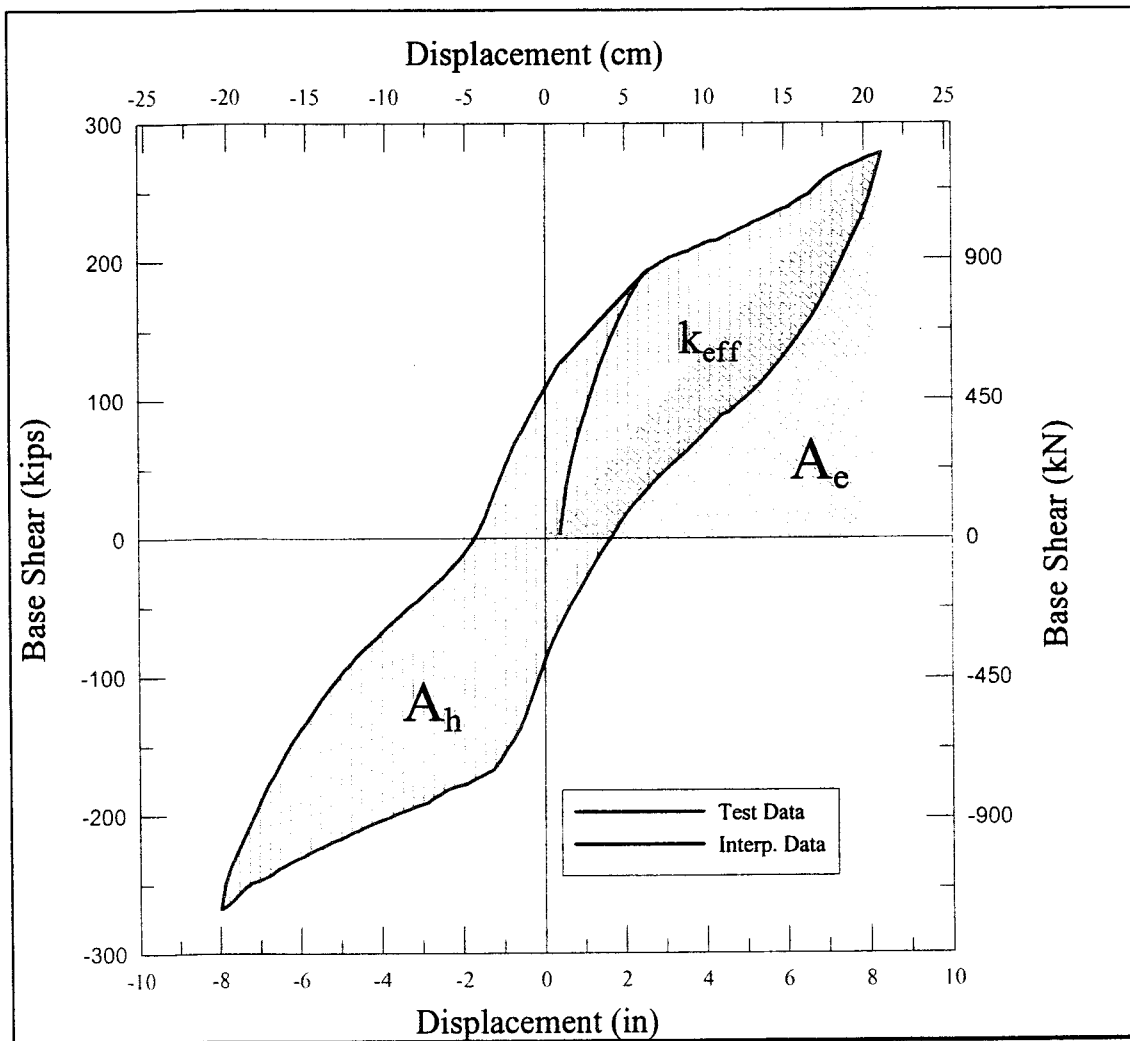
Figure 3-8 Procedure for Calculating Equivalent Viscous Damping Coefficient

4 TEST OBSERVATIONS

Testing of the *PRESSS* Five-Story Building was initially carried out at a fraction of the EQ-1 level. Following this, the seismic intensity was gradually increased up to the maximum level, as described previously. The performance of the wall resisting system was excellent. Virtually no damage occurred to the panels up to the EQ-3 level of testing. At this level some minimal cracking of the wall began to occur due to high levels of compression strain at the wall toe, which lead to spalling of the concrete during subsequent IT tests. Significant yielding of the UFP connectors occurred as expected, with no damage to the U-plates. The post-tensioned thread bars were able to increase lateral load resistance while preserving their self-centering characteristics up to and including the design level earthquake. Further details of the overall building performance will be presented in this section, as well as a comparison between prediction and test results in an effort to validate the analytical model. Descriptions of the performance of specific components of the resisting system, including the U-plates and post-tensioning bars, will also be addressed. Damage that occurred to other components of the building associated with the wall direction testing will be evaluated, with comparisons to the prediction being made where appropriate. It will be found that the overall performance of the building is extremely satisfactory, with virtually no damage occurring, even at levels beyond 2% drift.

4.1 Overall Analytical/Experimental Comparisons

Analyses were run using each level of earthquake on the *PRESSS* building, using the same record and intensity input into the control algorithm. The results from these analyses are shown in this section as they compare to the data recorded in the test. For the test building two sets of test data were taken. One data set used a data acquisition system to record strain gage and potentiometer readings most valuable in evaluating specific building results. The other data set was a record of the external actuator forces and the corresponding building displacements used to

control them. The force and displacement data were instantaneously recorded at each time step (0.012 seconds) by a computer controlled data acquisition system. These results are referred to as the control data and give an excellent measure of the overall performance of the building.

The results of the control record were then examined to determine a suitable bias for the data. The first scan of the test corresponding to a level 0.25 EQ-1 was set as the bias for tests up to EQ-2. During the initial lower levels of testing, some problems were encountered with the building displacement potentiometers, as seen by evaluating the maximum displacement envelopes for the different tests biased to 0.25 EQ-1. It was therefore determined that EQ-2 (Test 040) and subsequent tests would be biased to the first scan of EQ-2. The resulting maximum displacement envelopes for the wall direction testing are shown in Figure 4-1. The profiles are very close to linear at all stages, agreeing with assumed design profiles. At EQ3, the design intensity earthquake, the peak roof displacement was 8.28 in, or 92% of the design target displacement corresponding to 2% drift.

The best indicator of wall direction building performance from a force standpoint is the base moment time history. This is because the higher mode effects present in the base shear and floor force time histories do not heavily influence the base moment. Further details on the higher mode effects on the building will be described subsequently. Base moment time history comparisons between the analytical model and the test building results are shown in Figure 4-2 (a), (b), and, (c), representing earthquake levels EQ-2, EQ-3, and 1.5 EQ-3, respectively. The base moment for the test building was determined by multiplying the actuator forces by the story height plus the height to the centerline of the actuators (14") at that level. It should be noted that the bottom of the wall and columns represented the base line or zero elevation level for the building; thus the height of the grouting pad and foundation below zero elevation were not considered in the base moment calculations. Since floor forces were not directly available from

71
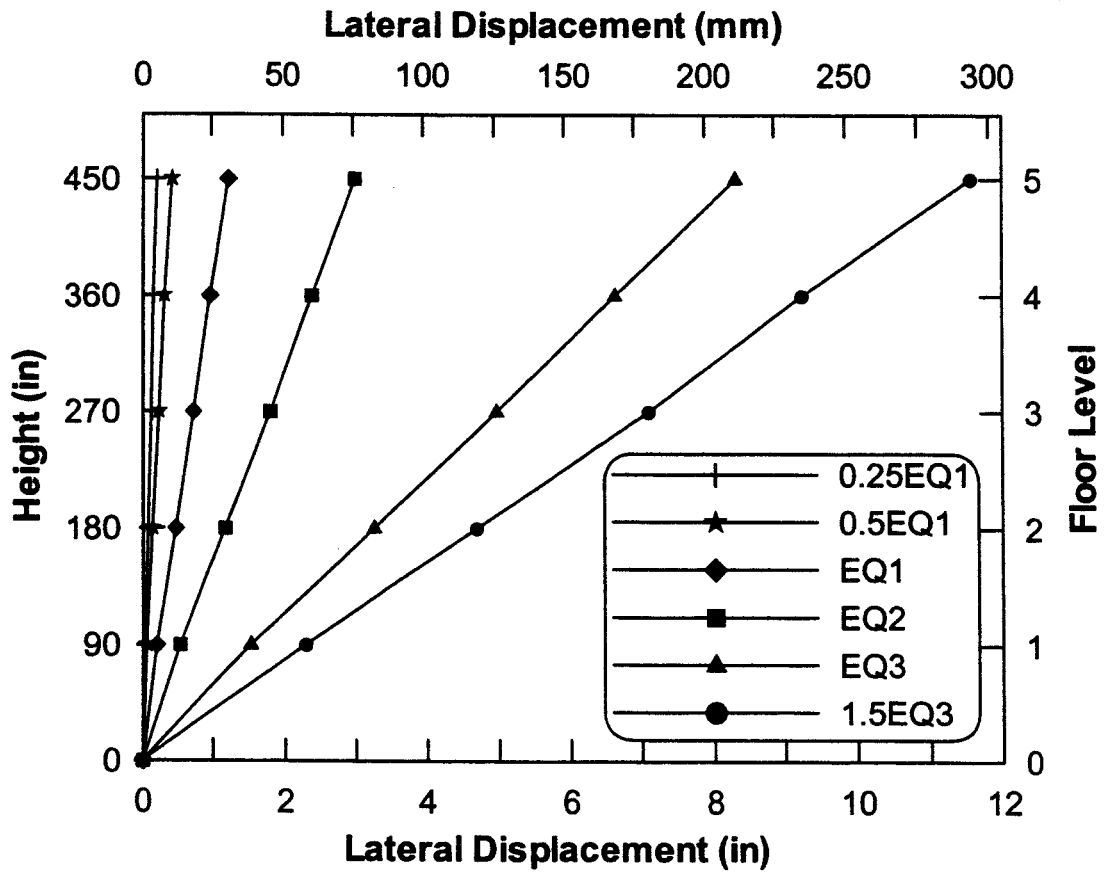
Figure 4-1 Test Maximum Displacement Envelopes
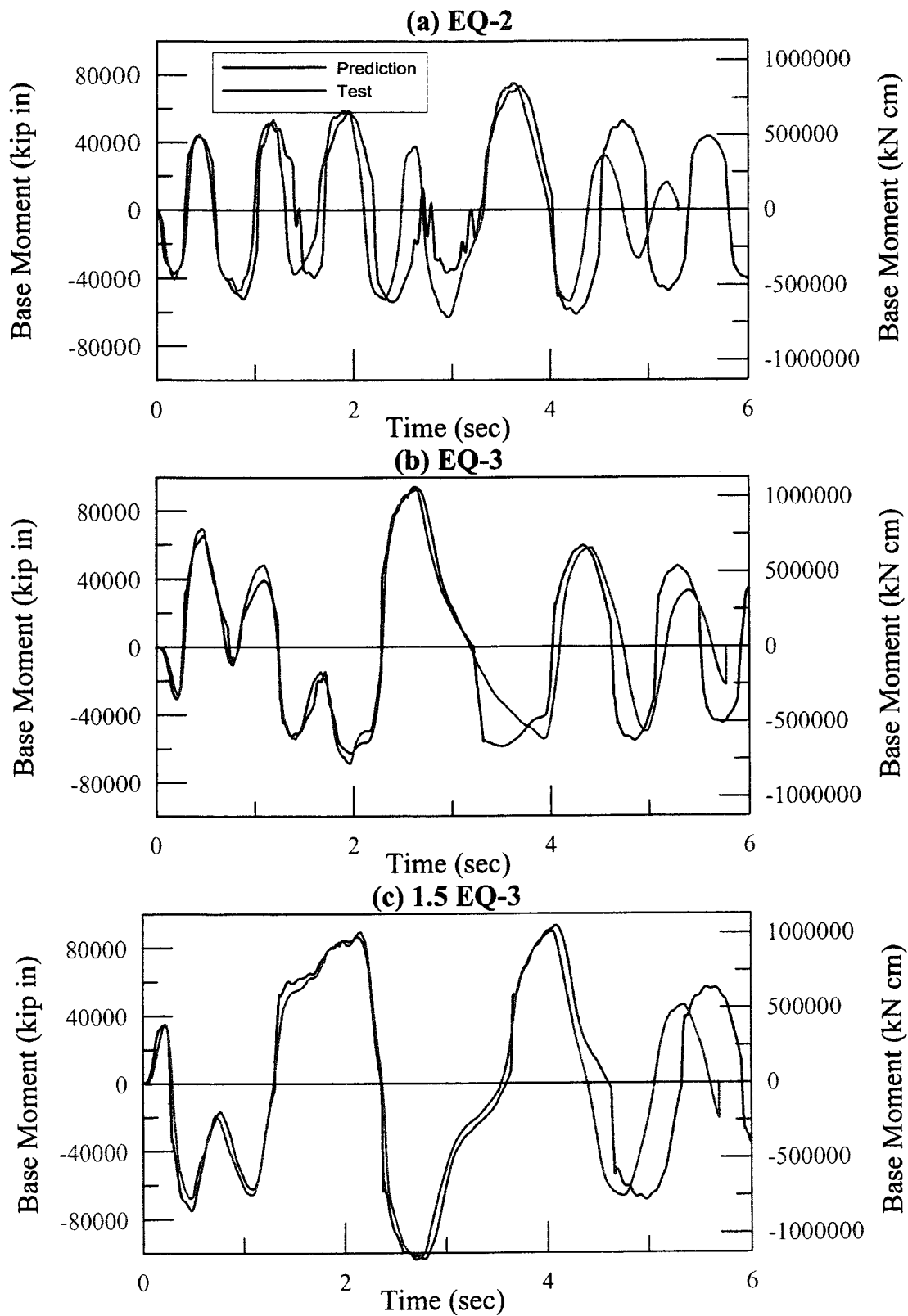
Figure 4-2 Base Moment Time History Comparisons

the Ruaumoko program, the values had to be calculated from the shear in the column element and the frame elements representing the wall members. The shears in the two walls and the column member were summed per floor at each floor level for each time step using the Dynaplot post processor program. The floor forces were then determined as

$$F_i = S_i - S_{i+1}$$

where F is the floor force, i is the floor level, and S is the sum of the wall and column shears. The base moment for the analytical model was taken as these floor forces multiplied by the actuator height to acquire an equivalent representation of the base moment in the analysis to that in the test.

As shown in Figure 4-2, the analytical model and test results match up extremely well. The spikes that occur in the prediction results are a result of the wall base coming in contact with compression springs. This causes an impact load resistance that is distributed throughout the model. The model was initially run at a time step of 0.006 seconds and decreasing this to 0.003 seconds reduced the spike to the level shown in Figure 4-2. It was found that further reduction in the analysis time step did not cause further reduction of these spikes; therefore the time step of 0.003 was determined to be adequate. Although an impact load would occur as the test structure panels come in contact with the foundation in a real earthquake situation, it was not evident in the test results due to the slow nature of the pseudodynamic test. These forces are further reduced in the test structure by the distributed nature of the contact provided by the grout layer between the wall base and foundation, as distinct from the discrete two-point contact of the analytical model.

Another indicator of overall building performance is the top floor displacement time history. Top-level time history comparisons between the analytical model and the test building results are shown in Figure 4-3 (a), (b), and, (c), representing earthquake levels EQ-2, EQ-3, and 1.5 EQ-3, respectively. The displacements shown are the average of displacements recorded at either side of the wall panels on each floor level. The displacement data for each floor was taken

(a) EQ-2

(b)EQ-3

(c) 1.5 EQ-3
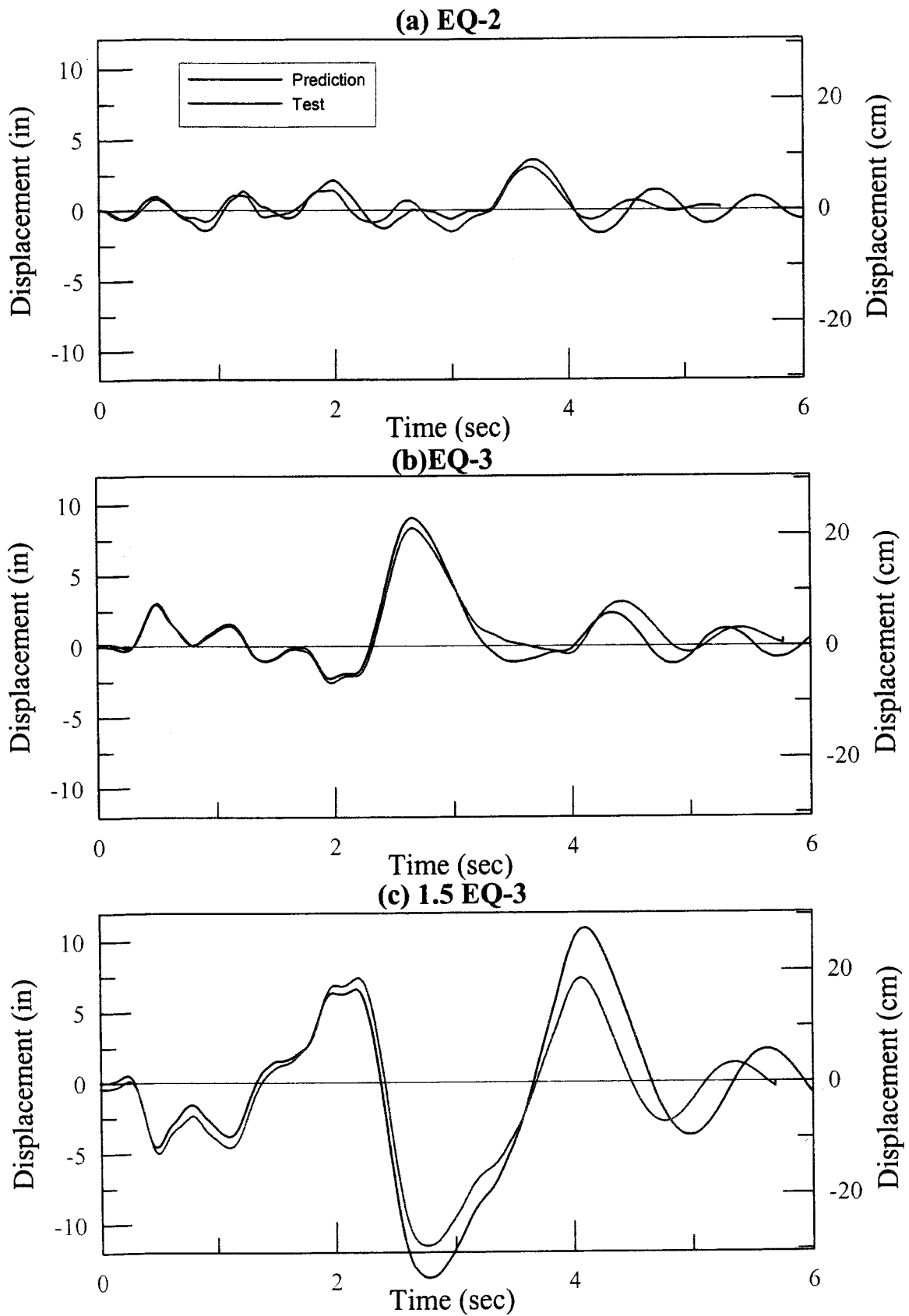
Figure 4-3 Top Level Displacement Time History Comparisons

a level approximately 2 inches higher than the actual floor level. This had virtually no impact on the actual floor displacements therefore no adjustments to these values were made, aside from the initial biasing mentioned previously.

The prediction displacement time history for each of the earthquake records shown in Figure 4-3 matches the test results reasonably well. Prediction peak displacement values are up to 10% larger than the test results. Figure 4-3 (c) shows a difference in the initial displacement at the beginning of 1.5 EQ-3. This is due to the small residual displacement that occurred after EQ-3 and the subsequent IT tests.

The base shear time history test results also compared well to the results from the analytical model. The base shear on the test structure was taken as the sum of the actuator forces applied to the building at each time step increment. The base shear on the analytical model was found by summing the floor forces that were determined form the member shears. The effects of the higher mode forces are evident in the base shear time histories shown in Figure 4-4. The analytical model is extremely sensitive to the higher frequency shaking of the input record for EQ-2 as shown in Figure 4-4 (a). The modified EQ-3 input records provided some filtering of these high frequencies as shown in both the analytical and test results in Figure 4-4 (b). The higher mode effects in the prediction base shear then became most evident in the free vibration cycles for all the earthquake records shown.

The higher mode forces in the prediction base shear was partially a result of the impact load that occurs when the base springs come in contact with the wall in the analytical model, after uplifting. This effect was most evident when looking at the floor force levels in the analytical model. Figure 4-5 shows the predicted floor forces, base shear, base moment, and top displacement in comparison to the respective experimental results for 1.5 EQ-3. The figure also shows predicted gravity column story shears at each floor level. The higher mode forces are evident at all floor levels, with the fourth level most minimally effected. This implies

76

(a) EQ-2

(b) EQ-3

(c) 1.5 EQ-3
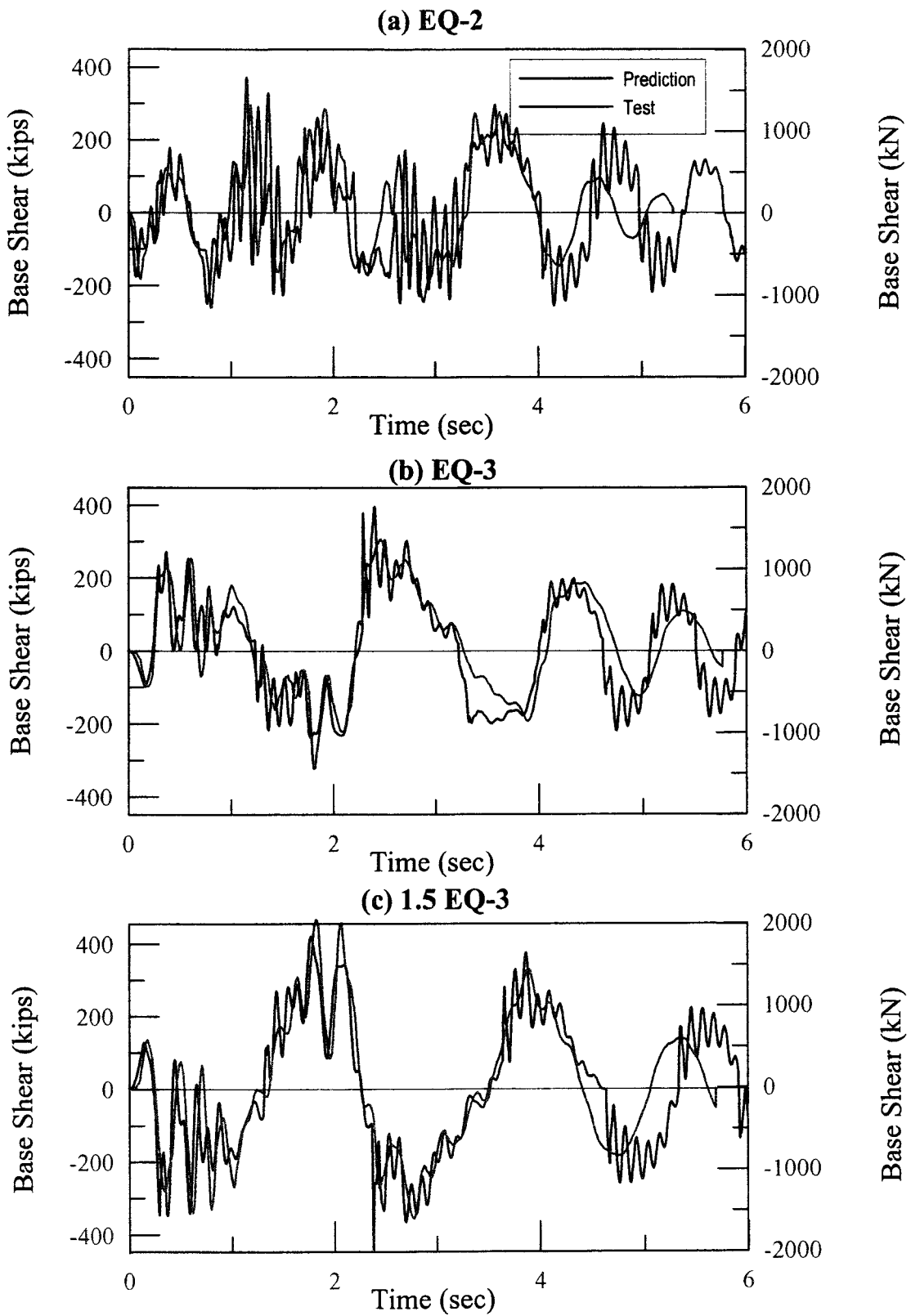
Figure 4-4 Base Shear Time History Comparisons
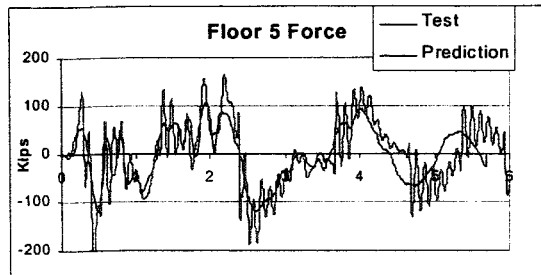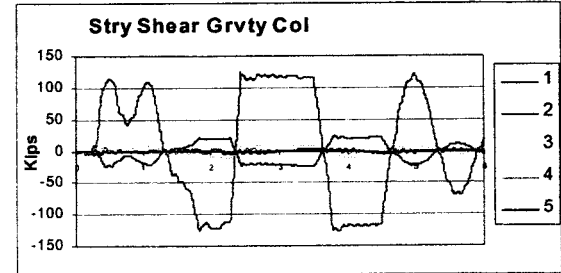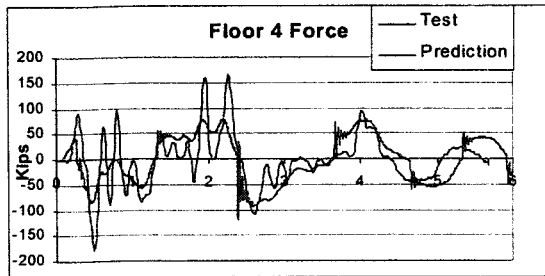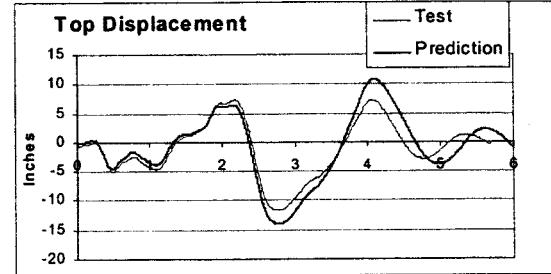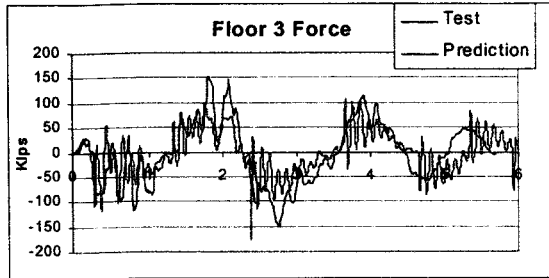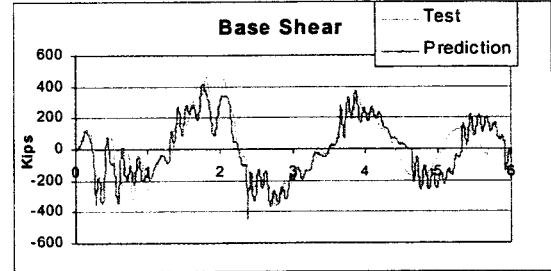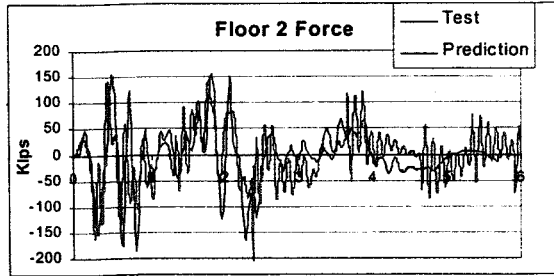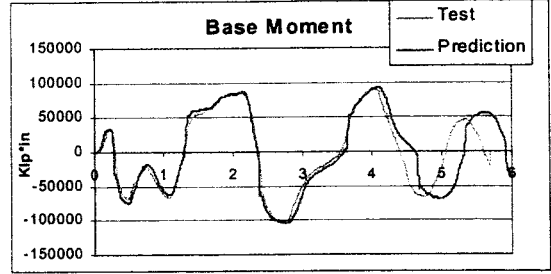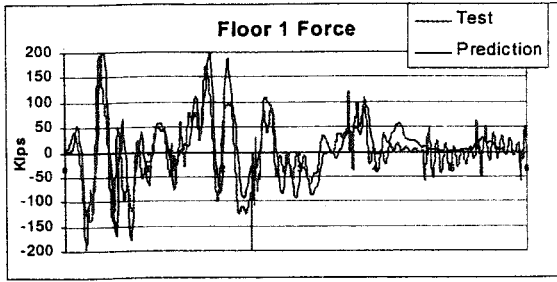
Figure 4-5 Analytical Results k_{bs}=10,000 kip/in

78

that the impact force was having some type of second mode effect on the prediction results, because a second mode shape would have a near zero value at that level.

In order to better evaluate the effect of these impact forces, the base spring stiffness was reduced first by a factor of two and then by a factor of five. Analytical models with these new spring stiffness values were run at the 1.5 EQ-3 level. Figures 4-6 and 4-7 show analytical results for base spring stiffness values of 5,000 kip/in and 2,000 kip/in, respectively. These results are displayed in the same format as Figure 4-5. Figure 4-6 shows that the initial reduction had a significant impact on limiting the effect of the impact force on the structure, while causing virtually no difference in base shear, base moment, and top displacement results. Further reduction of the base spring stiffness greatly reduces the effect of the impact force, as seen in the prediction floor force results in Figure 4-7. The peak base shear and base moment results still match experimental data very well, with the softening of the base springs having the greatest effect on top level displacement results. These results show that the impact force can be limited by changing this spring stiffness. Other means of limiting this effect are also possible. By distributing the base springs all along the base of the wall, instead of at the idealized center of compression as done in the analytical model, the effect could likely be eliminated completely or greatly reduced.

Although the reduction of base spring stiffness had almost no impact on the base shear and base moment results for the analytical model, this change did have a significant effect on the first mode period of the structure. The first mode period of the analytical model was 0.540 seconds. Reducing the base spring stiffness by a factor of two changed the models period to 0.625 seconds, while the reduction factor of five resulted in a model period of 0.812 seconds. Figure 4-5 through Figure 4-7 show that change in first mode has minimal impact on the overall
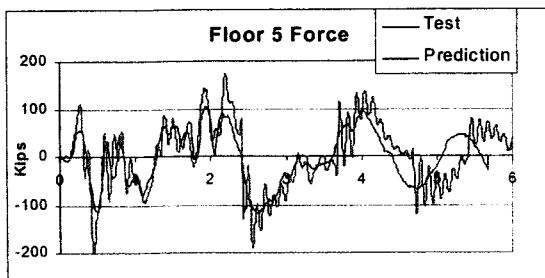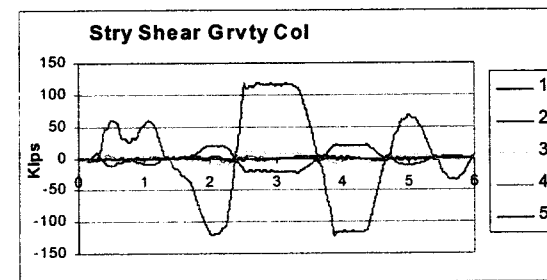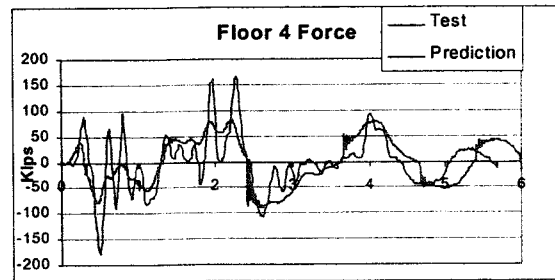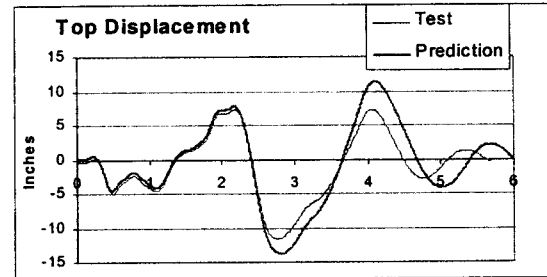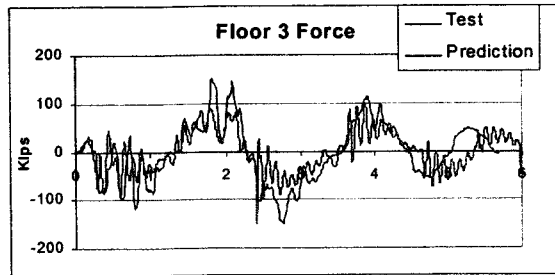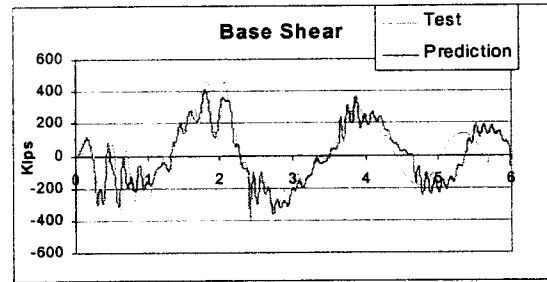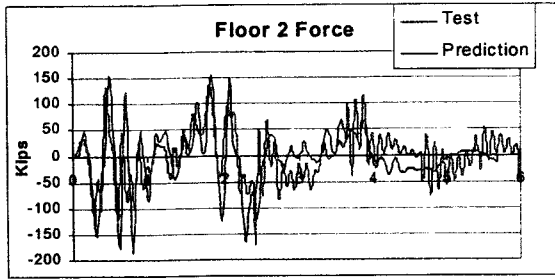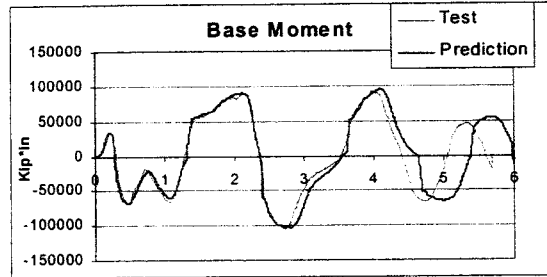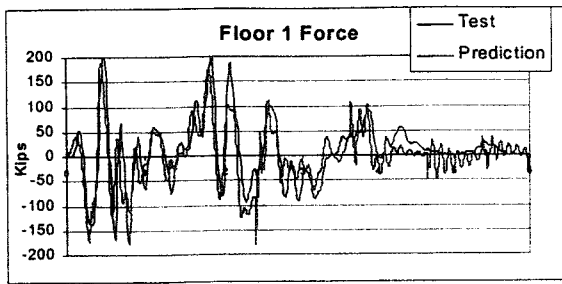
Figure 4-6 Analytical Results k_{bs}=5,000 kip/in
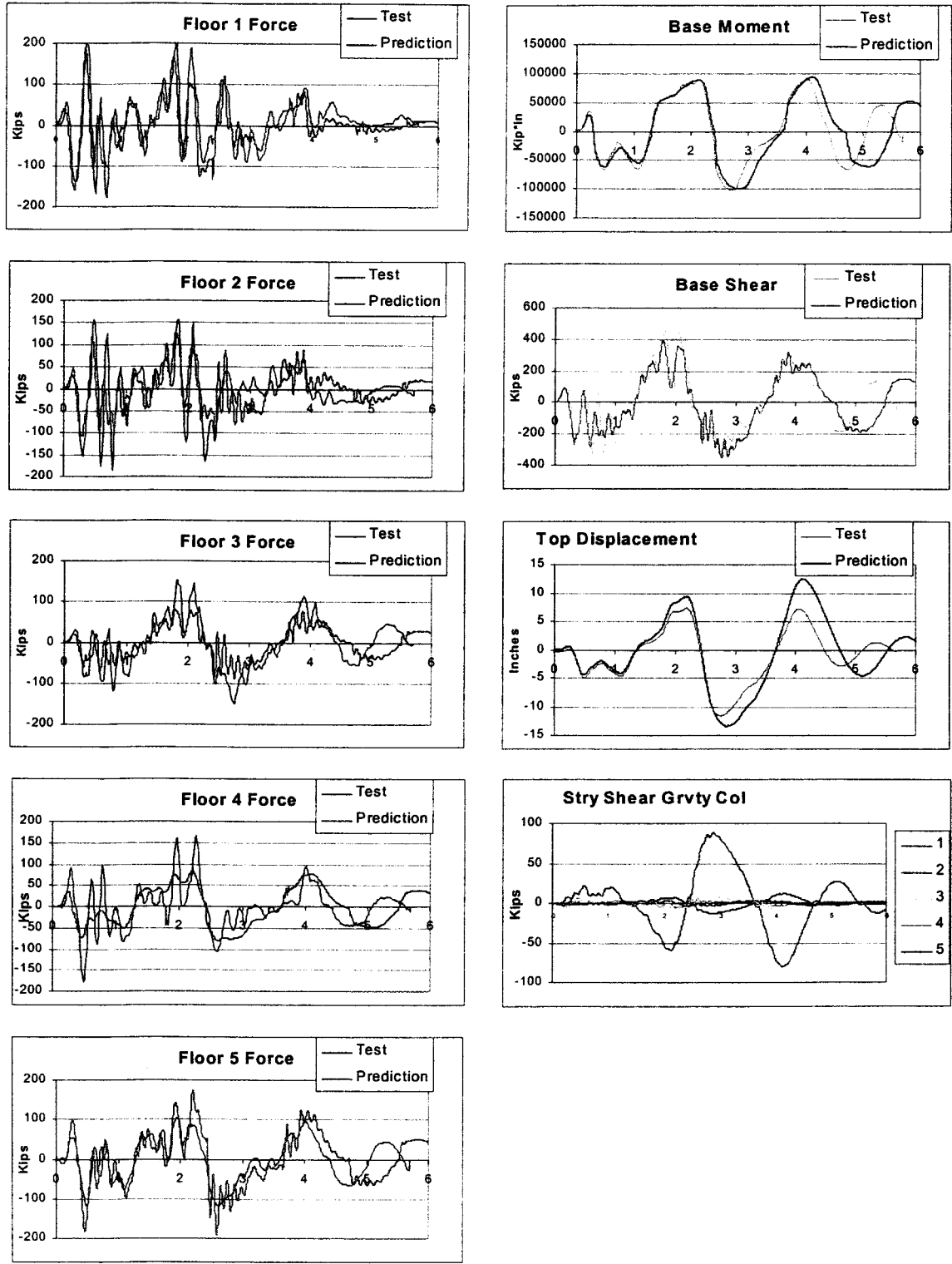
Figure 4-7 Analytical Results k_bs=2,000 kip/in

performance of the building. This is because the secant stiffness remains about the same for each of the models. The procedure of Force Based Design would indicate a significant change in required building strength based on this change in period due to initial stiffness, and also a significant change in expected response displacements. It is evident from these analyses that an initial stiffness based design approach, i.e. Force Based Design, is not accurate.

To get the most accurate overall experimental and analytical correlation it is helpful to view the Wall Base Moment Displacement Prediction-Response Envelope (Figure 4-8). The curve represents the pushover model with additional influence of the gravity and seismic frame columns. The data points represent peak base moment and displacement values from the various tests. With the additional resistance due to the columns accounted for the analytical results are practically matching the experimental results, in spite of the high mode effects as will be discussed subsequently.

4.2 Overall Experimental Results

In this section plots of story displacements, forces, and shears, together with base moment/roof displacement hysteretic response are given for different levels of seismic excitation.

The higher mode forces in the analytical model were related to the impact load, but were also present in the experimental results where impact was not significant. This was seen as early as the 0.5 EQ-1 test, even though the maximum displacement achieved was less than half an inch (Figure 4-9).

Figure 4-10 shows the influence of these higher modes on the floor force time history, with the fifth floor force opposing the other forces through most of the test. The story shear results (Figure 4-11) also show the higher mode influence with a peak inter-story shear of 150 kips occurring at the second level. This is of interest considering the wall had not yet "lifted off" (as evidenced by the linear Base Moment Hysteresis loop shown in Figure 4-12.
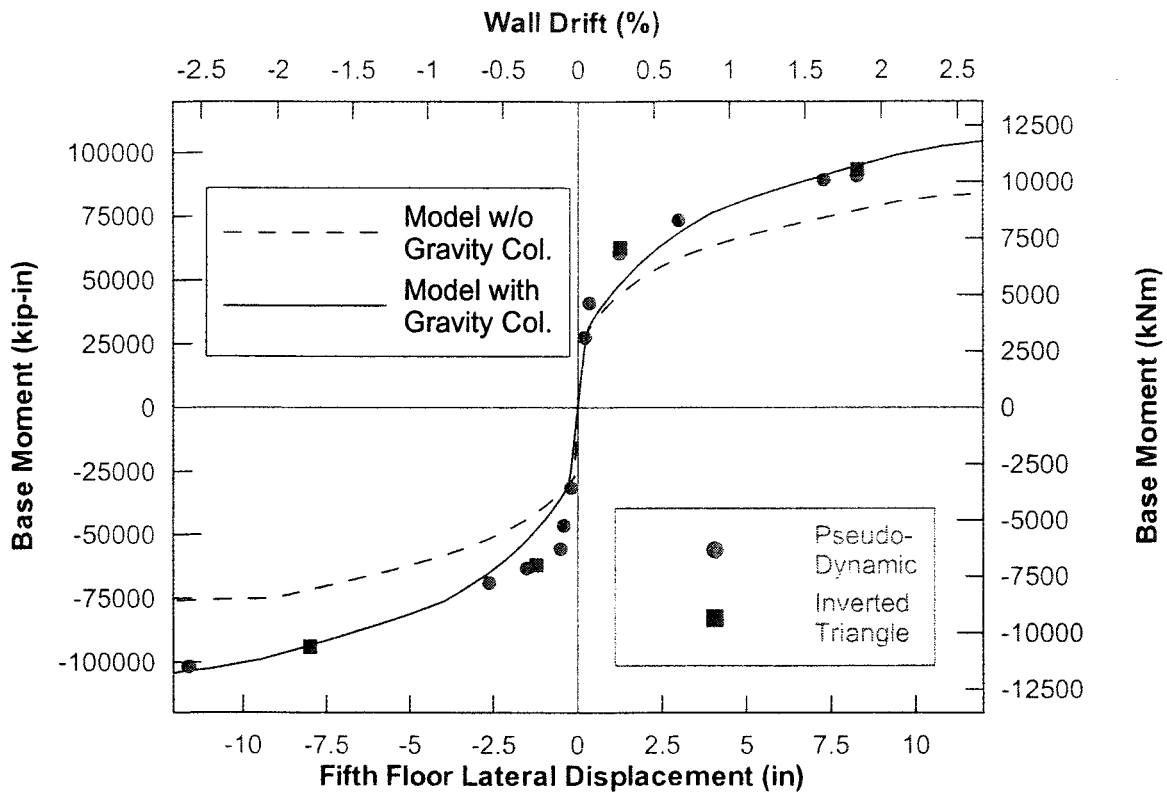
Figure 4-8 Wall Moment Displacement Prediction-Response Envelope
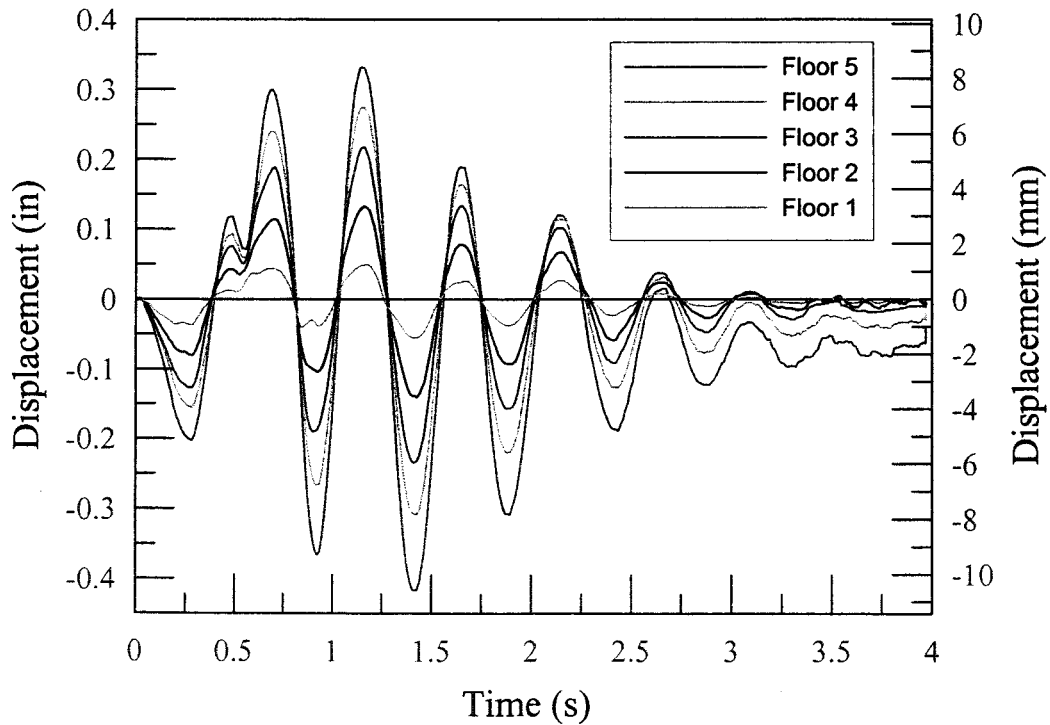
Figure 4-9 Floor Displacement Time History (0.5 EQ-1)
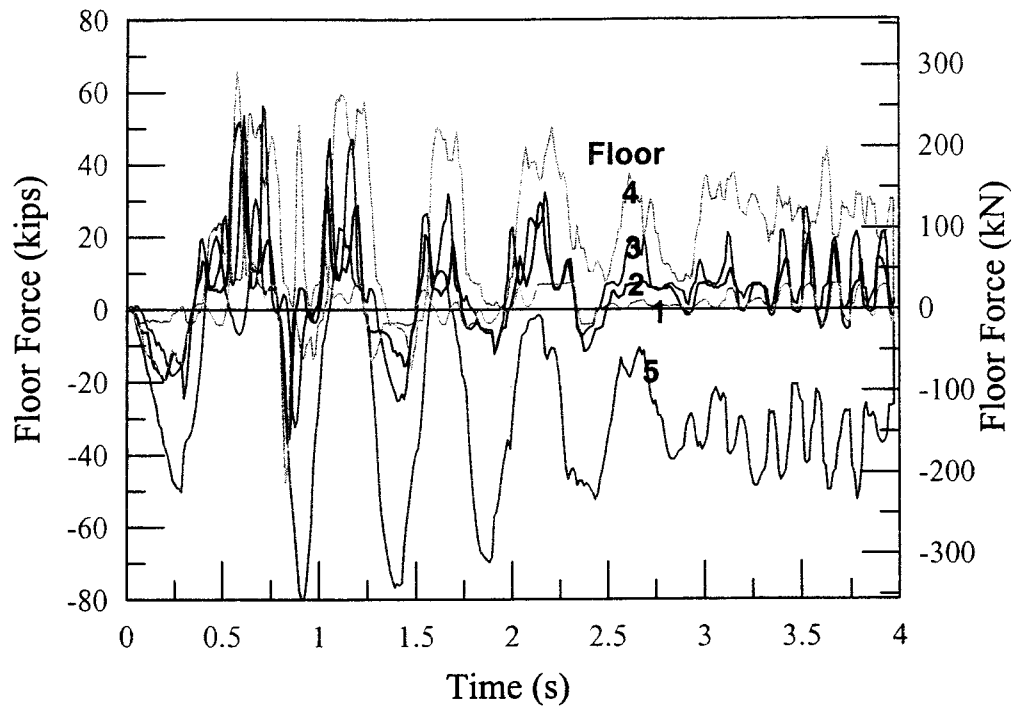
Figure 4-10 Floor Force Time History (0.5 EQ-1)
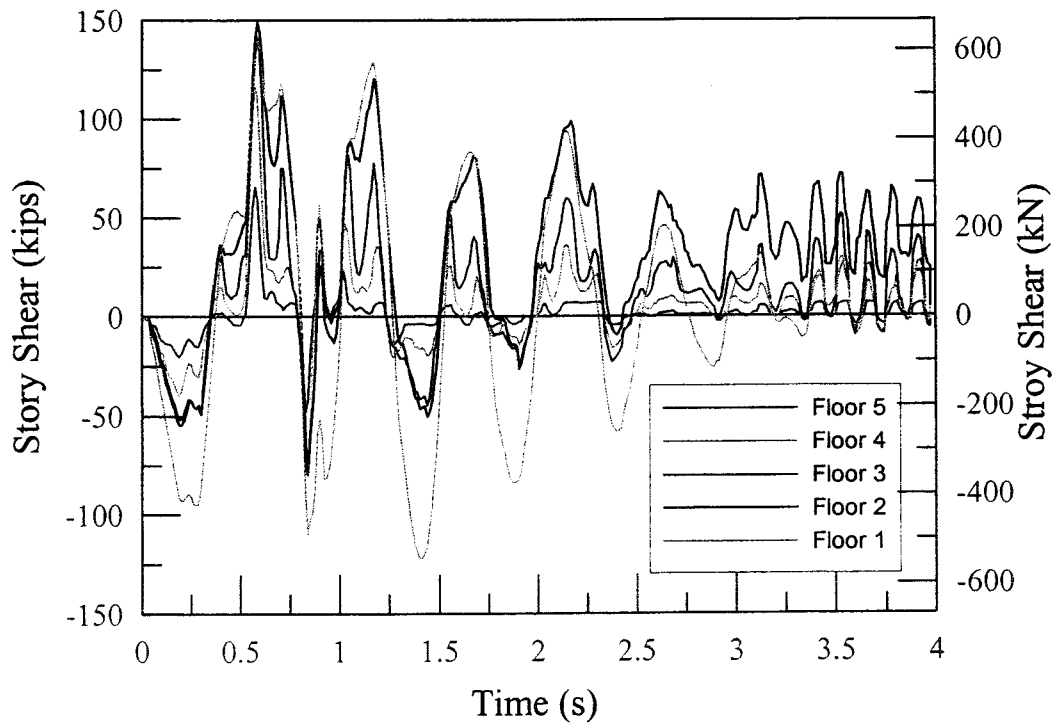
Figure 4-11 Story Shear Time History (0.5 EQ-1)
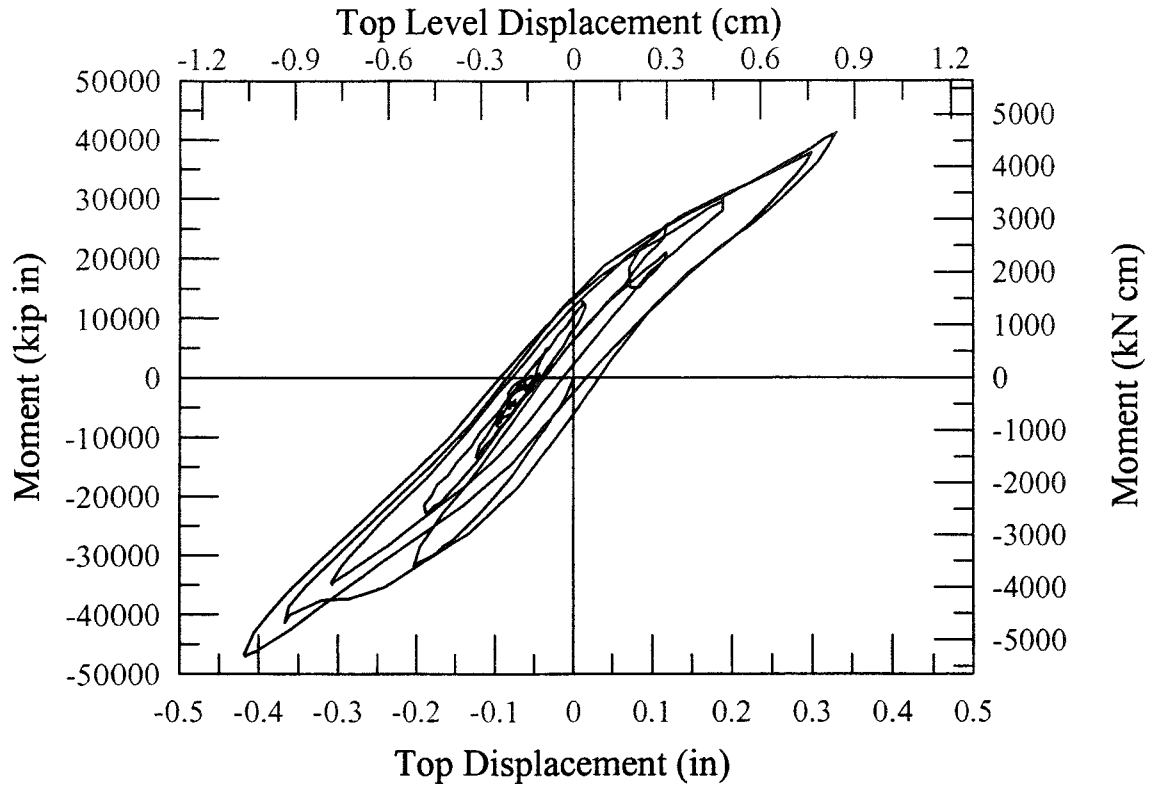
Figure 4-12 Base Moment Hysteresis (0.5 EQ-1)
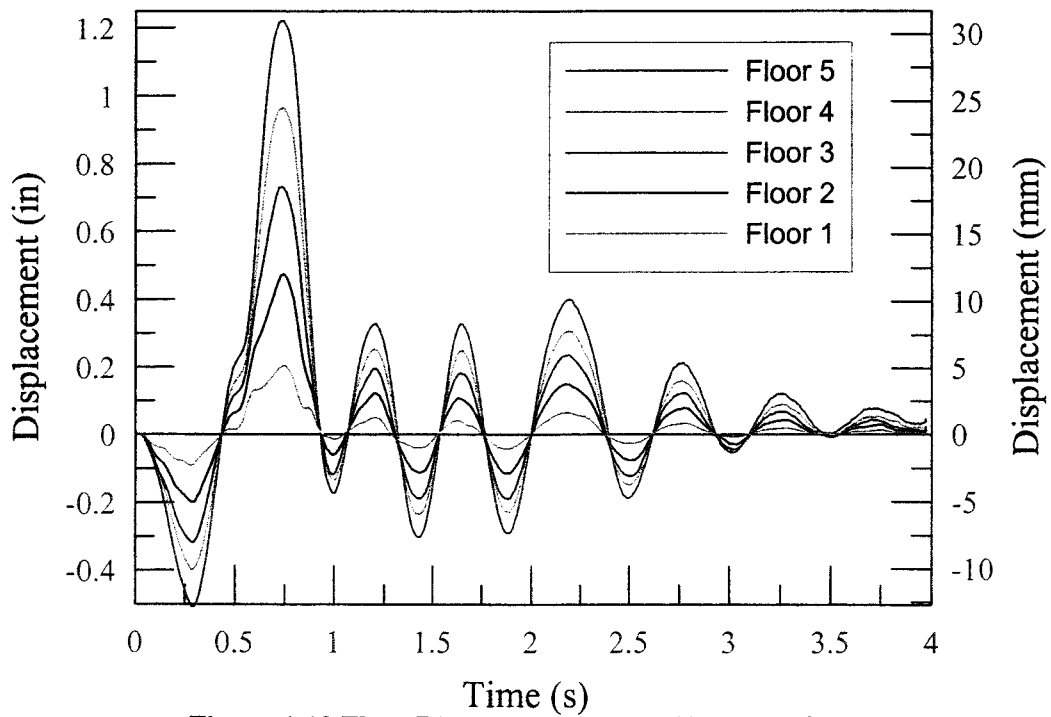
Figure 4-13 Floor Displacement Time History (EQ-1)
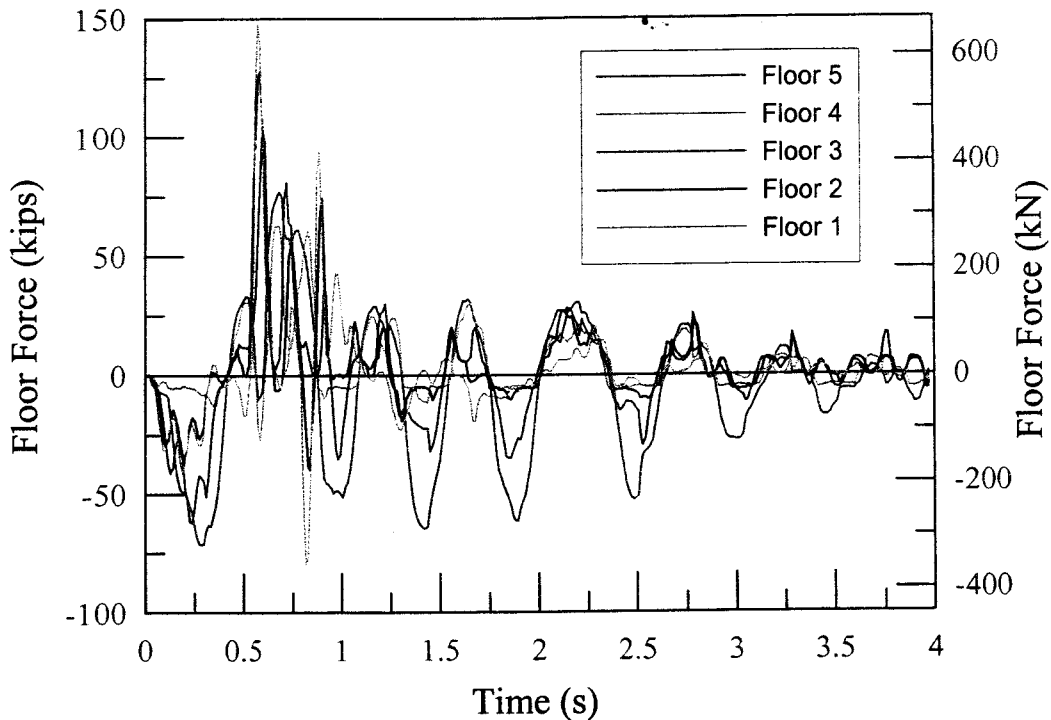
Figure 4-14 Floor Force Time History (EQ-1)

The test building achieved a peak displacement of 1.2 inches during the EQ-1 level test as shown in Figure 4-13. The 0.540 second first mode period of the analytical model correlates well with the experimental building period of approximately half a second as shown by the displacement time history results. The higher mode effects were even more substantial at this level of testing as shown by the floor force and story shear time histories in Figure 4-14 and Figure 4-15, respectively. "Lift off" of the wall occurred at this level of testing during peak positive displacement. This is evident from the nonlinear behavior of the base moment hysteresis loop shown in Figure 4-16. The figure also shows the self-centering characteristics of the split wall panel system by the "flag-shaped" hysteresis loops. The IT-1 inverse triangular load test followed the EQ-1 pseudodynamic test. Base moment hysteresis results (Figure 4-17) show hysteretic energy dissipation occurring as the wall "lifts off" and begins to rock.

The wall "lift off" which occurred in EQ-1 and IT-1 caused cracking and some crushing of the grout layer beneath the wall panels. The cracking changed the test building period slightly, generally increasing it as damage occurs as seen in the displacement time history (Figure 4-18).

87

The floor force time history results (Figure 4-19) are jumbled, showing the strong influence of higher mode frequencies in the EQ-2 record. These influences are also seen in the story shear results for this test (Figure 4-20). The base moment hysteresis plots for both EQ-2 (Figure 4-21) and the subsequent IT-2 (Figure 4-22) test, show further progress into the nonlinear behavior range of the wall panel system.

The trend of increasing period with damage continued in the EQ-3 record test as shown in the displacement time history results (Figure 4-23). Filtering of the original EQ-3 record, as discussed previously, significantly reduced the influence of higher (particularly 4th and 5th) mode frequencies in the test record. This is evident in both the floor force and story shear time histories (Figure 4-24 and Figure 4-25). Figure 4-26 shows the base moment hysteresis plot for the test building for the UBC Zone 4 design level earthquake. The building achieved a peak base
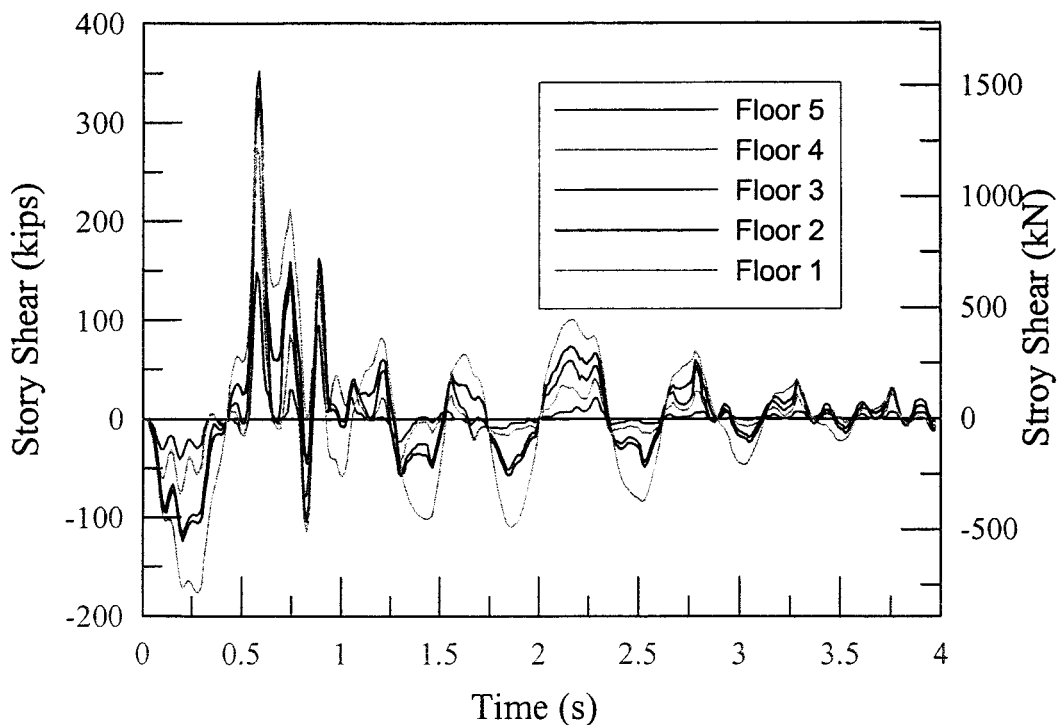
Figure 4-15 Story Shear Time History (EQ-1)
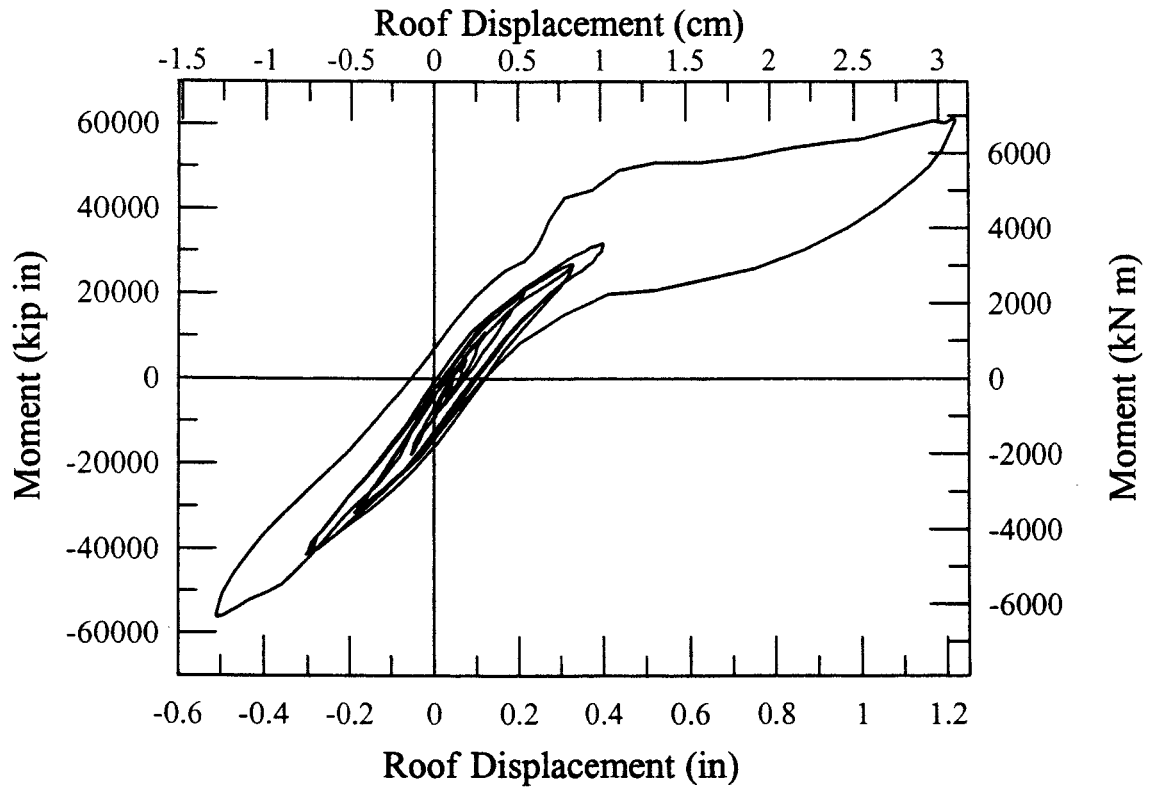
Figure 4-16 Base Moment Hysteresis (EQ-1)
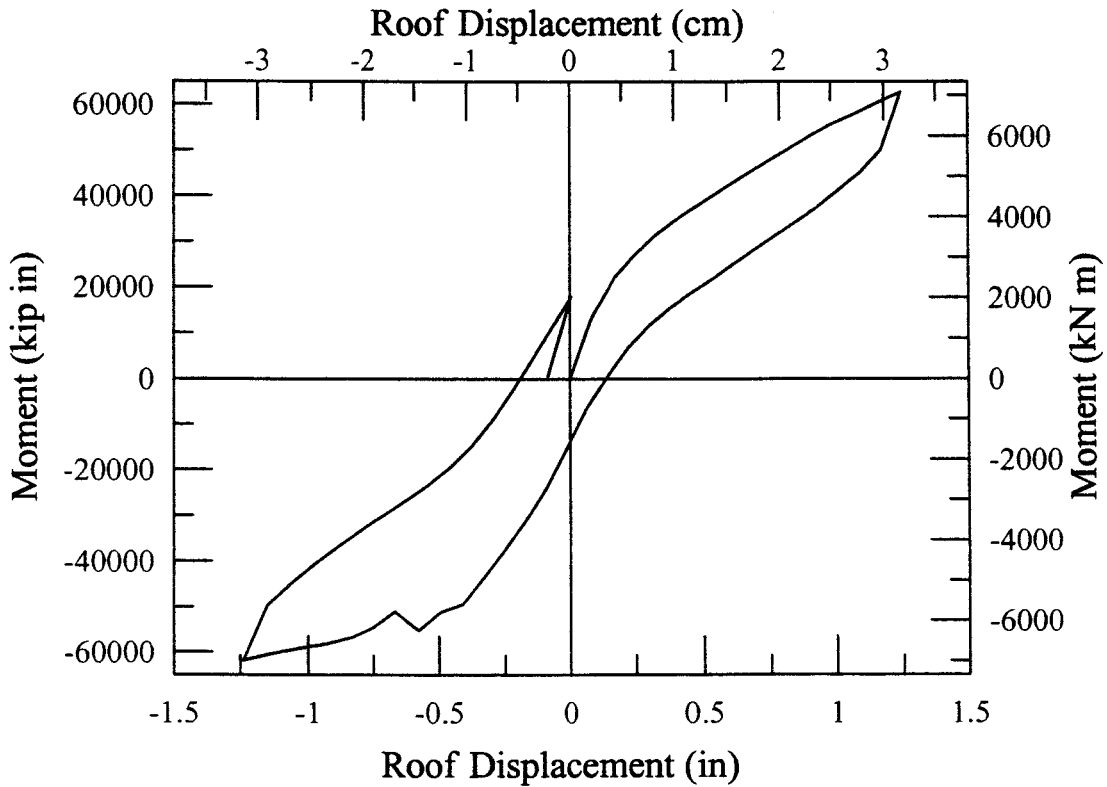
Figure 4-17 Base Moment Hysteresis (IT-1)

89
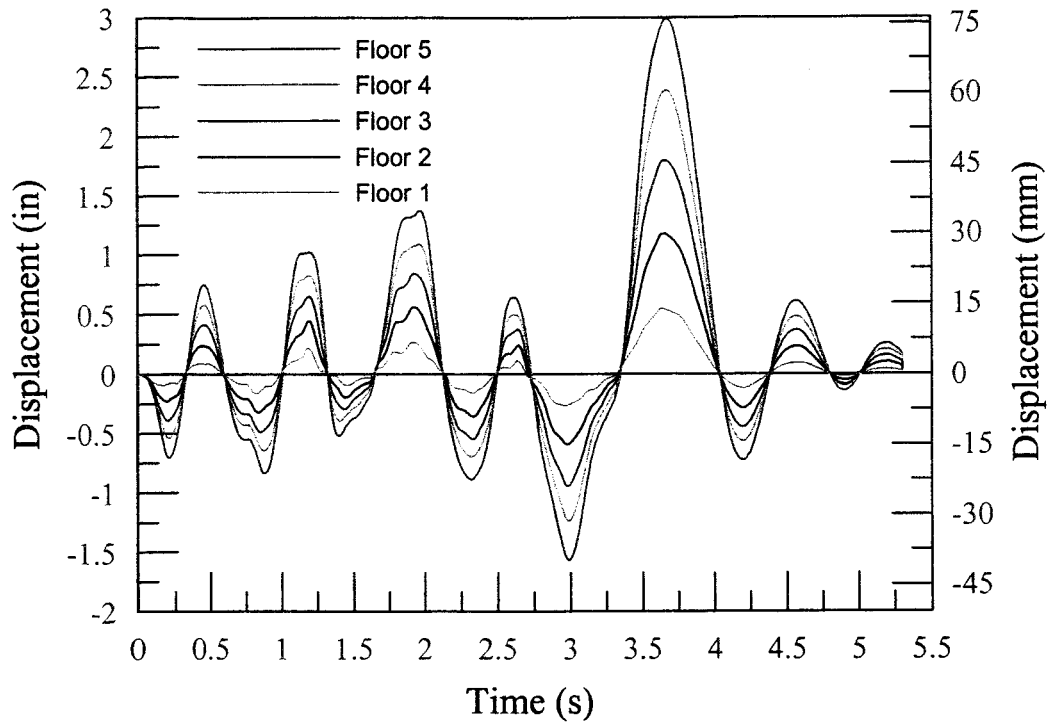
Figure 4-18 Floor Displacement Time History (EQ-2)
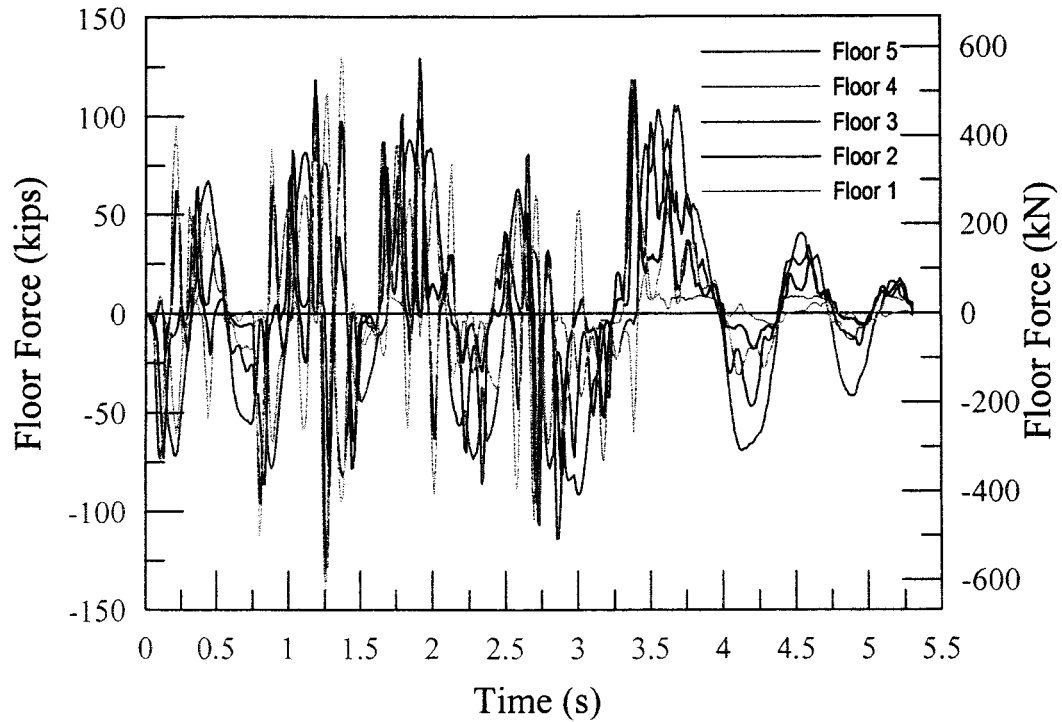
Figure 4-19 Floor Force Time History (EQ-2)
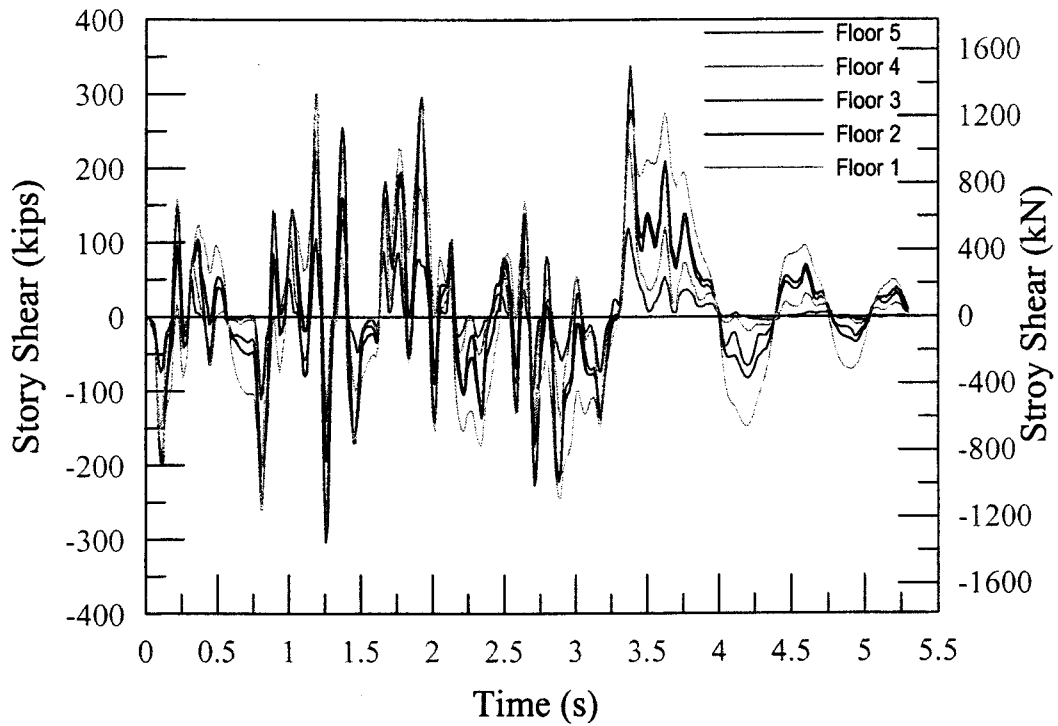
Figure 4-20 Story Shear Time History (EQ-2)
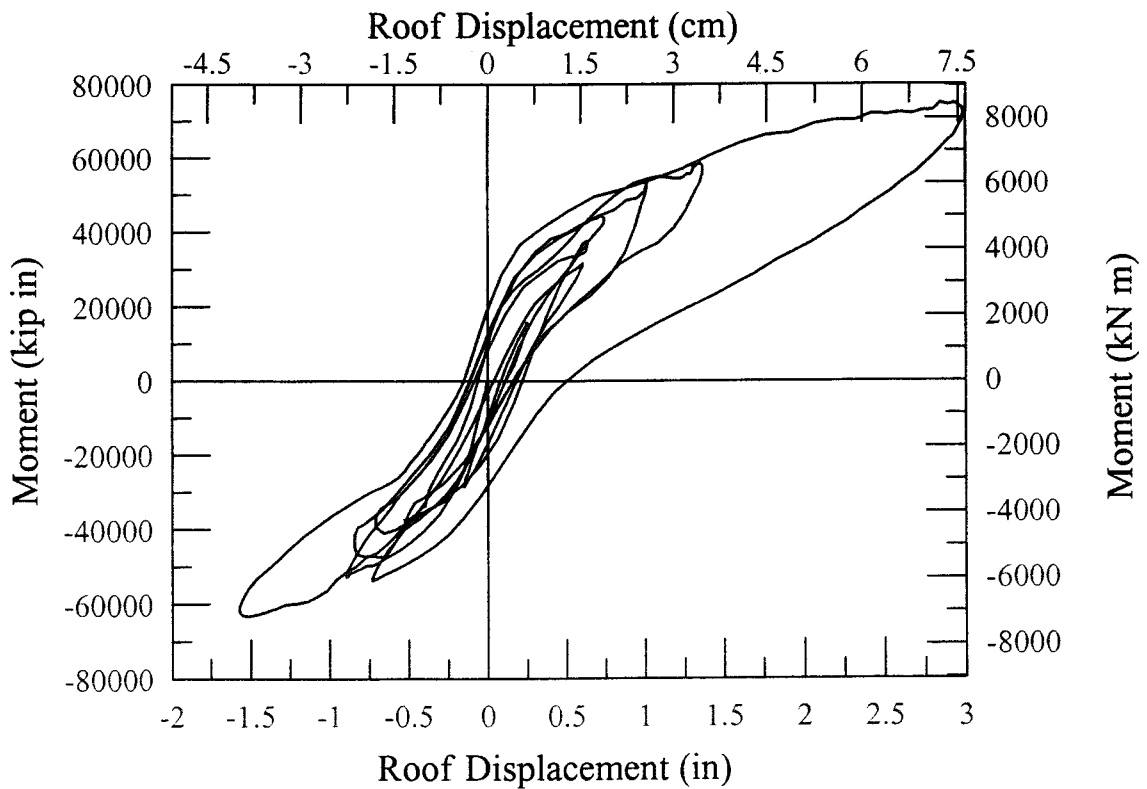
Figure 4-21 Base Moment Hysteresis (EQ-2)

91
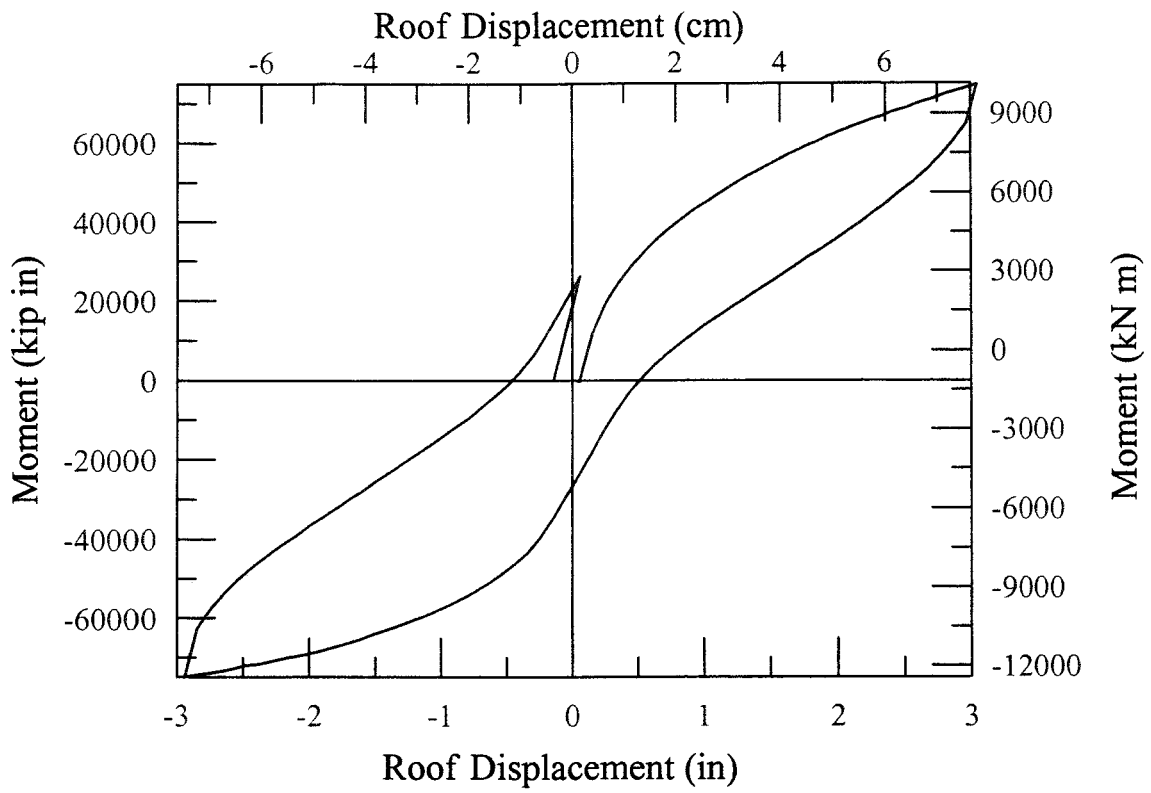
Figure 4-22 Base Moment Hysteresis (IT-2)
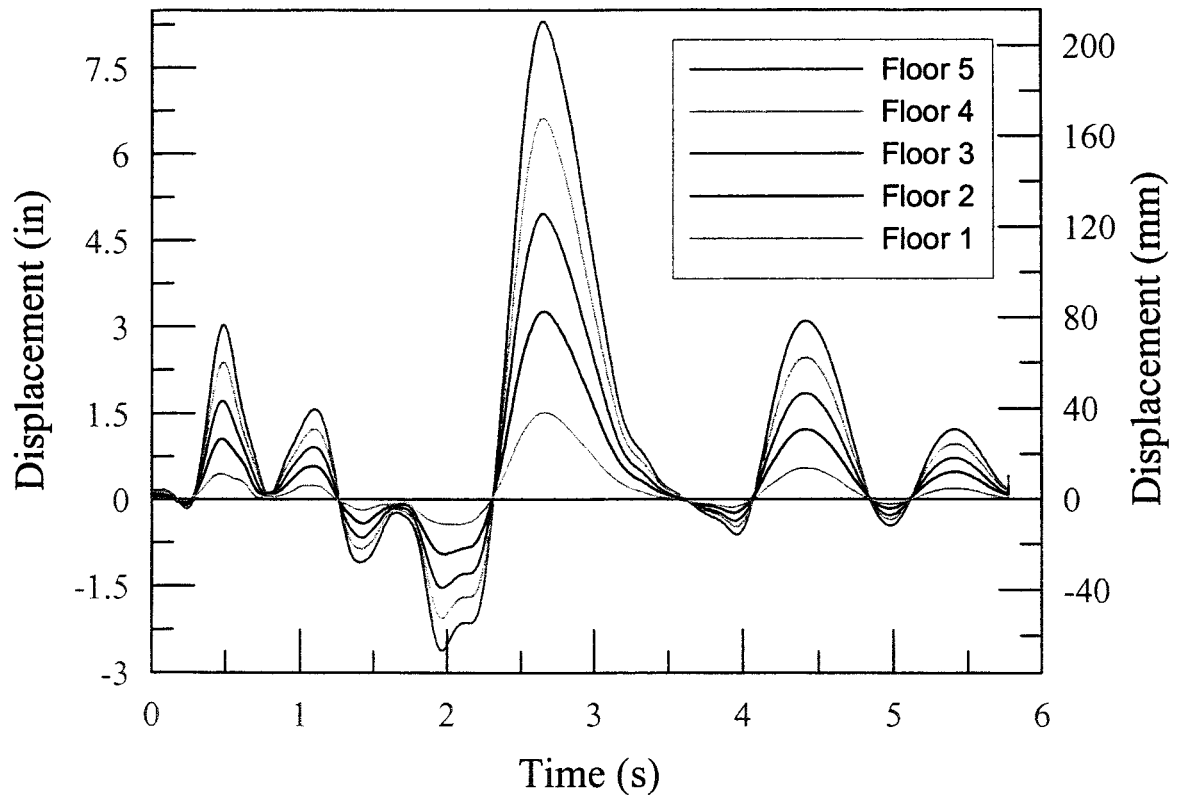
Figure 4-23 Floor Displacement Time History (EQ-3)
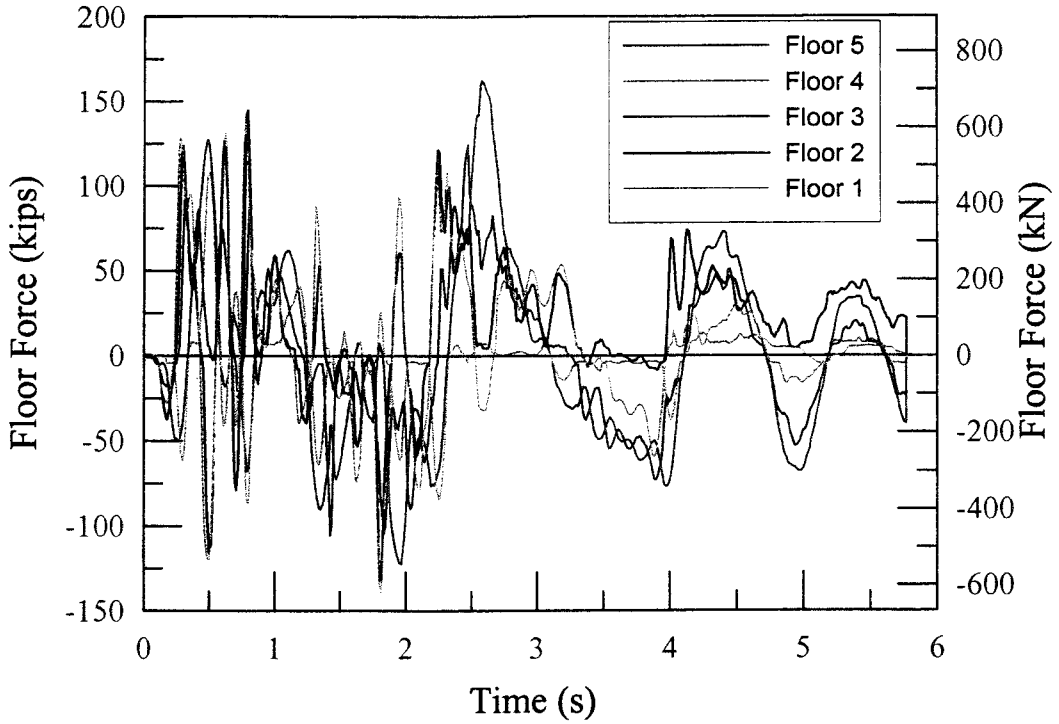
Figure 4-24 Floor Force Time History (EQ-3)
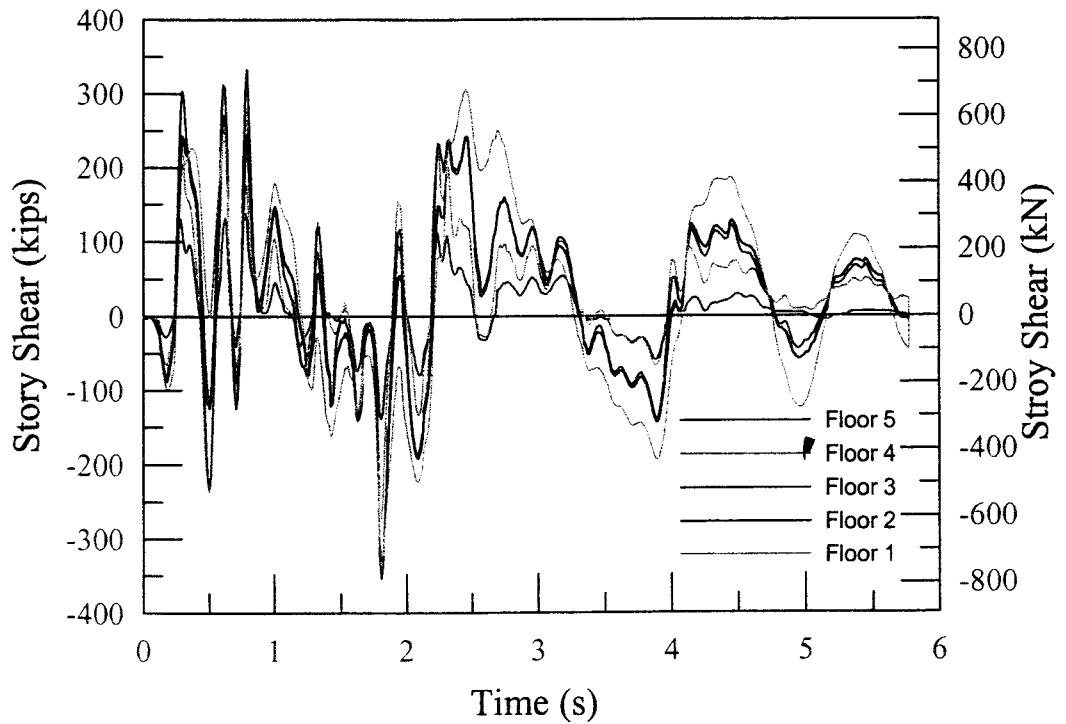
Figure 4-25 Story Shear Time History (EQ-3)

93
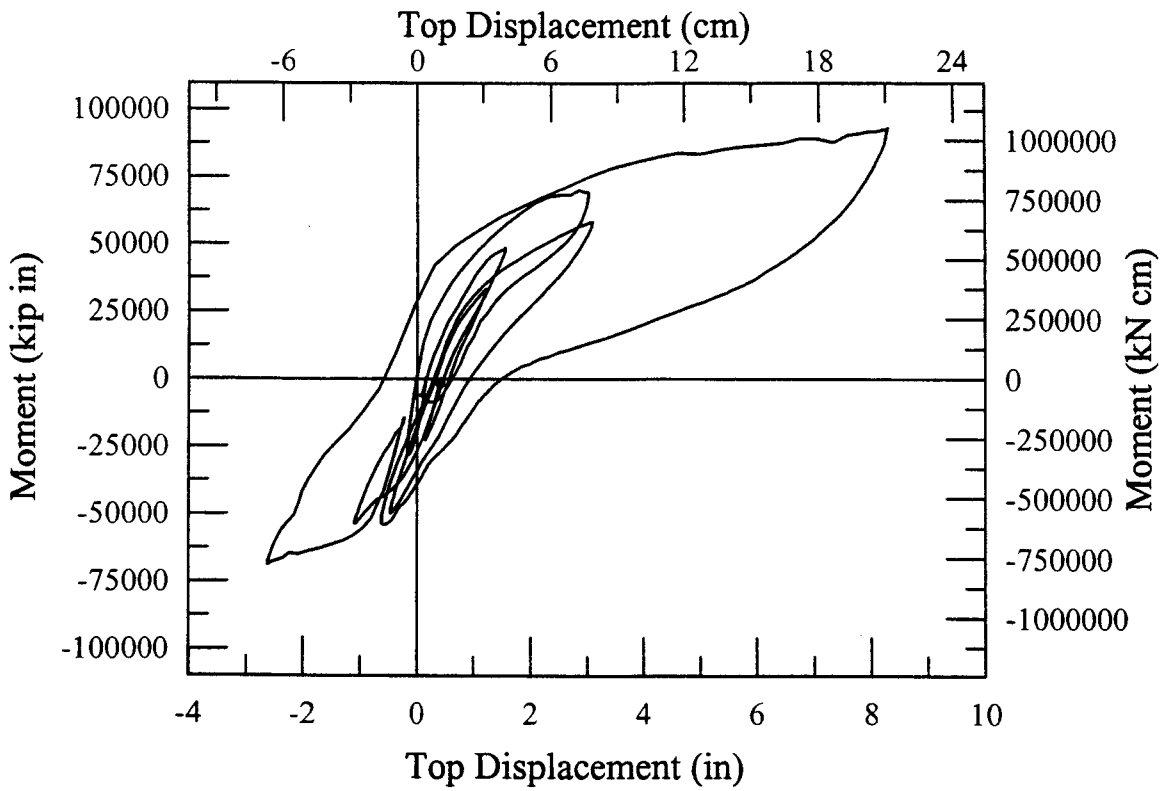
Figure 4-26 Base Moment Hysteresis (EQ-3)
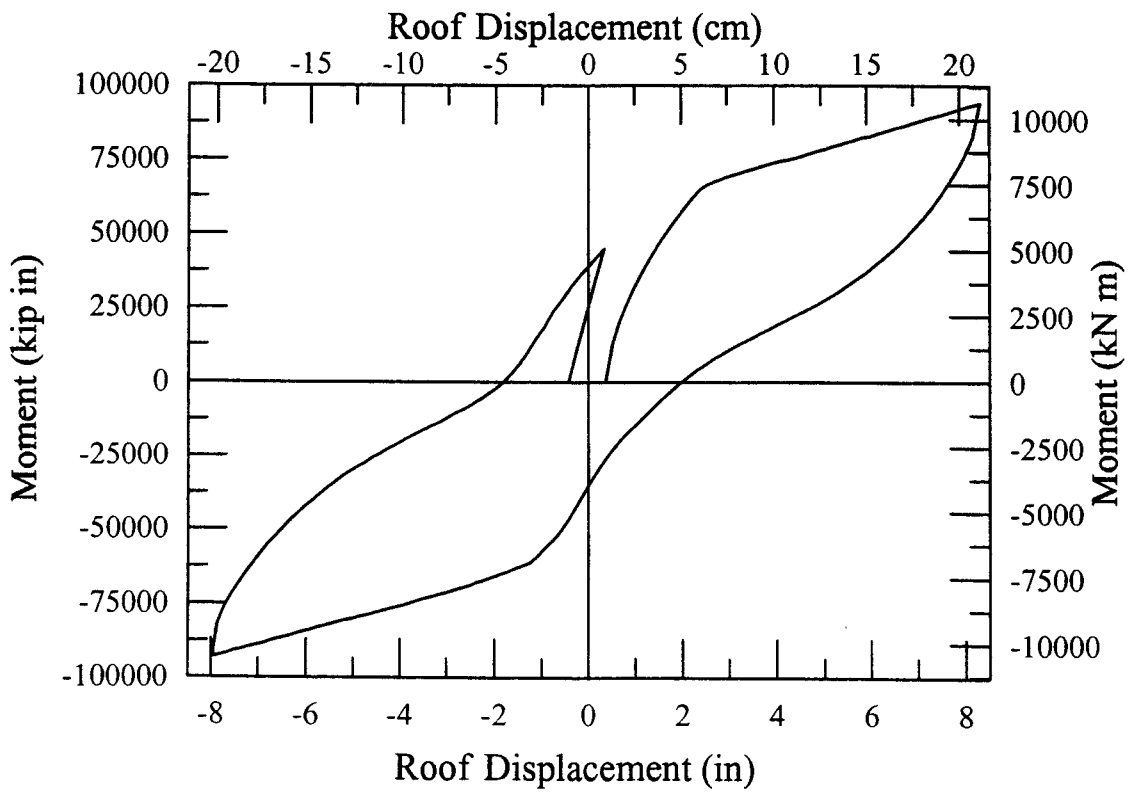
Figure 4-27 Base Moment Hysteresis (IT-3)

94

moment resistance of 90,500 kip inches (10,230 kNm) at a top floor level displacement of 8.28 inches (21 cm). The building showed excellent energy dissipation characteristics due to both the rocking action of the wall panels and the added energy absorption provided by the UFPs. The pinched behavior of the hysteresis loop due to the self-centering action of the post tensioning bars is also evident. The residual displacement after the design level earthquake due to this action was extremely low, less than one half inch, as shown by the black dot in Figure 4-26. Yielding of the post tensioning did occur during this test at a minimal level, as described subsequently. It is quite evident from this graph that the wall panel system provides excellent hysteretic behavior for the design level earthquake. The subsequent inverse triangular load test, IT-3, exercised the test building to the maximum displacement achieved in the design level earthquake in both directions. The base moment hysteresis loop for this test is shown in Figure 4-27.

It is well known that although the design level events proposed in various codes make a good effort to provide recommendations that will ensure safety should the inevitable earthquake occur, the possibility that these levels may be exceeded is significant. In an effort to evaluate the performance of the building at these higher earthquake levels, an input record was used that exceeded the design level earthquake accelerations by 50 percent. This resulted in a peak top-level displacement forty percent larger as shown in Figure 4-28. Floor force and story shear time histories continue to show the higher mode influences (Figure 4-29 and Figure 4-30). The base moment hysteresis plot for this test is shown in Figure 4-31. Again, the wall system showed good hysteretic behavior and energy dissipation. The peak base moment of 101,800 kip inches (11,500 kNm) occurred at a displacement of 11.58 inches (29.4 cm) in the negative direction. Even though yielding of the post-tensioning bars occurred in this and previous tests (starting with EQ-3), the residual displacement was still minimal. This displacement was less than one-quarter inch as shown by the black dot in Figure 4-31.

95
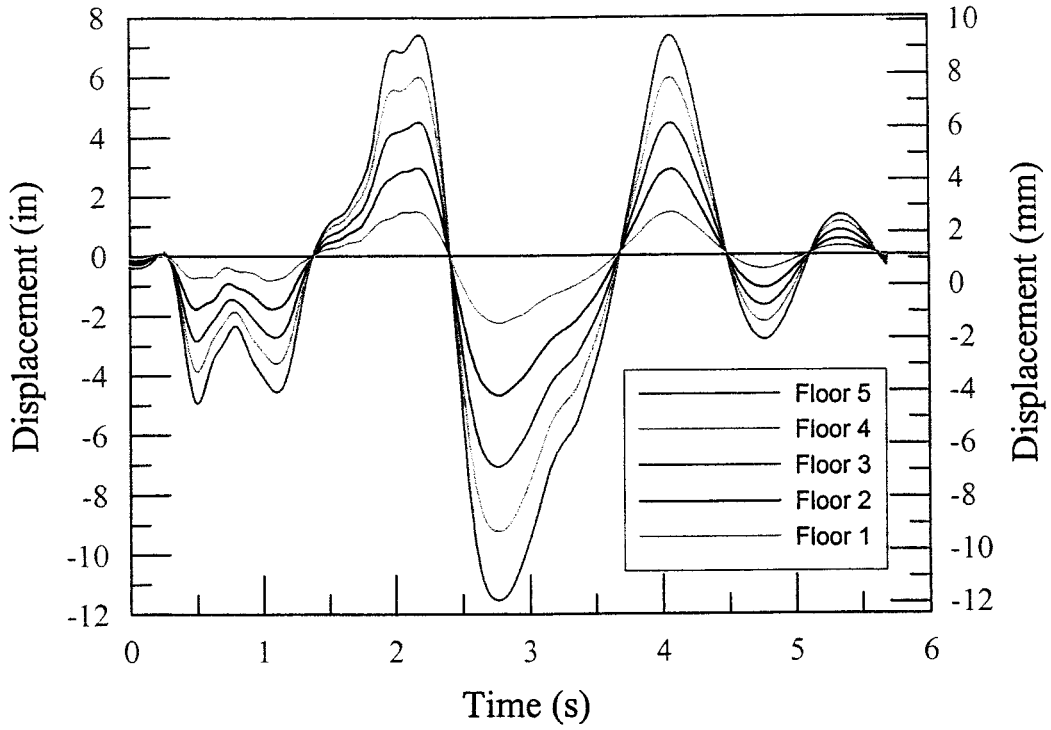
Figure 4-28 Floor Displacement Time History (1.5 EQ-3)
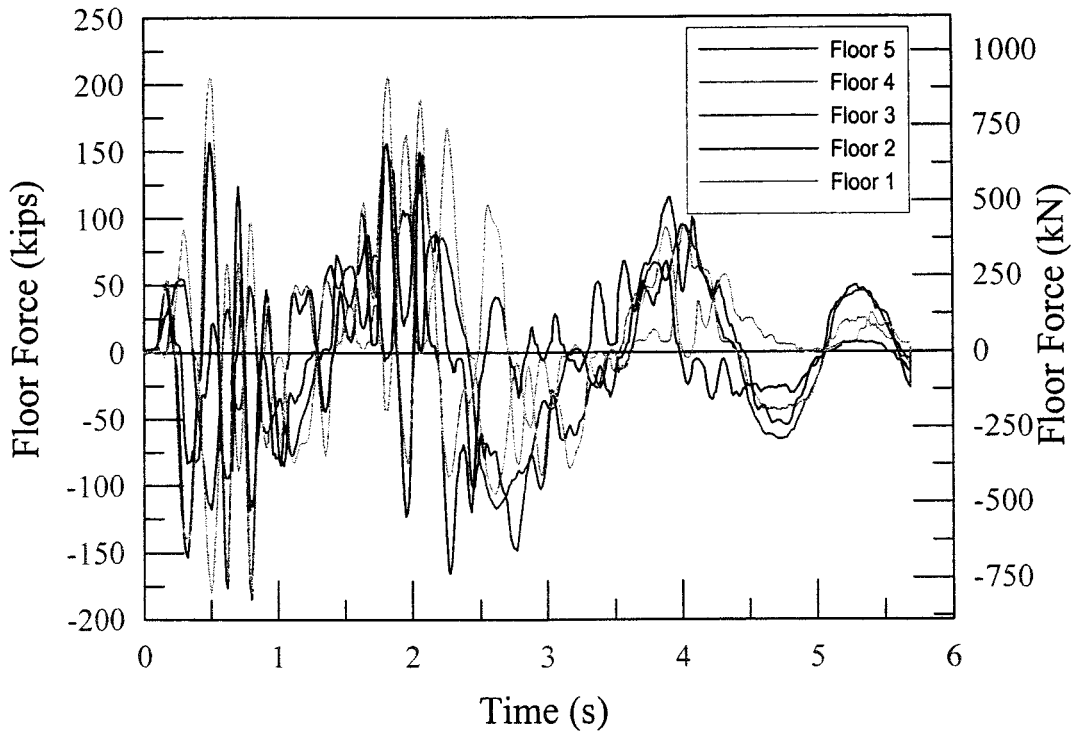
Figure 4-29 Floor Force Time History (1.5 EQ-3)

96
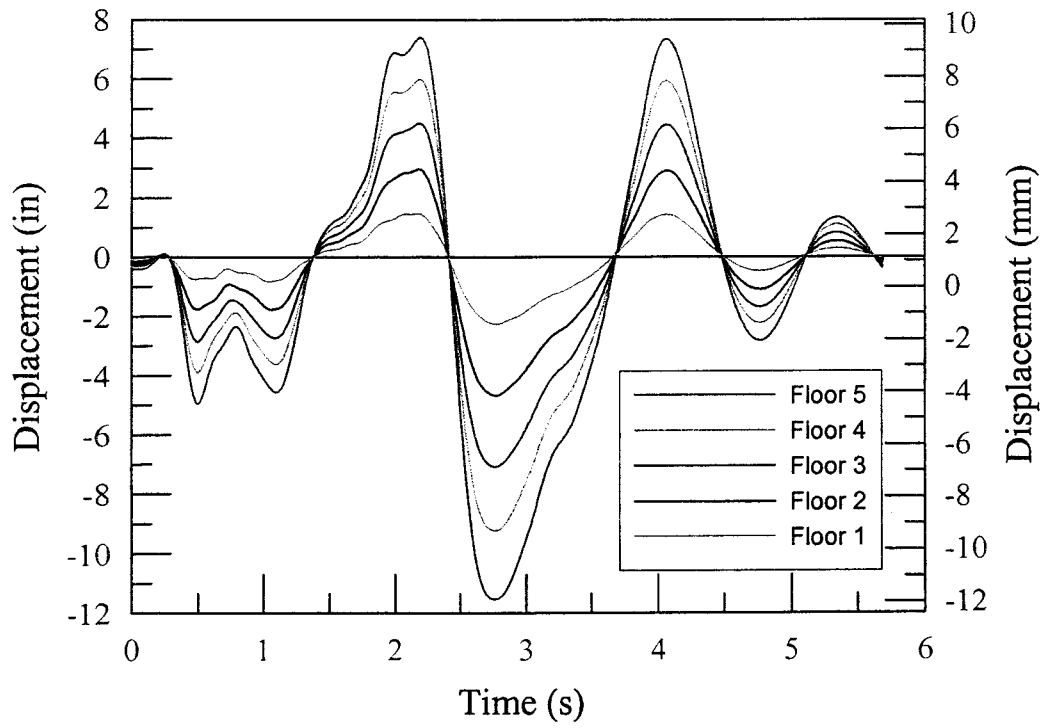
Figure 4-30 Story Shear Time History (1.5 EQ-3)
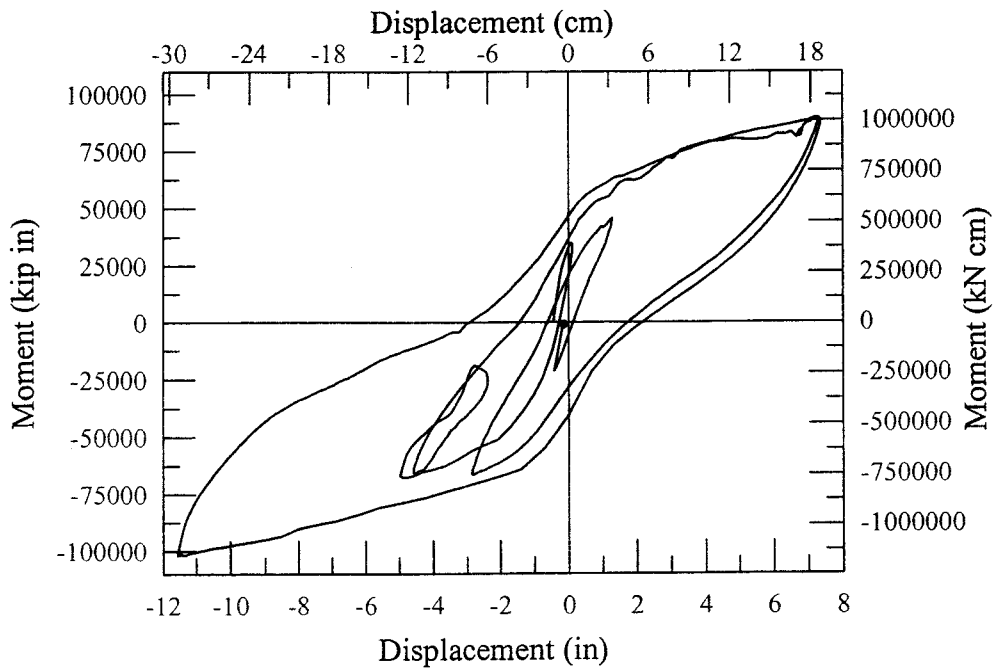
Figure 4-31 Base Moment Hysteresis (1.5 EQ-3)

97

Overall, the building performed quite well with only damage to the wall system limited to minimal cover concrete spalling at the toe and other minor damage to non-resisting components of the structure. Further details and observations on this will be discussed subsequently. The system could probably have been taken to even higher load levels, but due to the limitations of the actuator and test building connections the wall direction test was completed at this level. In order to allow the structural integrity of the frame direction testing to remain, no inverse triangular load tests was run after 1.5 EQ-3. The test was halted at peak positive and negative displacements during 1.5 EQ-3 to examine the structure instead of running the IT test.

It should be noted that the reaction tower erected for the wall direction testing of the *PRESSS* building was undergoing a significant rotation and uplift at its base during the final stages of testing. This had two impacts on the test being concluded at 1.5 EQ-3. Though base shear forces were significantly lower during the inverse triangular load test, the floor force at the top level is still significantly large. This would cause an overturning moment on the reaction tower that would come close to or exceed its capacity limits. Furthermore, the relative displacement between the reaction wall and the test building would also be significantly larger than in the pseudodynamic test, coming uncomfortably close to actuator displacement limitations. This also influences the decision not to apply IT tests after 1.5EQ-3.

4.3 Observations of Structural Resisting System Components

At the peak displacement during the IT tests the testing was paused in order to investigate the building, as well as for other reasons mentioned in Section 2.4. Pictures were taken and damage to the building was evaluated and recorded. This section will document the important details extracted from the record of descriptions as well as provide comparisons of specific elements in the Ruaumoko model and test building to further validate the analytical results. Further photographs of damage that occurred to the building are also available in the Appendix.

4.3.1   Wall Panel Performance

The jointed precast wall panels served as the earthquake resisting system for the
East/West direction of testing on the *PRESSS* Building. The panels performed exceptionally well
during all stages of the testing, with only minimal damage occurring at the design level
earthquake and subsequent tests.

The initial pseudodynamic and inverse triangular tests imposed forces and displacements
on the test structure up to levels equivalent to Zone 2 design requirements (represented by EQ-2
and IT-2). During these test stages no damage occurred to the wall panels, indicating that they
were performing well within their elastic range. However, it should be noted that this does not
correspond to the initial elastic stiffness that would be assumed in a force-based design. As soon
as lift-off of the wall occurs, the force-displacement characteristics of the building also change;
therefore, initial stiffness is a poor method of determining important building force and yield
characteristics. The only cracking that occurred before EQ-3 was along the grout interface
between the foundation and wall base. The grout cracking is expected because of the rocking
phenomenon that occurs in the wall panel system and that cannot be considered damage.

In an effort to more clearly describe the location of damage to the wall panels the location
of the wall panels will be noted. W1R is the panel on the same side as the reaction wall, west of
the building centerline, which also corresponds to displacement in the negative direction for the
test. W1 is the opposing panel, east of building centerline. Panels W2R and W2 are on top of
panels W1R and W1, respectively.

Initial cracking began to occur in the wall panels during the design level earthquake, EQ-
3. During the inverse triangular load test, IT-3, vertical cracks extending from the wall toe
upward four inches began to form. Horizontal cracks were also noted at the panel bases on the
west side of W1R and the east side of W1 with crack widths less than 0.1mm. This is due to the
high level of compression strain in the cover concrete. A crack was noted propagating from the

corner of the block-out at the wall base where the PT couplers are located in both W1 and W1R. Some spalling at the wall toe was also noted. Spalling at the west base corner of the PT coupler block-out was noted at the negative peak of IT-3 (-8.15", -20.7cm). Aside from the damage at the base, there was no other damage to the wall panels, including no cracking in the horizontal construction joint between the bottom and top panels.

The spalling of the wall base toes continued during 1.5 EQ-3. Figure 4-32 shows the damage that occurred to the exterior toe of W1 at the peak displacement during that test. The cover concrete beyond the armored section had spalled off and the confinement rebar can clearly be seen. The up-lift of the wall can also be seen noting the line of white paint that was at the top of the grout layer prior to testing.

The vertical displacements of the wall base were recorded using six potentiometers, three on W1R and three on W1. The locations and potentiometer labels are shown in Figure 4-34. The comparisons between model and test are reasonably good, even at earthquake levels 50 percent higher than design levels, with small discrepancies occurring at the peak displacement values as shown in Figure 4-34 and Figure 4-35. In these figures positive displacement represents lift-off and negative displacement represents concrete compression.

Figure 4-34 shows a comparison of the vertical displacements at the exteriors of the two walls. For the predictions, displacement time histories of the compression only spring elements in the model were recorded. The location of these springs in the model are a distance of 49.6" (1.26 m) from the panel center line, while test displacements were recorded at the panel extremities as shown in Figure 4-33. In order to account for this, displacements taken at the potentiometer where extrapolated to a point at the same distance from the panel centerline as the base springs in the analytical model. Note that considerable displacement in the negative direction occurred in the test results. This shows the influence of contact with the high strength grout beneath the panel base. As previously mentioned this stiffness may have contributed to the difference between analytical and test results causing an impact load.
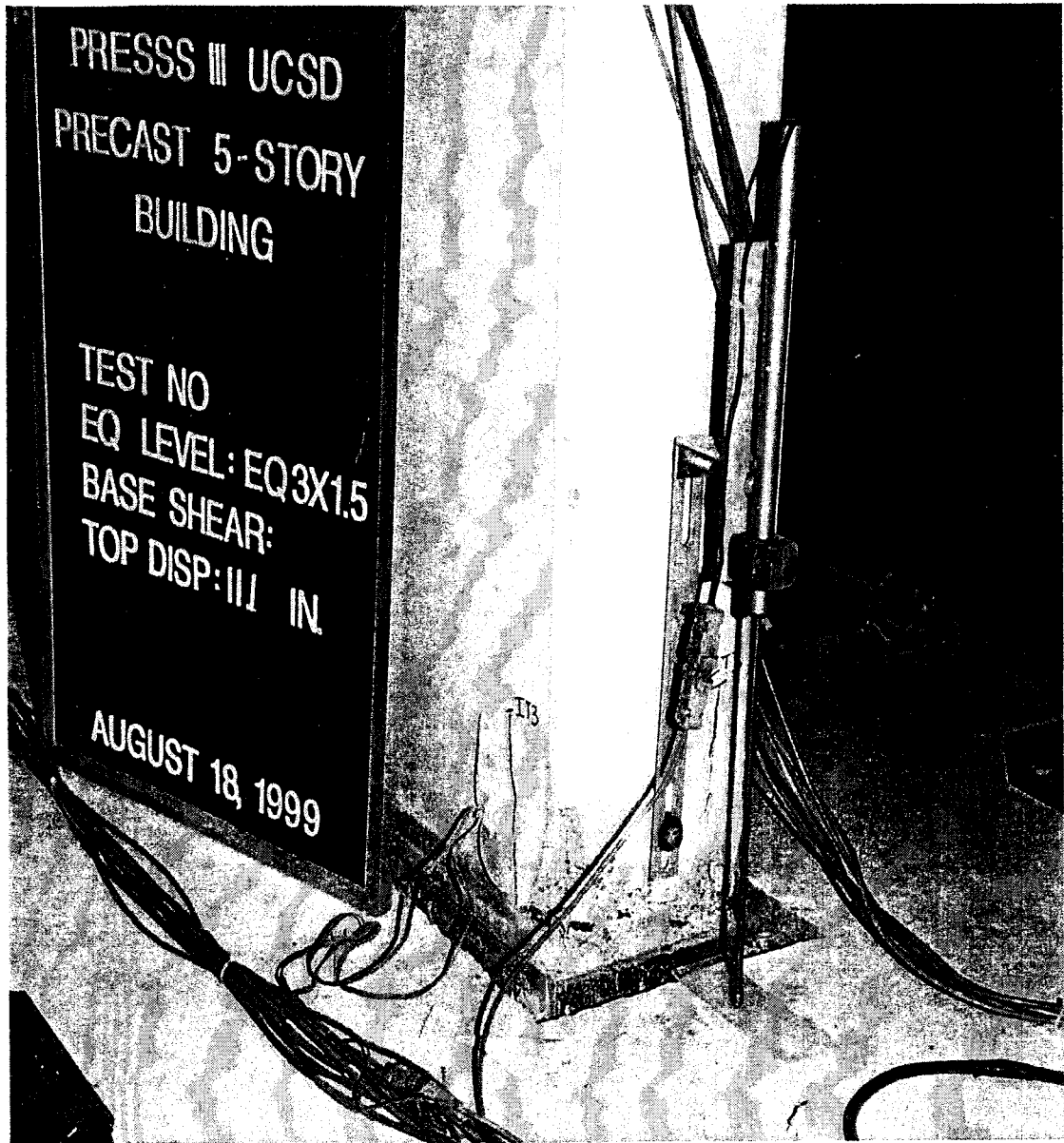
Figure 4-32 Damage to W1 During 1.5 EQ-3

W1RVBW

W1R

W1RVBS   W1RVBN

W1VBS   W1VBN

W1

W1VBE
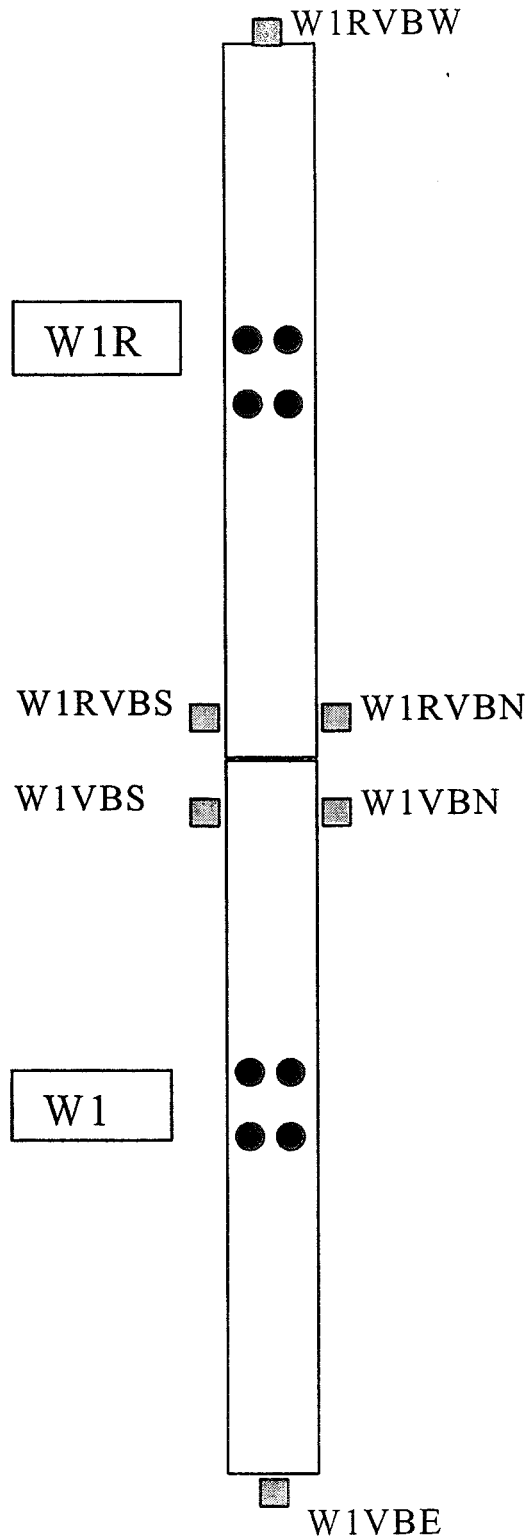
Figure 4-33 Wall Potentiometer Locations (Base Plan View)

Figure 4-35 shows vertical displacements at the interior of the wall system. The displacement data for W1R interior was taken as the average of W1RVBN and W1RVBS and the displacement data for W1 interior was taken as the average of W1VBN and W1VBS. The compression only spring elements were at a location 53" (1.35 m) from panel centerline, which is reasonably close to the location of the pots at the interior. The compression loads at the interior wall base were considerably lower than at the exterior, therefore there is better correlation with analytical data. There is also evidence of compression of the grout layer, approximately one-tenth inch (2.5mm). The prediction tends to slightly overestimate the interior displacements at the peaks.

At peak displacement during 1.5 EQ-3, small cracks in the grout at the exterior ends of the construction joint at the base of W2R and W2 began to occur.
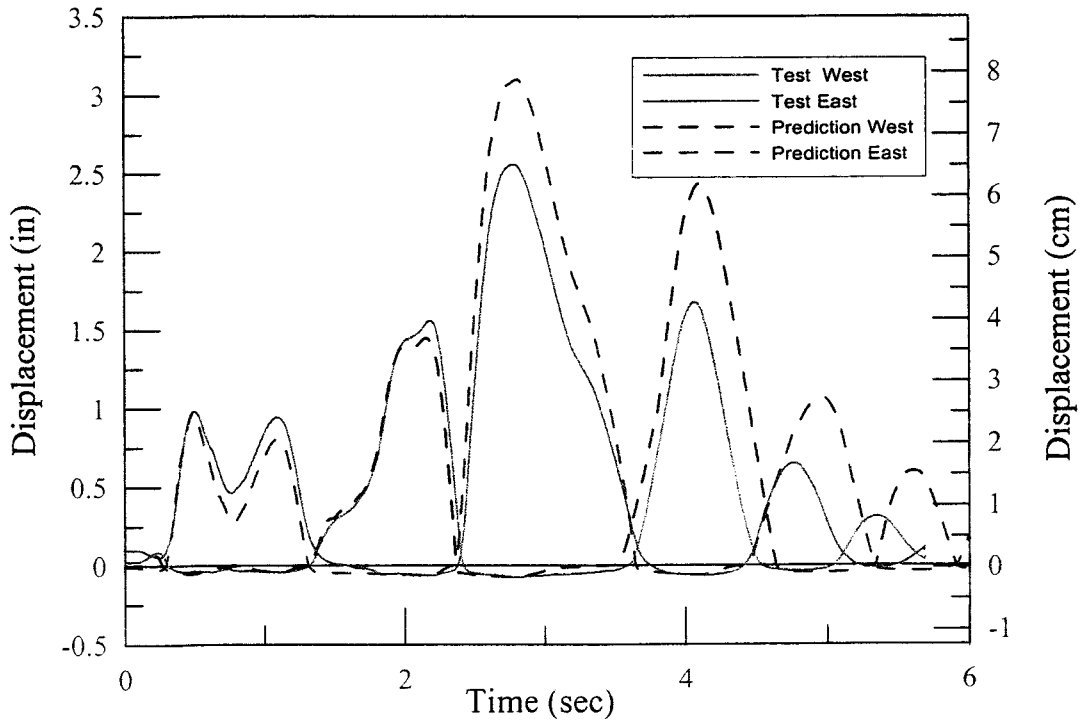
Figure 4-34 Wall Base Exterior Displacement Comparison (1.5 EQ3)
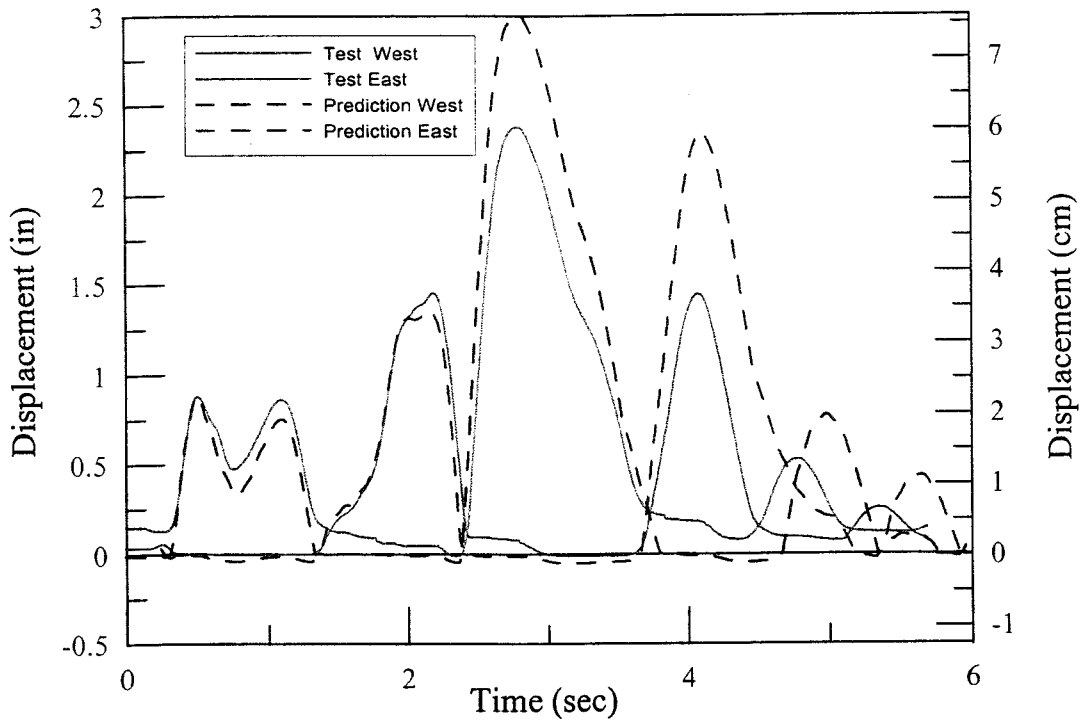
Figure 4-35 Wall Base Interior Displacement Comparison (1.5 EQ3)
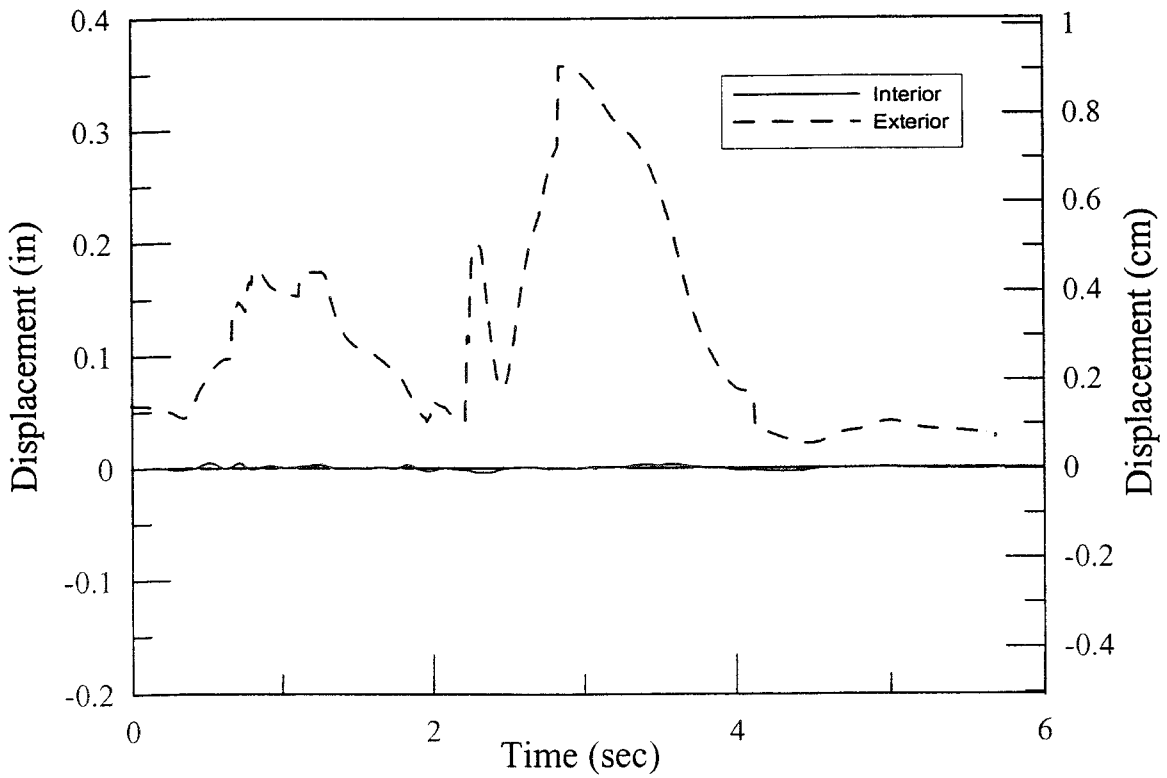
Figure 4-36 Wall Horizontal Joint Displacement (1.5 EQ-3)

104

Figure 4-37 shows results of the displacement pots located at the base of W2R measuring the vertical displacement across the horizontal joint between W1R and W2R at the exterior and interior of those panels. The data for these results was biased to scan one of the EQ-2 test. The initial offset of the exterior displacement indicates that there may have been some slipping of the vertical potentiometer during testing between EQ-2 and 1.5 EQ-3. However, it is still evident that opening at the exterior of the horizontal joint did occur over one-quarter inch (0.64 mm) at peak top floor displacement. The interior vertical gap displacement was insignificant and the joint remained closed. This is do to the shear action of the U-plates. As the earthquake forces push the building in one direction, those forces are resisted in part by the U-plates causing a vertical shear force that serves to keep the interior joints between panels closed.

4.3.2 U-Plate Performance

The performance of the U-shaped flexible plates was outstanding. They provided significant energy dissipation through flexural yielding and added significantly to the building strength. Figure 4-37 shows a comparison between analytical model and test structure relative displacements along the vertical joints at 1.5 EQ-3. The test displacements were measured using vertical displacement pots located across the base level U-plates (shown in Figure 4-38) and at the top of the wall. The values were found to be virtually identical, with the difference after the vertical displacement pots located across the base level U-plates (shown in Figure 4-38) and at the top of the wall. The values were found to be virtually identical, with the difference after the peak displacement attributed to yielding of the PT springs in the analytical model. The displacement time histories of each UFP spring per floor in the analytical model were also found to be the same, indicating the UFP springs were activated only by first mode response. This is due to the basic geometry of the wall system and the fact that these wall panels remain elastic. Therefore, the relative vertical displacement (biased to EQ-2) of the UFP at the base of the

building was directly compared to the displacement time history of the UFP spring element at level one in the model.

As shown in Figure 4-37, correlation between analytical and test relative displacements at the vertical joint was very good. This is of major importance to the designer because it represents one of the critical design issues for the U-plates and the structure overall — the UFP maximum displacement capacity. It has been shown that stainless steel plates provide excellent hysteretic properties and virtually no strength degradation even at levels over 10% strain, a remarkable property of the material. Furthermore, at increased cycles of the plates, as would occur during an earthquake event, significant strength increase due to cyclic strain hardening occurs. However, if the designer does not carefully take into consideration the maximum displacement of these elements, the reliable flexural yielding performance could avert to shear tearing of the plates along the weld and eventually result in fracture. A correction of the initial displacement of the analytical results would further improve the correlation. Figure 4-38 shows the vertical offset between panels W1R and W1 at the south side of the walls at peak top level displacement for 1.5 EQ-3. The displacement pot used to measure the relative vertical displacement between panels can be seen to the right of the UFPs. It is also evident that the displacement of the U-plate is near its limit.
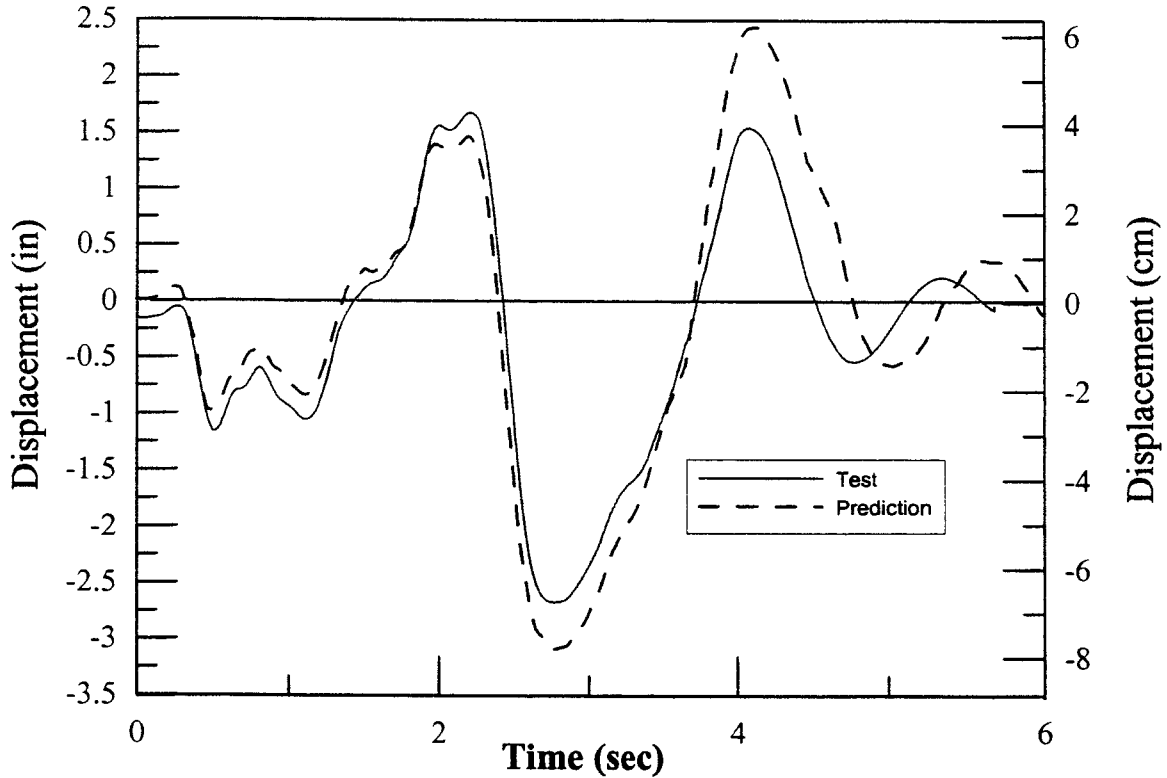
Figure 4-37 Panel Vertical Joint Relative Displacement Comparison (1.5 EQ-3)

The U-plates performed equally well for the design level test. The force time history

results of the UFP spring element for EQ-3 are shown in Figure 4-39. This force value is the

same for all the UFP springs as the relative displacement mentioned previously was the same.

The yield value for the UFP springs in the analytical model was 37.3 kips (166 kN). This resulted

in a peak value of 41 kips (182.5 kN) due to the secondary stiffness characteristics of the element.

The strains in the U-plates during testing were recorded using four high yield strain gages

placed on the bottom two U-plates shown in Figure 4-38. Two gages were located approximately

2 in. (5.1 cm) above the termination of the weld on each side of each plate as noted in Figure 4-

40. The figure also shows a plot of the strain time history of those gages. The data for this plot

was unbiased since the initial level of strain in the plates was related to the bent condition of the

plates following fabrication, corresponding to approximately 10 percent strain. Therefore, the
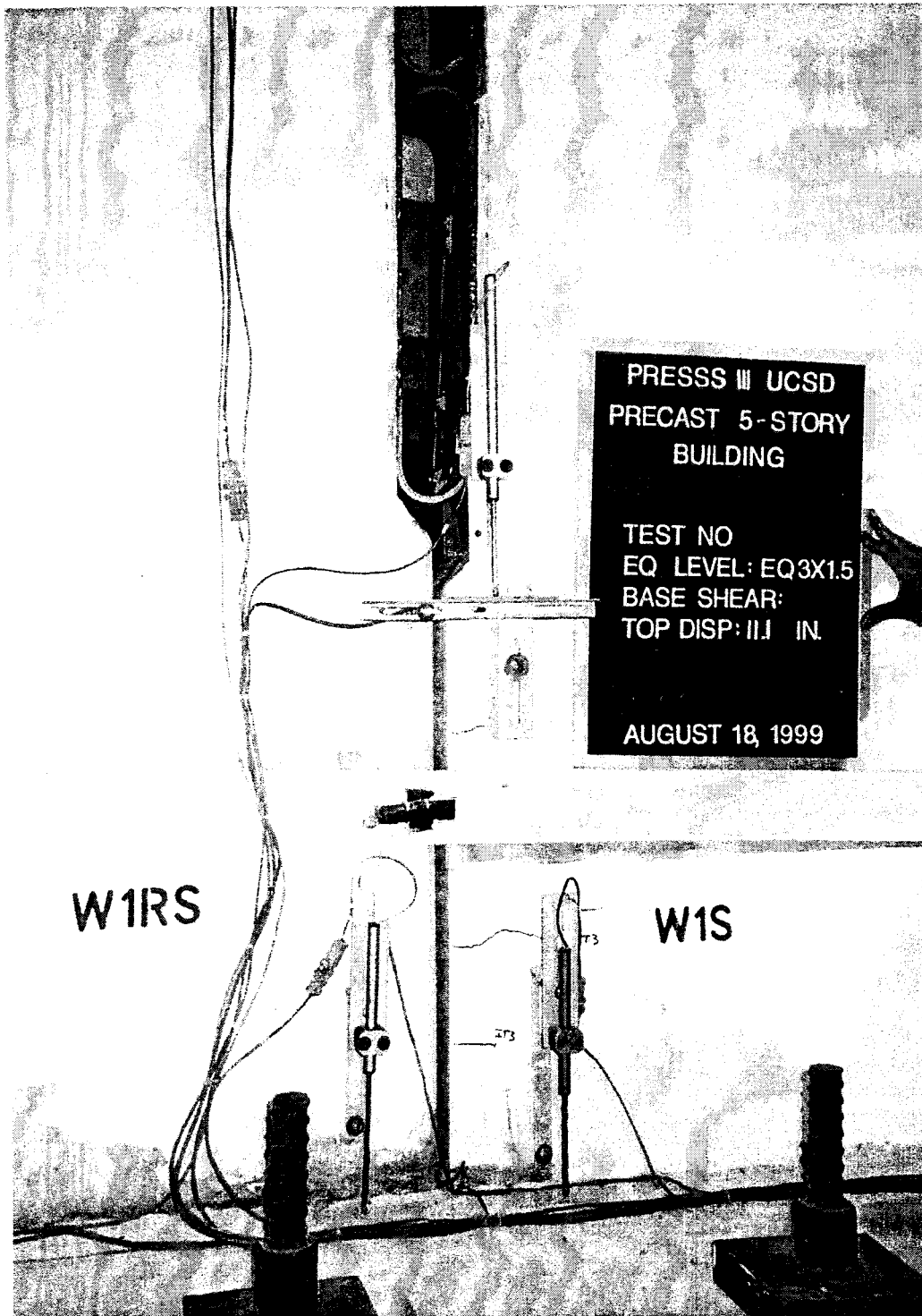
Figure 4-38 UFP Offset Picture

change in strain should be noted. Note that the maximum strain in Figure 4-40 is about 60,000 microstrain, which is less than the strain of 100,000 microstrain caused by deforming the plate to its circular shape. Reasons for the lower than expected strain changes during testing are not clear.

4.3.3 Post-Tensioning Performance

The post-tensioned threaded bars were designed to remain elastic up to and during the design level earthquake event. The force time history for the PT springs in the analytical model were taken from the design level earthquake prediction. The values are shown in Figure 4-43 and Figure 4-44. The strain recorded experimentally in the PT bars remained at an elastic level therefore the strain could easily be converted into force in the post-tension bars using the strain and an elastic modulus of 29,000 ksi (199,900 MPa). Since one spring was used to model the
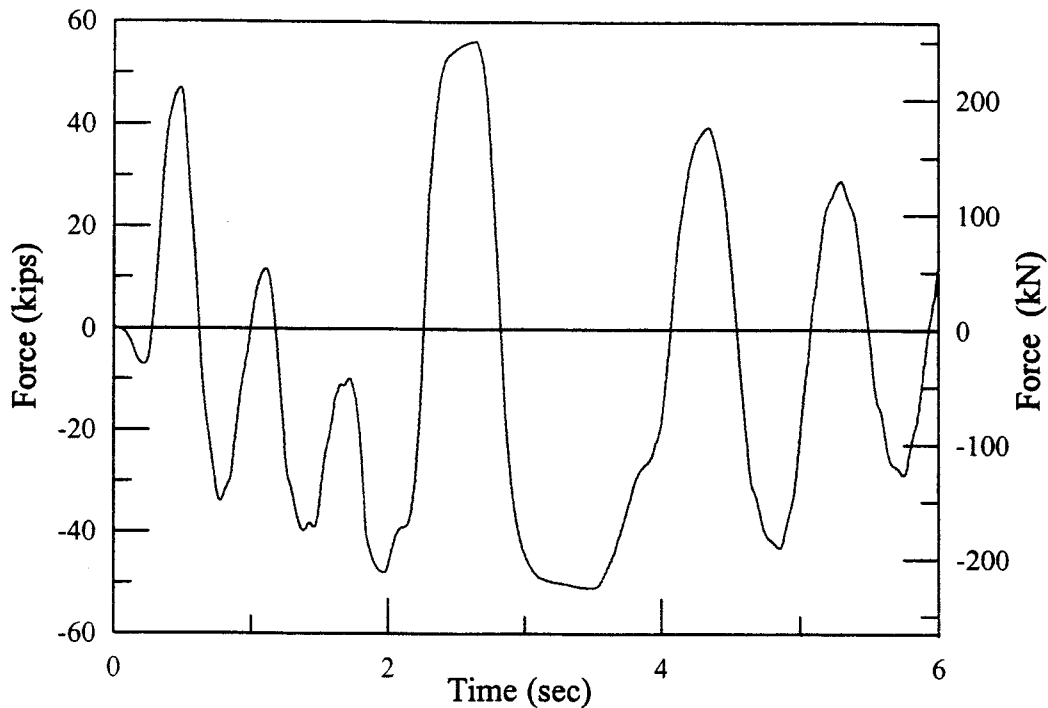
Figure 4-39 UFP Prediction Force Time History (EQ-3)
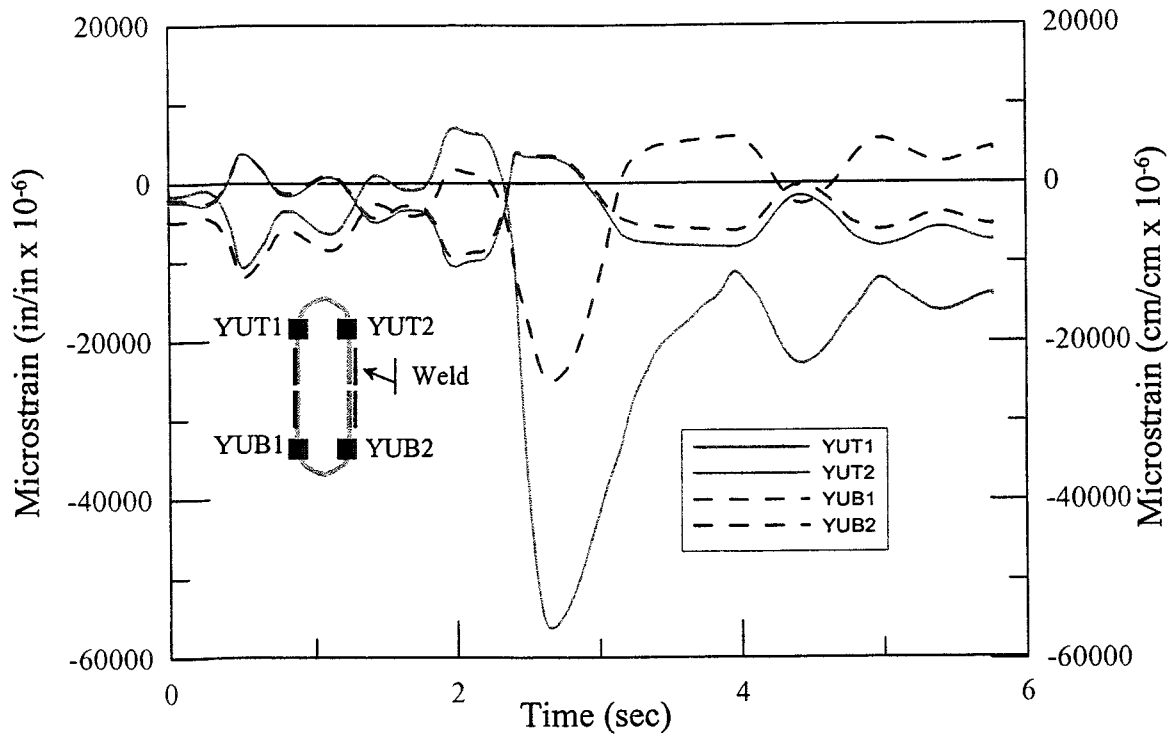
Figure 4-40 W1R PT Force Time History
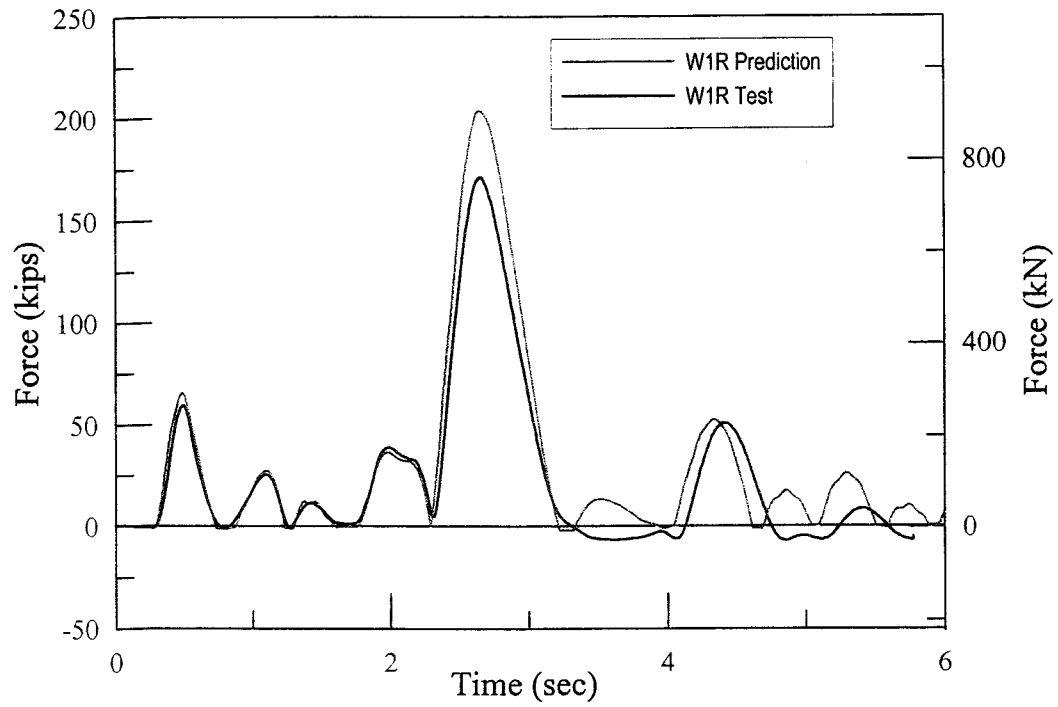
Figure 4-41 W1R PT Force Time History

110
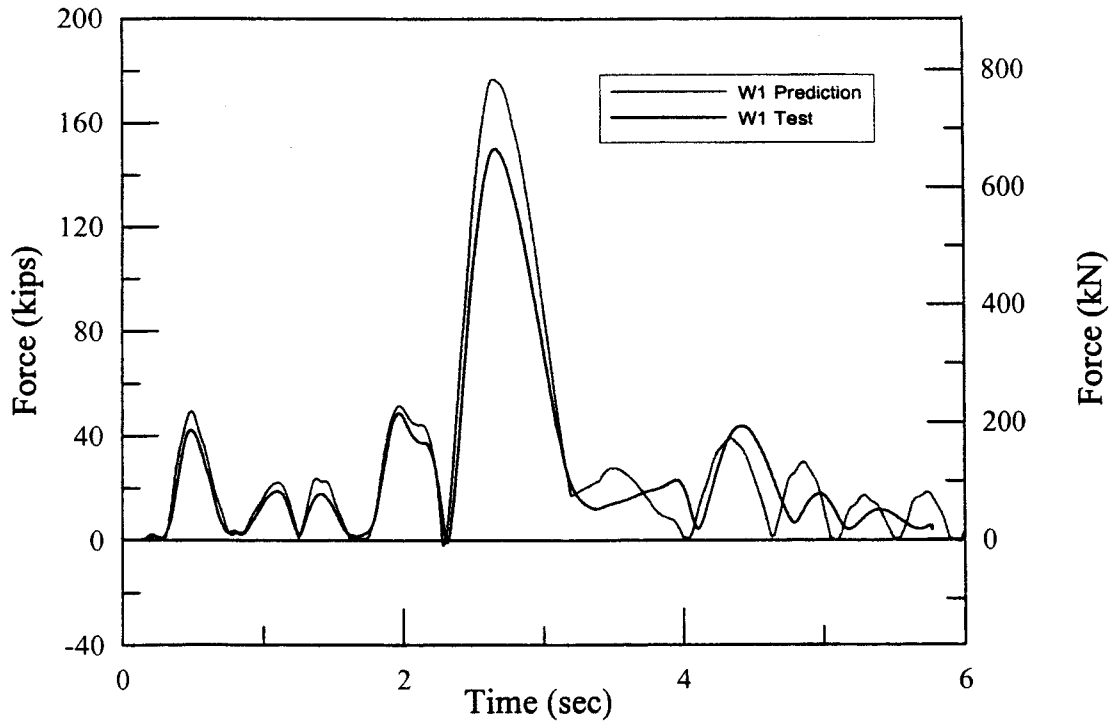
Figure 4-42 W1 PT Force Time History

four bars, the sum of the bar forces was calculated. The experimental results match reasonably

well with the analytical model, which overestimates the post-tensioning force for both W1 and

W1R. The reason for the overestimate in PT force is due to the constraints of the PT spring. The

spring is attached to a rigid link representing the base of the wall, whereas the PT bars extend the

full length of the wall. The rotation at the top of the wall where the PT bars are attached is not

exactly equivalent to the rotation of the rigid link at the base. This is the likely cause of the

overestimate. These plots represent the change in force in the PT bars and do not include the

initial post-tension force of 41 kips per bar, which corresponds to 164 kips for the four bars added

together.

Yielding of the post-tension bars did occur in the subsequent IT test and 1.5 EQ-3.

However, the bars went only slightly into the inelastic range and recovered their initial stiffness

111

characteristics. This would require a re-post-tensioning after the earthquake event in order to restore the initial post-tension force levels.

The PT bars and the rest of structural resisting elements of the test structure performed very well during the test and most likely could have ridden out an earthquake event of even larger intensity without failure, the limiting factor being the displacement capacity of the UFPs.

4.3.4   Comparison of Design and Recorded Force Envelopes

It is of interest to examine the envelopes, with height, of various actions developed in the wall. To this end, Figure 4-43 compares the envelopes of story overturning moment, story shear force, and floor forces obtained from testing the building at the EQ-3 design level. In this arrangement, the envelopes correspond to the design inverted diagonal distribution of forces. The floor forces represent the actual force levels applied to the floors by the two actuators at each floor level.

The increase in the maximum recorded base moment over the design level (see Figure 4-43 (a)), of approximately 25 percent, represents the overstrength resulting from the U-shaped energy dissipators having higher strength than the design value; and also, to a lesser extent, due to lateral resistance provided by the columns of the building, which were ignored in the design approach.

At levels above the base, it will be observed that the experimental distribution of moment is almost liner with height, whereas the design distribution is concave upwards. This discrepancy in shape is the result of higher mode effects. It is noted that the linear distribution of moment with height conforms to recommendations for cantilever structural walls made by Paulay and Priestley (Paulay, 1992).

The discrepancy between the design and experimental shear force distribution is much more marked than for moments. As can be seen in Figure 4-43 (b), the maximum base shear at the design level of excitation was 63 percent higher than the design level. The great majority of

112

this excess shear demand is the consequence of higher mode effects. It is also notable that the shear demand reduced only gradually with height.

Paulay and Priestley (Paulay, 1992) have recommended a dynamic shear amplification for a five-story cantilever wall structure of 40 percent to account for higher mode effects. This shows a reasonable agreement with the experimental value, when the overstrength due to flexural enhancement, apparent in Figure 4-43 (a), is included.

The biggest differences between experiment and design levels were in the floor forces levels. As seen in Figure 4-43 (c) the floor force levels greatly exceeded the design values at all heights of the building. It is also clear that the floor forces do not show any tendency to reduce in the lower levels, as would be expected from a predominately first mode response. For the wall direction of response, a rough approximation to the floor forces levels for design purposes would be to apply 75 percent of the design base shear as a floor force at each level.

Note that these high floor forces levels, while not significantly influencing the moment demand at the base, are important since they represent the magnitude of diaphragm forces that must be transmitted from floors to lateral force-resisting elements. These high force levels caused considerable problems in the testing of the PRESSS building.

4.4 Observations of Non-Resisting System Structural Components

Some of the non-resisting structural components did not fair as well as the structural resisting system during testing. Much of this can be attributed to the higher mode effects present in the test. This especially affected the components used to transfer the floor forces to the resisting system. Note that these high floor forces are important since they represent the magnitude of diaphragm forces that must be transmitted from floors to the lateral force-resisting elements. Recognizing the potential impact of higher mode effects, Ms. Suzanne Nakaki and Professor John Stanton, the building designers (Stanton et al., in press), had designed the diaphragm-to-wall and diaphragm-to-frame connections for force levels corresponding to 50

113

percent higher than the top story design level at each floor. These values were significantly surpassed during testing; causing much of the damage that will be described in this section.

4.4.1 Double Tee and Floor Panel Performance

The diaphragm system performed quite well in spite of the significantly higher than anticipated floor forces imposed on the building (Section 4.3.4). At the IT-1 level of testing the only cracks that appeared were on the fourth and fifth levels. Cracks began to propagate across the topping on the hollow core panels between the actuator connection panels and the hollow core planks. This cracking was expected due to the uplift of channel system supporting the floor panels as the wall rotates. Crack widths were minimal, approximately 0.05 mm. No cracking in the double tee sections was noted at this level.
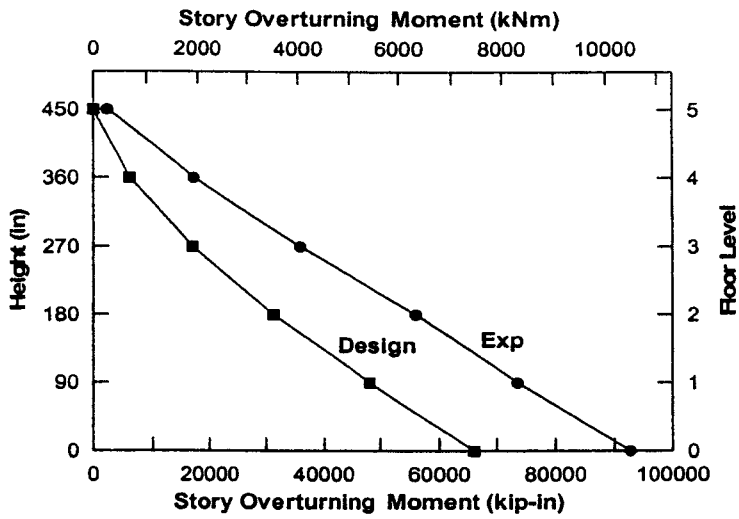
(a)
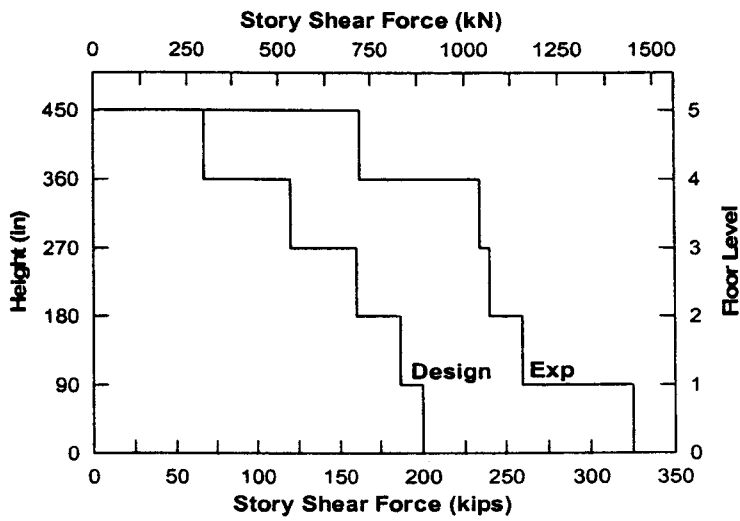
(b)
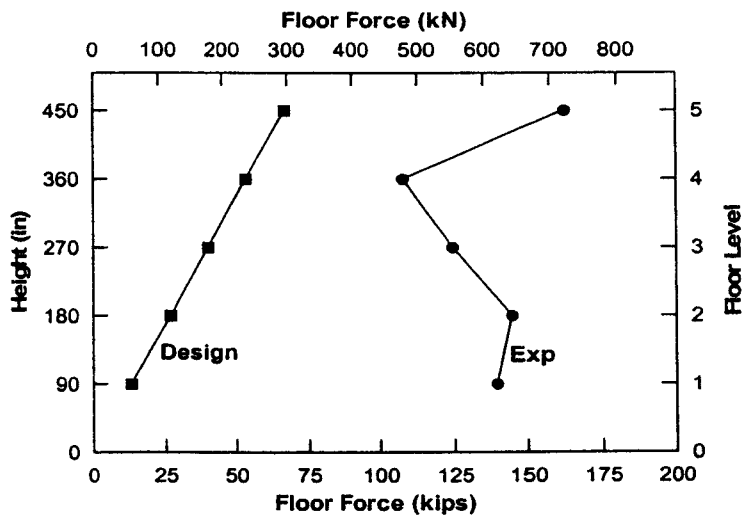
(c)

Figure 4-43 Design and Experiment Envelopes

The IT-2 level test caused further propagation and opening (to 0.1mm) of the cracks noted previously for the floor panels, while no damage was noted in the double tees. A 3/8" lift up of the south side of the double tees on the first level was noted at positive maximum displacement. The EQ-3 level of testing was paused at peak displacement of 8.28" and widening of the fourth and fifth level cracks was noted.

The subsequent IT-3 test showed the first significant signs cracking to the double tee sections. This was directly below the actuator connection locations due to the vertical force the actuators applied to the structure. The cracking was minimal, and such localized force concentrations on this area would not occur during a real earthquake event. More importantly no cracking was evident around the region of the double tee-to-wall connection and no vertical sliding of the connection device was notable. In the negative direction failure of the steel tabs between the gravity beam and the double tee occurred at all floors due to the differential movement between the two components. At the floor panel levels widening of the previously mentioned cracks to 0.3 mm occurred. New cracks also began to form between the hollow core and frame actuator connection panels. A diagonal crack running across the hollow core panels due to torsion effects on these elements was evident. A crack of 2.2 mm width was noted between the pre-tensioned beam and the frame actuator connection panels due to rotation of the beam.

At the peak displacement of 1.5 EQ-3 there was significant raising of the double tees on the first floor relative to the TCY Gap beams. This caused a significant stress in the X-plates connecting the top of the double tees to the top of the beam. At the negative peak displacement a crack between the channel and double tee at the connection to the wall was noted indicating the high levels of shear forces in the area. Further widening of the cracks on the fourth and fifth floors continued. Figure 4-45 shows the crack between actuator and hollow core panels at the fifth level at peak negative displacement during 1.5 EQ-3.

116

The diaphragm system provided the necessary transfer of the earthquake loads to the resisting system and suffered only minimal damage even at levels up to 50 percent higher than design intensity earthquakes and floor forces significantly higher than designed for.

4.4.2 Gravity Frame Performance

The gravity frame provided an increased resistance to the earthquake forces input to the structure. Figure 4-45 shows the flexural cracks marked on the gravity column. These cracks began to occur at IT-2, along with some flexural cracking in the seismic frame columns bases, and continued through the subsequent tests up to IT-3. At IT-3 no more significant extension of the gravity column flexural cracking occurred, but significant lift-off of the column base due to column rotation began to occur. The cracking of the seismic frame bases occurred in the grout region. Lift off of the base of the gravity columns is evident in Figure 4-45, taken at peak displacement during 1.5 EQ3.

During the IT-3 test minor cracking of the gravity beams began to occur on the first through third levels. Incipient spalling was also evident where the gravity beams frame into the gravity columns. As the column rotates in the direction of top level displacement, the solid actuator connection panel bears on the corner of the gravity beam being pushed up ward by the column rotation. As displacements increased the damage became worse. At the top level during 1.5 EQ-3 the gravity beam corners began to spall off exposing the reinforcing.
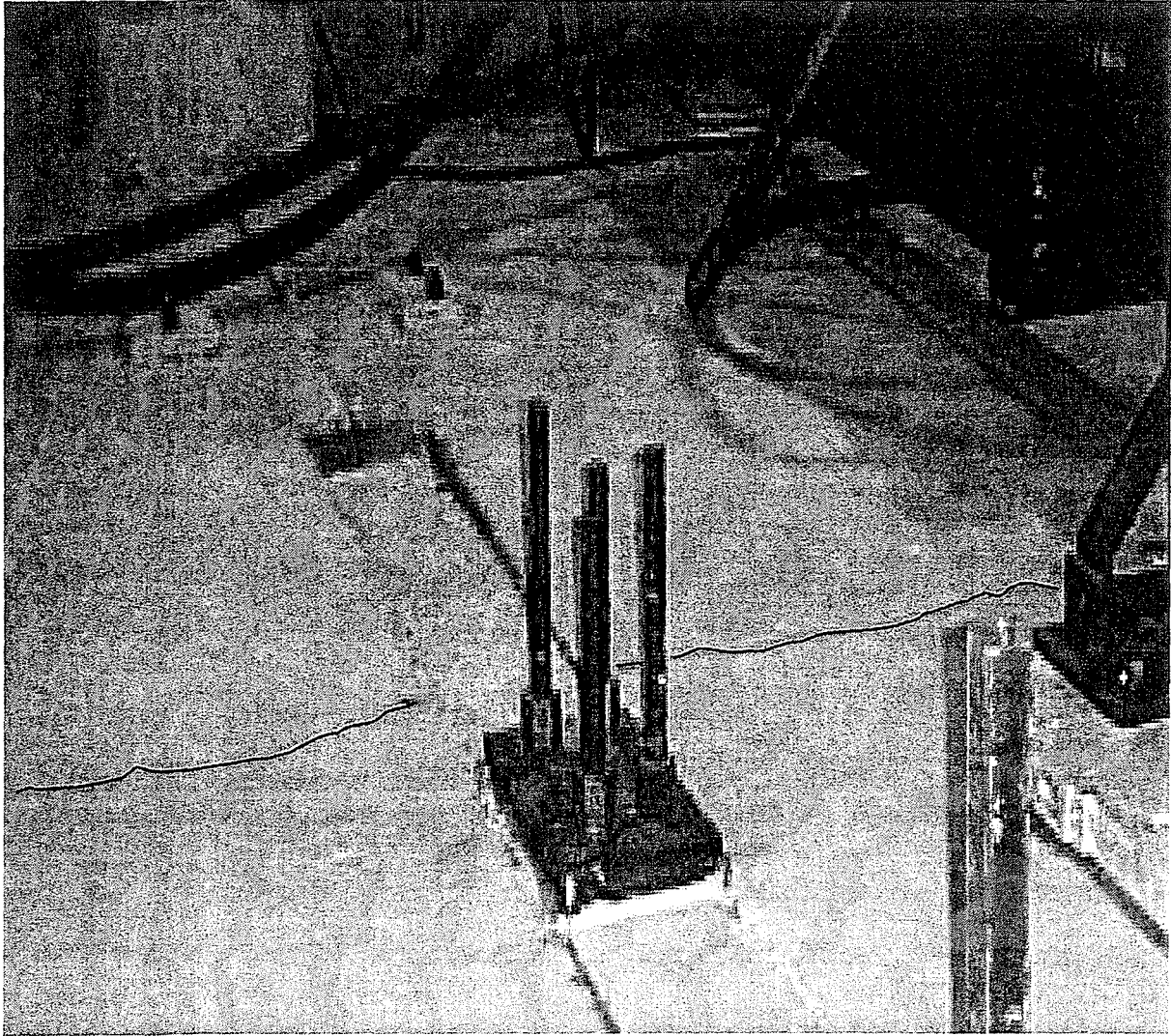
Figure 4-44 Hollow Core Crack Picture (1.5 Eq-3)

The sign in the image reads:

PRESSS III UCSD
PRECAST 5-STORY
BUILDING

TEST NO
EQ LEVEL: EQ3X1.5
BASE SHEAR:
TOP DISP: 11.1 IN.

AUGUST 18, 1999
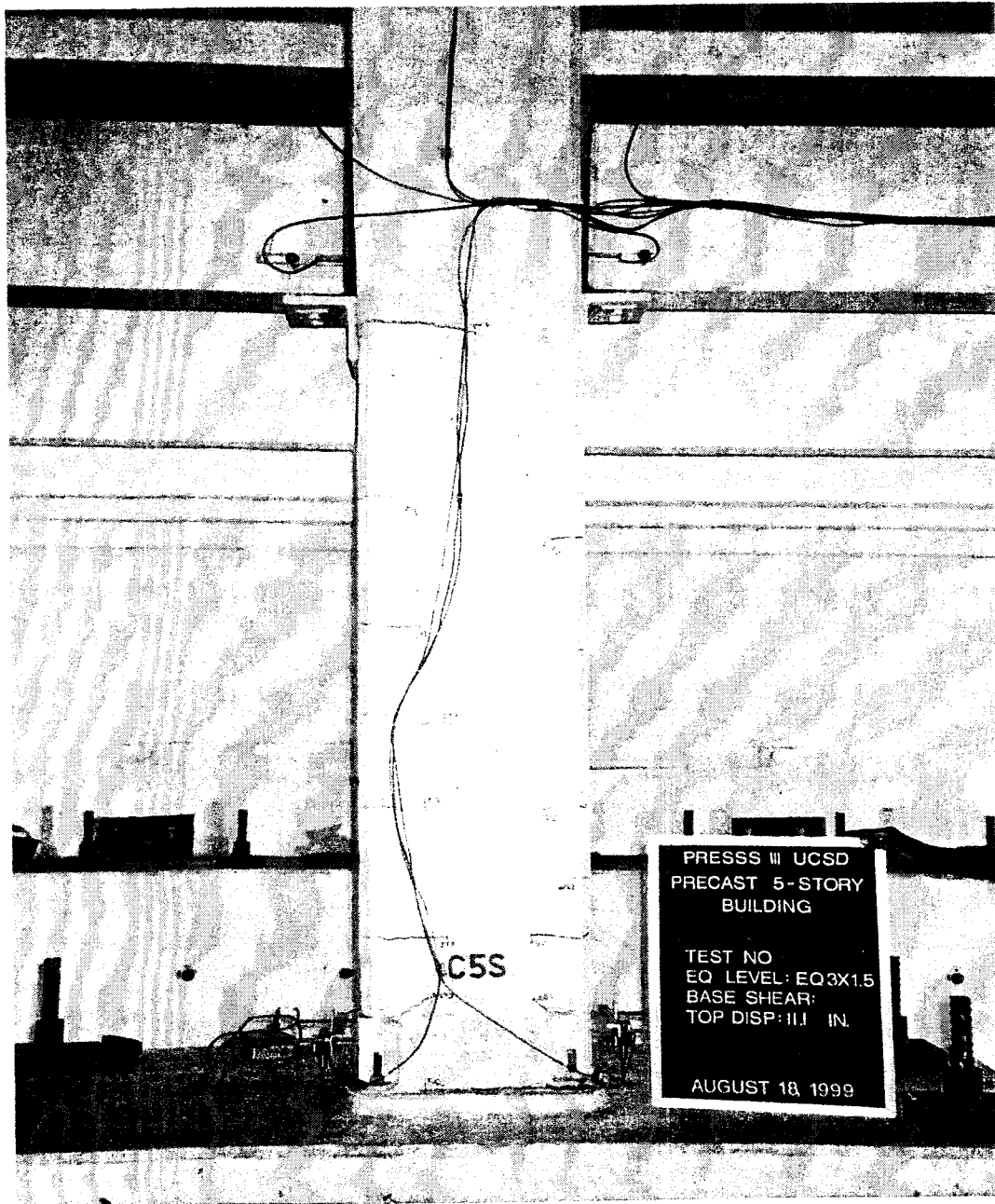
Figure 4-45 Gravity Column Flexural Cracking

4.4.3 Out of Plane Performance

The out of plane performance of the wall panel system was excellent as well. The frame direction of the *PRESSS* Five-Story Building was tested after the conclusion of the wall direction testing. The results associated with the frame direction are presented elsewhere (Pampanin et al., in press). The building was taken to increasingly higher loads as in the wall direction, with the final tests on the building being Inverse Triangular load tests to maximum drift angles exceeding 4 percent. This forced the lower levels of the wall to be subjected to a flexural drift of 4 percent between the base and floor level 1.

No visible signs of cracking occurred in the tests leading up to and including the earthquake input, EQ-2. The maximum top floor displacement at this level was 6.84 inches (17.4 cm), with a maximum base shear of 333.2 kips (1483 kN). Figure 4-46 shows the minimal amount of flexural cracking that occurred at IT-5, the final test on the building. The maximum top floor displacement and base shear for this test was 18.48 inches (46.9 cm) and 369.9 kips (1646 kN), respectively. The maximum crack width was less than 0.1 mm, and closed upon removal of load.
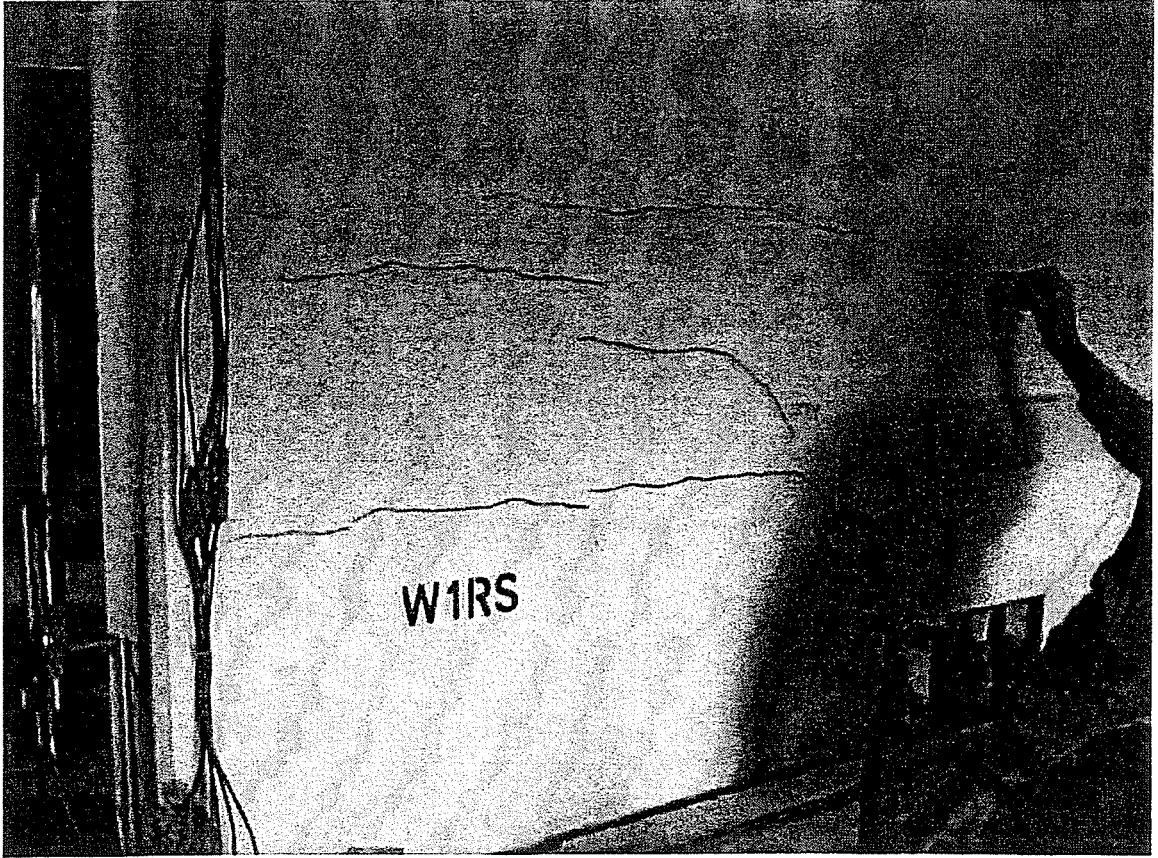
Figure 4-46 Out of Plane Flexural Cracking

5 CONCLUSIONS

5.1 Overall Wall Direction Performance

The superior performance of the PRESSS Five-Story Building in the wall direction of testing is evident from the results presented in this report. The precast wall panel system, implementing Non-Linear Elastic (NLE) and energy dissipation behavior characteristics, proved to be an ideal lateral seismic load-resisting system, responding to earthquake loads exceeding design levels with well-predicted behavior. Under the UBC Zone 4 design level earthquake, the building achieved a maximum base moment resistance of 90,500 kip inches (10,230 kNm) at a top floor level displacement of 8.28 inches (21 cm) and a peak base shear resistance of 335 kips (1490 kN).

The Displacement Based Design (DBD) procedure was further validated by this test, proving the fundamental accuracy of the procedure on a real building under imposed loads equivalent to a real earthquake. The equivalent viscous damping value of 15.5 percent calculated from the IT-3 tests correlates well with the DBD assumption of 20 percent damping, when the 5 percent assumed elastic damping is added.

It was shown that with adequate consideration to detailing, the inherent dry jointed properties associated with precast concrete are not a limitation but an advantage in such systems. The combination of the unbonded post-tensioning steel's NLE behavior at the foundation joint, with the added energy dissipating behavior of the UFPs at the vertical joint, resulted in a system capable of providing hysteretic damping behavior while retaining self-centering capability. These component behavior mechanisms were verified in an actual building environment, where behavior unaccounted for in component tests performed in earlier phases of the *PRESSS* program was present. The grouted splice sleeve components provided connection across the construction joint at mid-height of the building that was adequate to resist horizontal shear slip of the panels.

By limiting the strain in the PT bars to remain at elastic levels, the PT force remained intact to provide resistance to shear slip at the foundation joint through friction behavior. By detailing the high compression regions at the base of the panels with proper levels of confinement, the large compression forces could be carried to provide moment resistance.

Furthermore, the higher mode floor force effects must be taken into consideration. By not recognizing the impact of the higher mode forces, connection detailing may be undersized for forces that would be seen in an earthquake.

Not only did the test results show that the precast wall system provides excellent seismic load resistance, they also show that the force and displacement characteristics of the system can be accurately predicted with simple design analytical models.

5.2   Analytical Modeling Performance

The main goal of the theoretical work done at UCSD was to produce a simple analytical model, one that any typical design firm could reproduce with minimal effort, one that could provide an accurate prediction for force and displacement behavior of a building employing jointed precast panels as a lateral load resisting system. This goal was successfully achieved as demonstrated by the comparisons of analytical and test behavior described in the Test Observations section of this report.

The original model had some inaccuracies that minimally influenced the model's performance as validated by subsequent analyses described in Chapter 3. Even so, the original model provided predictions of overall forces that were as much as20 percent below peak levels as shown by the original prediction pushover in Figure 4-7. The cause of the discrepancy is related to low UFP yield values and the analytical model not taking into account the added stiffness of the columns in the building. The column stiffness can be assessed by approximating the column moment resistance and adding that moment to the analytical model predicted value as described in 4.1.1.

123

The results of the component comparisons showed fair accuracy, demonstrating that the geometric behavior of the wall could correctly be modeled using the combination of frame and rigid link elements. Assumptions made for the force-displacement characteristics of the post-tensioning bars were validated by the test and provided accurate correlation between analysis and test.

It is apparent that some improvement could be made in modeling the specific components of the panel system, namely the compression-only and UFP springs. The "spikes" which occur in the analytical model results are a consequence of the foundation being simplified as two springs at the centers of compression for each panel. This results in an impact force that is distributed through the model, which shows up as spikes in the analytical force results. Furthermore, adding vertical mass to the model may increase this dynamic load on the foundation elements. A distributed spring foundation system could eliminate this effect, or added damping elements in parallel with the single compression-only springs.

One other spring element in the model, the UFP spring, could also be improved. Although peak forces in the element matched well with the test UFP results as presented in Chapter 4, the force time history showed only moderate agreement. Experiments done on the UFP at a component level, as described in Chapter 3, were based on a more sinusoidal input. The behavior of the stainless steel in a more dynamic type of input appears to be different, as shown from the pseudodynamic test results; and further investigation in this area needs to be done. It is evident that the work hardening material properties of the stainless steel complicate the analysis of its post-yield behavior. A train type record may improve this behavior by capturing the effect of cycling UFP elements through many earthquake records. It must be noted that this only had a limited impact on the overall analytical/test correlation; and more importantly, the yield force in the UFP *could* be well predicted.

Finally, the discrepancy in floor force levels between model and test need to be better evaluated. Adding column elements linked to the wall in the Ruaumoko model could further

improve the analysis. This, again, had minimal impact on the force displacement characteristics showing that the simple analytical model could prove to be a useful tool for precast panel building design.

5.3 Design/Model Recommendations

Detailed design recommendations for precast concrete seismic structural systems are being proposed as part of the third phase of the *PRESSS* program (Stanton et al., in press). The Stanton et al. report will document detailed design recommendations for both the frame and wall precast systems. Recommendations for development of a simple precast wall analytical model that will produce accurate building force and displacement design values are made subsequently.

The assumptions made to create the analytical model used to predict the behavior of the *PRESSS* test building are straight forward and can be applied to design any building using precast wall panel seismic resisting systems based on basic panel geometry and the subsequent recommendations for the other elements.

The frame elements in the model are the wall panels and rigid links. Since the panels can be designed to remain elastic throughout the earthquake event, they can be represented by frame elements using the gross section properties of the wall. These members can be zero weight elements since this weight can be input in the form of external nodal forces as will be described later. The rigid links should use member properties one hundred times those for the wall members, or rigid links specific to the analysis program should be used. Nodes can be placed at each story level to serve as connection points between the panels and other elements. The mass that will be distributed to the lateral load resisting elements through the diaphragm should be correctly evaluated. Once the mass is determined for each floor level it can be lumped at the nodes at each story height. The wall members and rigid links should be placed according to panel geometry.

125

The compression-only base springs can be modeled as bilinear elastic springs with a zero yield force in the direction of lift-off and a zero secondary slope stiffness. The initial compression stiffness should be evaluated according to foundation characteristics. The value for the model was based on a concrete foundation compression displacement of 0.05 inches (0.13 cm) at 500 kips (2225 kN) force. The location of these springs can be at the center of compression of the wall panel base calculated as follows:

- **Interior Base Compression-Only Springs.** The depth of the rectangular stress block is

$$a = \frac{P - V_u}{0.85 f'_c b_w} \tag{5.1}$$

  where P is the axial load on the wall including the PT force, the weight of the panels, and any additional gravity load on the panels; b_w is wall width and V_u is the sum of the shear yield forces in the UFPs along the vertical joint.

- **Exterior Base Compression-Only Springs.** The depth of the rectangular stress block is the same as above only the shear of the UFP is added to the panel axial load such that

$$a = \frac{P + V_u}{0.85 f'_c b_w}$$

$$\tag{5.2}$$

The distances of the base rigid links will be from the panel centerline to the center of compression of the stress blocks as calculated.

Modeling of the PT springs is done using an element with bi-linear hysteresis characteristics. The initial stiffness, k_{pt}, can be found

$$k_{pt} = \frac{E_{pt} A_{pt}}{\lambda_{pt}} \tag{5.3}$$

where E_{pt} is the elastic modulus of the post-tensioning, A_{pt} is the sum of the cross-sectional area for the PT bars per panel, and λ_{pt} is the unbonded length of the PT bars. Yield value can be calculated based on the specified yield stress of the type of post-tensioning used. A secondary stiffness of two percent is suggested to account for the post- yield behavior of the PT bars.

The post-yield characteristics of the U-shaped flexural plates are a much more complicated issue. The Al-Bermani hysteretic behavior was used in the UCSD analytical model, but it is felt that a simplified bilinear hysteresis spring would work equally as well. The initial stiffness of the UFP was determined by using component tests and matching hysteretic behavior. However, a good approximation based on the plates tested is

$$k_u = \frac{12 E_{ss} I}{\lambda_{ub}^{\ 3}} \tag{5.4}$$

where E_{ss} is the elastic modulus of the stainless steel, I is the moment of inertia of the UFP, and λ_{ub} is the length of the bent portion of the plate, or half the circumference corresponding to the centerline radius of the UFP. The yield shear value can be determined from the plastic moment capacity of the plate

$$V_u = \frac{M_p}{\dfrac{\lambda_u}{2}} \tag{5.5}$$

where λ_u is the center-to-center distance between the U flanges. It should be noted that although this agreed well with the tests performed at UCSD, the thickness of the plates tested were all the same. Plates of different thickness may not have agreeing stiffness with the suggested approach. The nodes connecting the UFP spring should be constrained in the global X-direction and the spring should only have stiffness in the global Y-direction.

By implementing this simple analytical model, the designer can determine accurate force-displacement characteristics, and by using a time history analysis program such as Ruaumoko,

different input accelerations can be used, as they are best suited to the specific location of the building. The simplicity of the analytical model is a direct result of the jointed connection mechanisms inherent in precast concrete. This is further evidence of the great advantages of precast concrete for seismic structural design.

5.4   Impact on Seismic Design

As shown in the tests performed in this project, the precast wall system is a viable solution for building design in seismic areas. With the results of this test, it is the goal of members of the PRESSS Project to provide design recommendations to be used in future design codes. This will offer a cost efficient and working solution to engineers to be used in new construction. Further details on this will be presented in Design Guidelines for Precast Seismic Structural Systems (Stanton et al., in press). The excellent test results support the view that Precast Seismic Structural Systems, due to their low cost and excellent earthquake performance, will become the standard for construction as we advance into the Third Millennium.

Appendix A

Coding For Ruaumoko Dynamic Time History Analysis

Ruaumoko File


```
PRESSS TEST WALL            !  Units kips and inches
2 0 1 1 1 0 0 0 0 0                         ! Control Parameters
43 45 9 5 1 2 386.4 2.5 5.0 0.003 6.0 -1.5 ! Frame and Time-history
1 1 1 1 1 10 0.7 0.1                        ! Output and Plotting Option
0  0                                        ! Iteration Control
```

NODES

			Fixidity			Coupling			
Node	Xcor	Ycor	x	y	z	x	y	z	Output
1	0.0	-3.0	1	1	1	0	0	0	0
2	49.6	-3.0	1	1	1	0	0	0	0
3	102.6	-3.0	1	1	1	0	0	0	0
4	104.6	-3.0	1	1	1	0	0	0	0
5	157.6	-3.0	1	1	1	0	0	0	0
6	207.2	-3.0	1	1	1	0	0	0	0
7	0.0	0.0	0	0	0	0	0	0	0
8	49.6	0.0	1	0	0	0	0	0	0
9	102.6	0.0	0	0	0	0	0	0	0
10	104.6	0.0	0	0	0	0	0	0	0
11	157.6	0.0	1	0	0	0	0	0	0
12	207.2	0.0	0	0	0	0	0	0	0
13	49.6	90.0	0	0	0	0	0	0	0
14	103.6	90.0	0	0	0	13	0	0	0
15	103.6	90.01	0	0	0	13	0	0	0
16	157.6	90.0	0	0	0	13	0	0	0
17	49.6	180.0	0	0	0	0	0	0	0
18	103.6	180.0	0	0	0	17	0	0	0
19	103.6	180.01	0	0	0	17	0	0	0
20	157.6	180.0	0	0	0	17	0	0	0
21	49.6	270.0	0	0	0	0	0	0	0
22	103.6	270.0	0	0	0	21	0	0	0
23	103.6	270.01	0	0	0	21	0	0	0
24	157.6	270.0	0	0	0	21	0	0	0
25	49.6	360.0	0	0	0	0	0	0	0
26	103.6	360.0	0	0	0	25	0	0	0
27	103.6	360.01	0	0	0	25	0	0	0
28	157.6	360.0	0	0	0	25	0	0	0
29	49.6	450.0	0	0	0	0	0	0	0
30	103.6	450.0	0	0	0	29	0	0	0
31	103.6	450.01	0	0	0	29	0	0	0
32	157.6	450.0	0	0	0	29	0	0	0
33	228.6	0.0	0	0	0	0	0	0	0
34	228.6	90.0	0	0	0	13	0	0	0
35	228.6	180.0	0	0	0	17	0	0	0
36	228.6	270.0	0	0	0	21	0	0	0
37	228.6	360.0	0	0	0	25	0	0	0
38	228.6	450.0	0	0	0	29	0	0	0
39	220.6	0.0	1	0	0	0	0	0	0
40	220.6	-3.0	1	1	1	0	0	0	0
41	236.6	0.0	0	0	0	0	0	0	0
42	236.6	-3.0	1	1	1	0	0	0	0
			Fixidity			Coupling			
Node	Xcor	Ycor	x	y	z	x	y	z	Output

```
  43    228.6    -3.0      1 1 1   0 0 0   0

ELEMENTS
              Node
Nm.  Type  1    2
  1    1    7    8
  2    1   10   11
  3    2    8   13
  4    2   13   17
  5    2   17   21
  6    2   21   25
  7    2   25   29
  8    2   11   16
  9    2   16   20
 10    2   20   24
 11    2   24   28
 12    2   28   32
 13    3   13   14
 14    3   15   16
 15    3   17   18
 16    3   19   20
 17    3   21   22
 18    3   23   24
 19    3   25   26
 20    3   27   28
 21    3   29   30
 22    3   31   32
 23    4    1    7        !BASE SPRING
 24    5    2    8        !PT SPRING
 25    4    3    9        !BASE SPRING
 26    4    4   10        !BASE SPRING
 27    5    5   11        !PT SPRING
 28    4    6   12        !BASE SPRING
 29    6   14   15        !U SPRING
 30    6   18   19        !U SPRING
 31    6   22   23        !U SPRING
 32    6   26   27        !U SPRING
 33    6   30   31        !U SPRING
 34    1    8    9
 35    1   11   12
 36    7   33   34        !GRVTY COL
 37    7   34   35        !GRVTY COL
 38    7   35   36        !GRVTY COL
 39    7   36   37        !GRVTY COL
 40    7   37   38        !GRVTY COL
 41    9   40   39        !GRVTY COL BS
 42    8   43   33        !GRVTY COL PTS
 43    9   42   41        !GRVTY COL BS
 44    1   39   33        !GRVTY COL RL
 45    1   41   33        !GRVTY COL RL


PROPS (see Section 3.3 for Descriptions)
1 FRAME                              !Rigid base
  1 0 0  0 0 0                              ! Parameters
  5.2e5 2.2e5  8.64e4 0.  8.39e7 0         ! Elastic properties
```

131

```
2 FRAME                                      !Wall
   1 0 0   0 0 0                                    ! Parameters
   5.2e3  2.2e3  864  736  839808  0.0             ! Elastic Properties

3 FRAME                                      !Rigid wall links
   1 0 0   0 0 0                                    ! Parameters
   5.2e5  2.2e5  8.64e4  0.  8.39e7  0             ! Elastic properties

4 SPRING                                     !Compression only base springs
   1 15 0   0  10000   .1 .1 0 0 0 0.0 0.0 0.0 0.0    ! Parameters
   0.1 -800   10000 -10000 10000 -10000             ! Yield Surface

5 SPRING                                     !PT springs
   1 2 0 0 197 0.1 0.1 0 0.02 0 164.0 0.0 0.0 0.0    ! Parameters
   375 -375   10000 -10000 10000 -10000             ! Yield Surface

6 SPRING                                     !U Plate springs
   1 26 0 0 186.6 0.1 0.1 0 0.015 0 0 0.0 0.0 0.0    ! Parameters
   51.3 -51.3   10000 -10000 10000 10000            ! Yield Surface
   0.001   0.001                                     ! Hysterisis

7 FRAME                                      !Grvty Col
   1 0 0   0 0 0                                    ! Parameters
   5.4e3  2.3e3  1814  1814  49000  0.0             ! Elastic Properties

8 SPRING                                     !PT springs GC
   1 2 0 0 154   0.1 0.1 0 0.02 0 498.6 0.0 0.0 0.0    ! Parameters
   3004 -3004   10000 -10000 10000 -10000           ! Yield Surface

9 SPRING                                     !Comp. only base springs GC
   1 15 0   0  10000   .1 .1 0 0 0 0.0 0.0 0.0 0.0    ! Parameters
   0.0 -6400   10000 -10000 10000 -10000            ! Yield Surface

WEIGHT 0
        Lumped Nodal Weight
Node      x      y
  13    175.5  0.0
  16    175.5  0.0
  17    175.5  0.0
  20    175.5  0.0
  21    175.5  0.0
  24    175.5  0.0
  25    175.5  0.0
  28    175.5  0.0
  29    175.5  0.0
  32    175.5  0.0




LOADS
        Static Load
Node  x       y       z
1    0.0     0.0     0.0
2    0.0     0.0     0.0
3    0.0     0.0     0.0
```

```
4      0.0        0.0       0.0
5      0.0        0.0       0.0
6      0.0        0.0       0.0
7      0.0      -120.88        0.0
8      0.0        0.0       0.0
9      0.0      -113.12         0.0
10     0.0      -113.12         0.0
11     0.0        0.0       0.0
12     0.0      -120.88        0.0
13     0.0        0.0       0.0
14     0.0        0.0       0.0
15     0.0        0.0       0.0
16     0.0        0.0       0.0
17     0.0        0.0       0.0
18     0.0        0.0       0.0
19     0.0        0.0       0.0
20     0.0        0.0       0.0
21     0.0        0.0       0.0
22     0.0        0.0       0.0
23     0.0        0.0       0.0
24     0.0        0.0       0.0
25     0.0        0.0       0.0
26     0.0        0.0       0.0
27     0.0        0.0       0.0
28     0.0        0.0       0.0
29     0.0        0.0       0.0
30     0.0        0.0       0.0
31     0.0        0.0       0.0
32     0.0        0.0       0.0
33     0.0        0.0       0.0
34     0.0        0.0       0.0
35     0.0        0.0       0.0
36     0.0        0.0       0.0
37     0.0        0.0       0.0
38     0.0        0.0       0.0
39     0.0      -600.9         0.0
40     0.0        0.0       0.0
41     0.0      -600.9         0.0
42     0.0        0.0       0.0


EQUAKE
 3 2 0.003 1.0  -1


START
```

Appendix B

Photo Documentation

Reaction Tower

T NO.

LEVEL : EQ3

SE SHEAR :

P DISP : 8.1 IN.

UGUST 18, 1999
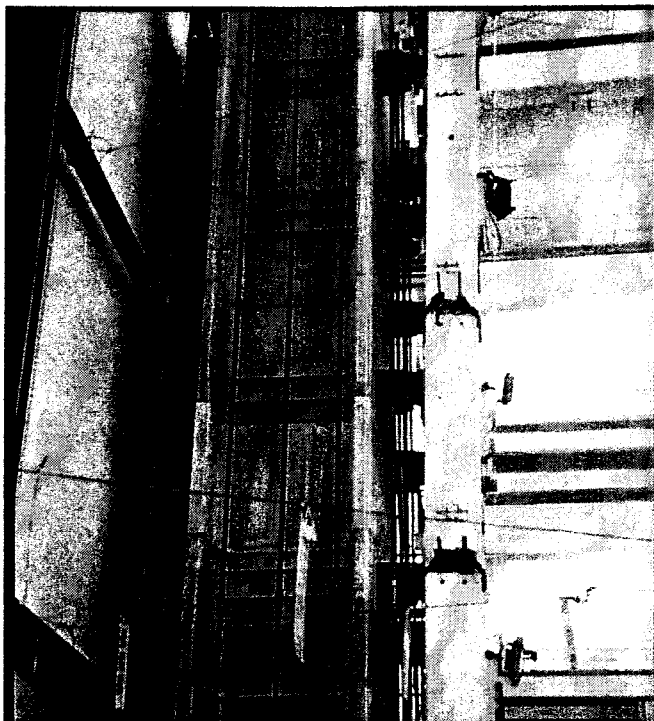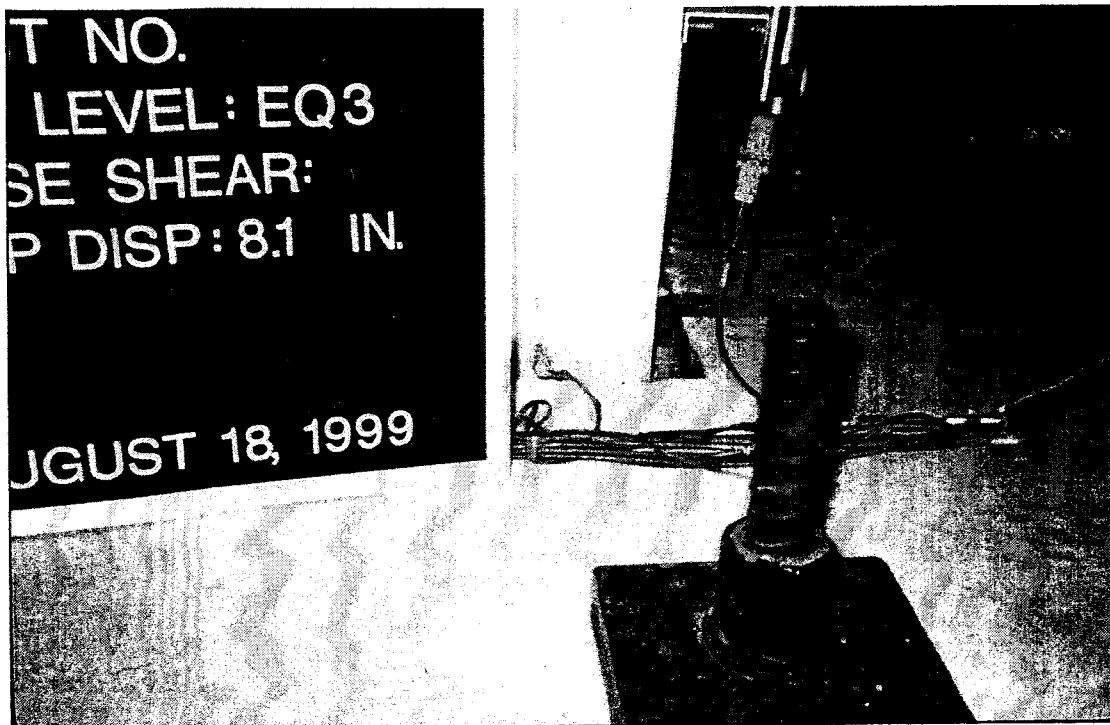
Exterior Wall Base (IT-3)
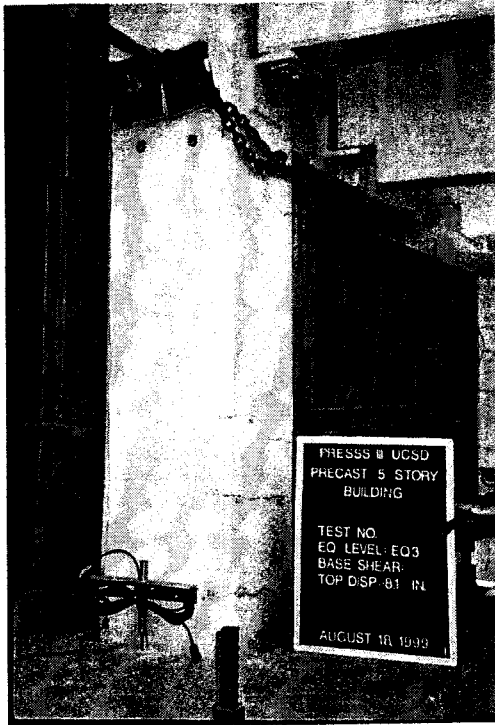
Exterior Column Non-Prestressed Frame (IT-3)
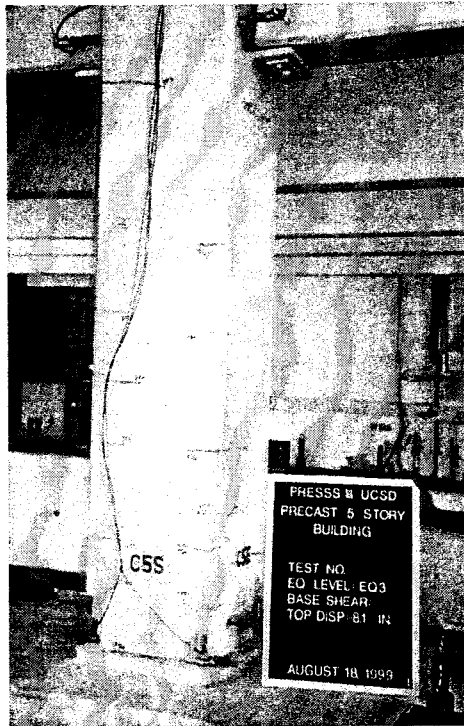
Interior Column Gravity Frame (IT-3)
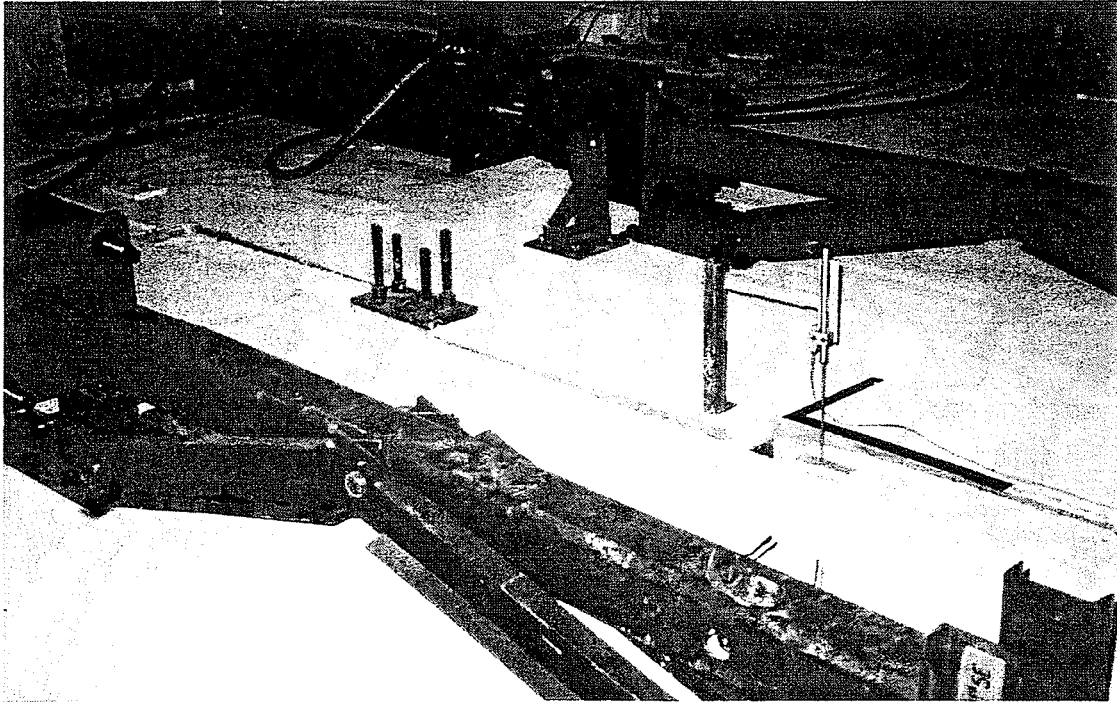
Wall Top Vertical Joint Offset (IT-3)
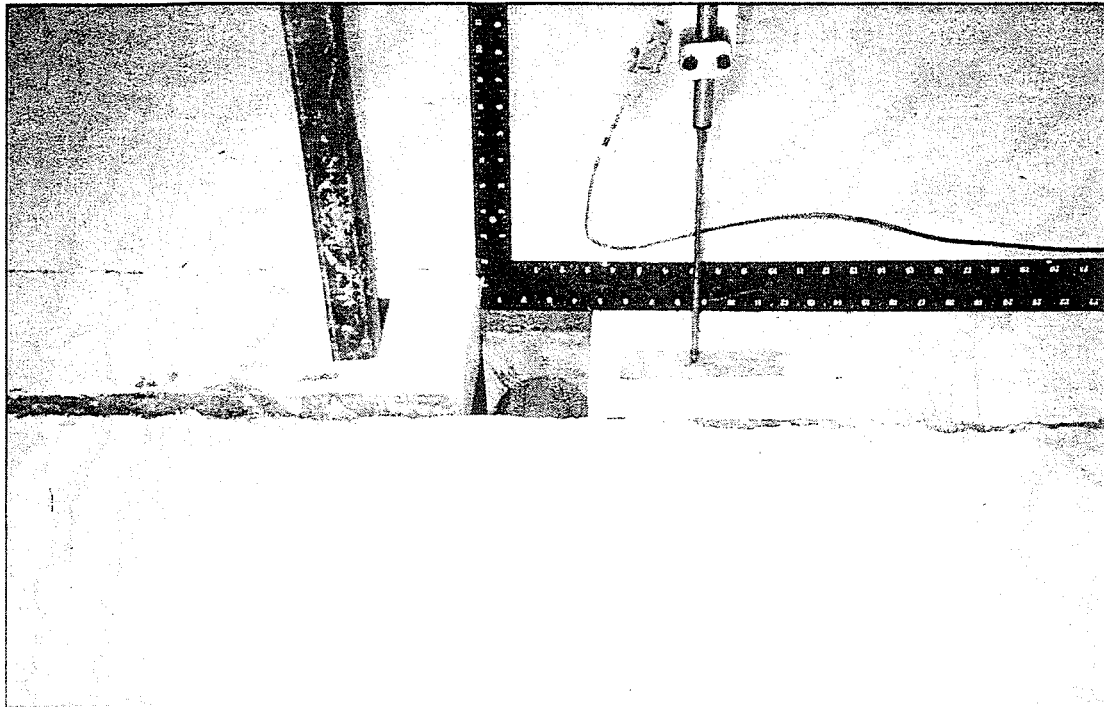
Wall Top Vertical Joint Offset (IT-3)

Wall Base Vertical Joint Offset (IT-3)

Wall Base Vertical Joint Offset (IT-3)

138
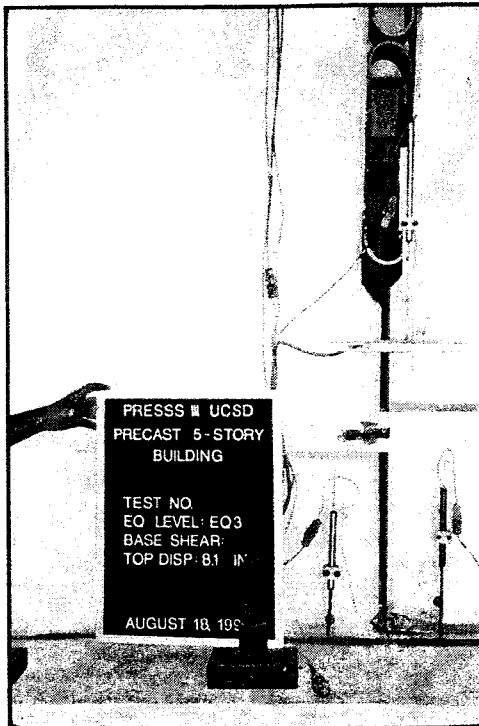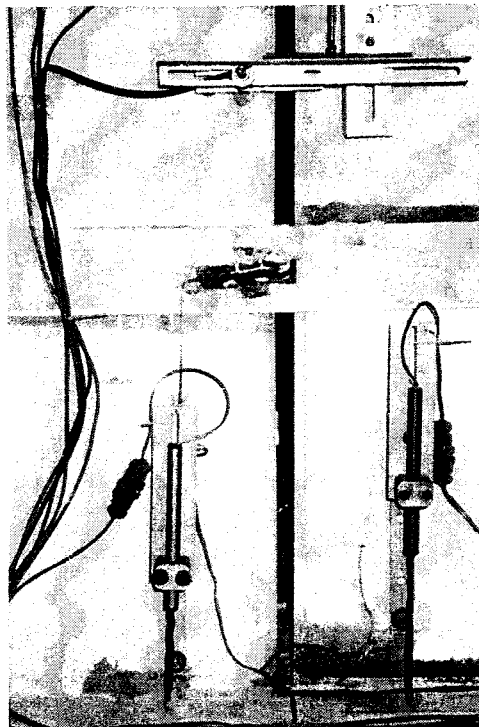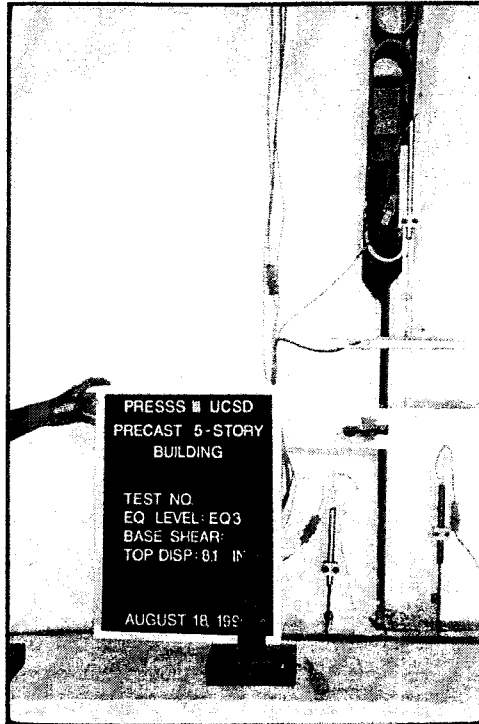
UFP Offset (IT-3)
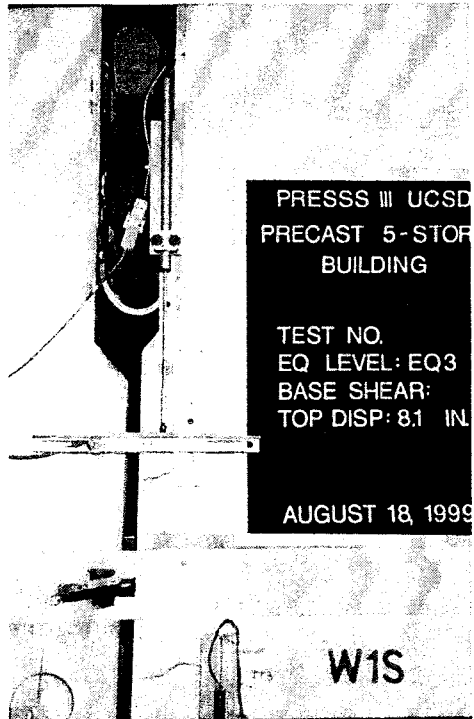
UFP Offset (IT-3)
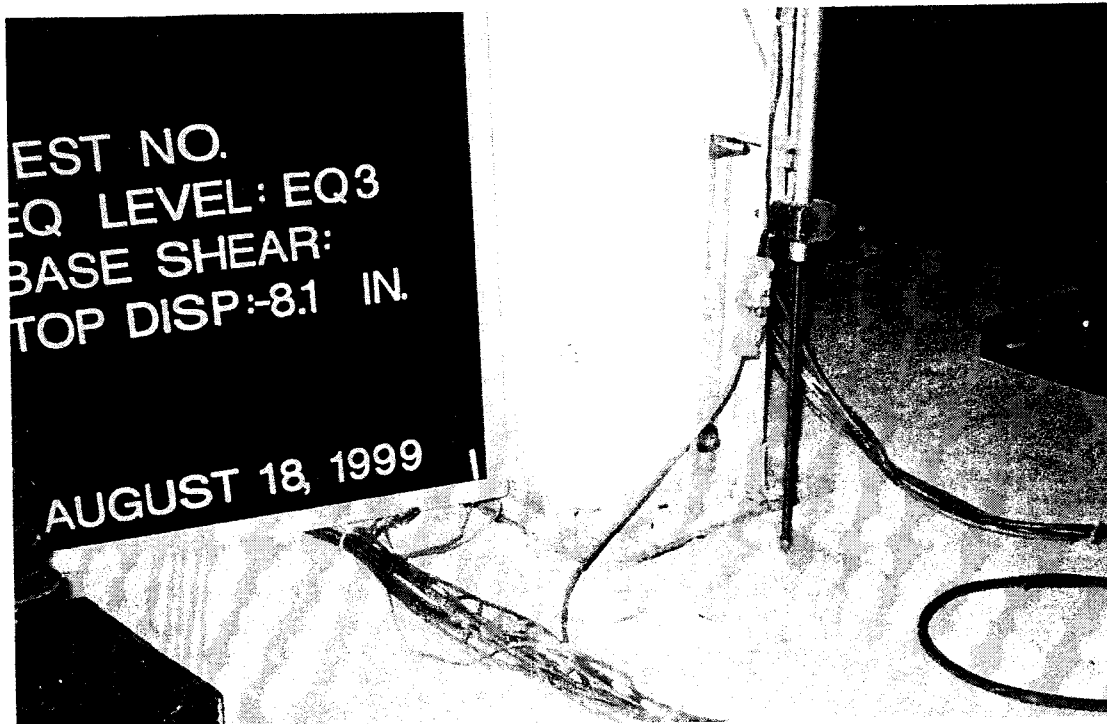
Exterior Wall Base (IT-3)
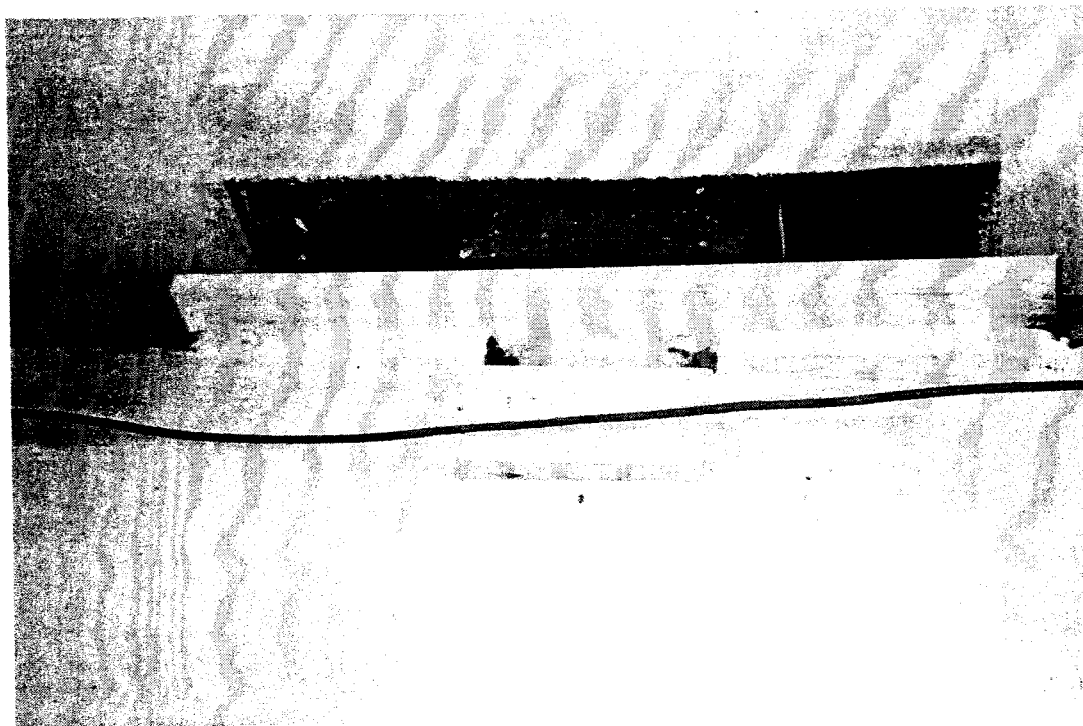
Double Tee Floor Connection (IT-3)
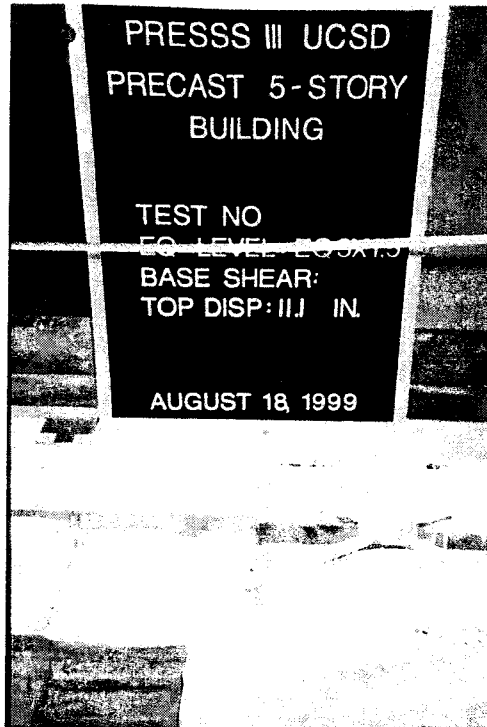
X-Plate Connection (1.5 EQ-3)
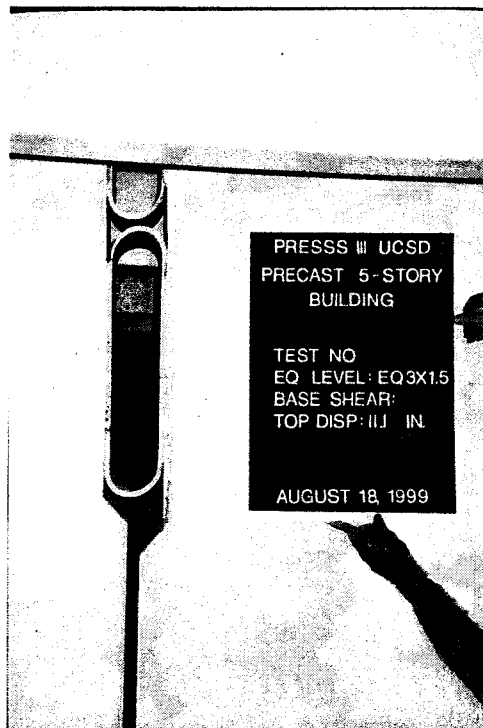
UFP Offset (1.5 EQ-3)
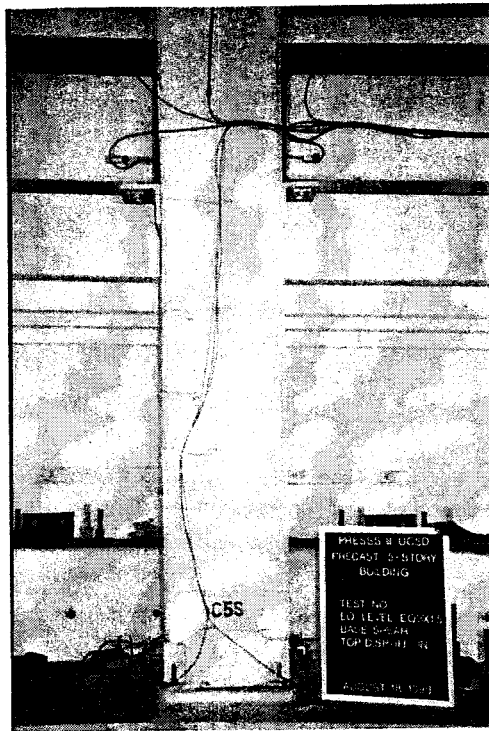
Interior Column Gravity Frame (1.5 EQ-3)
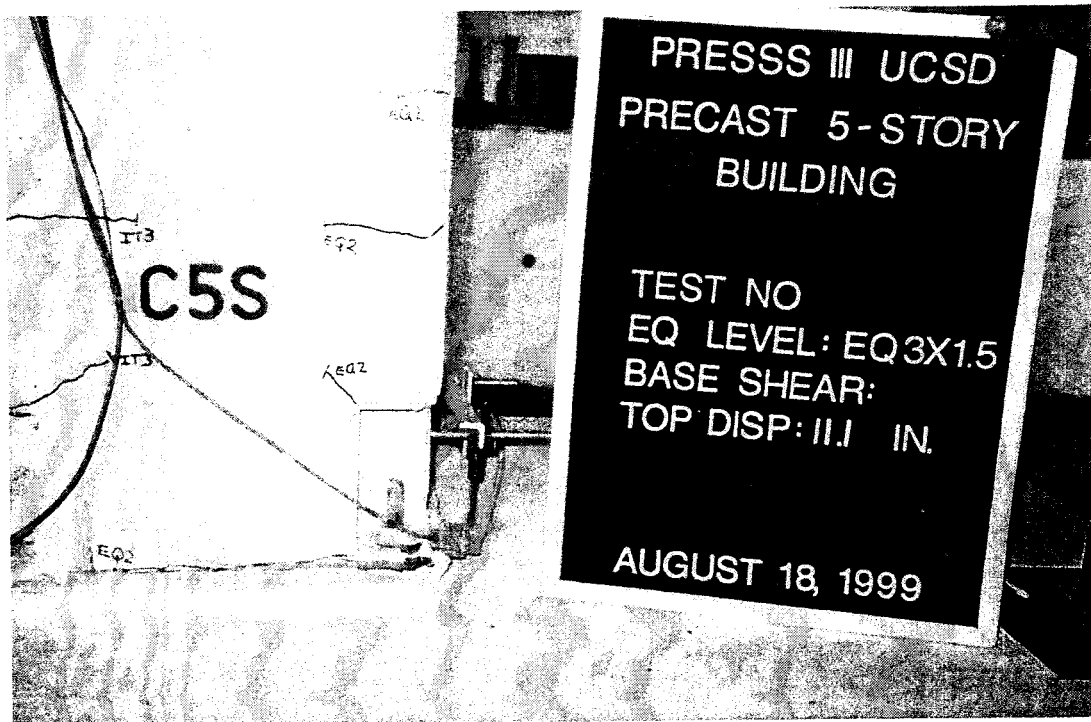
Interior Column Gravity Frame (1.5 EQ-3)
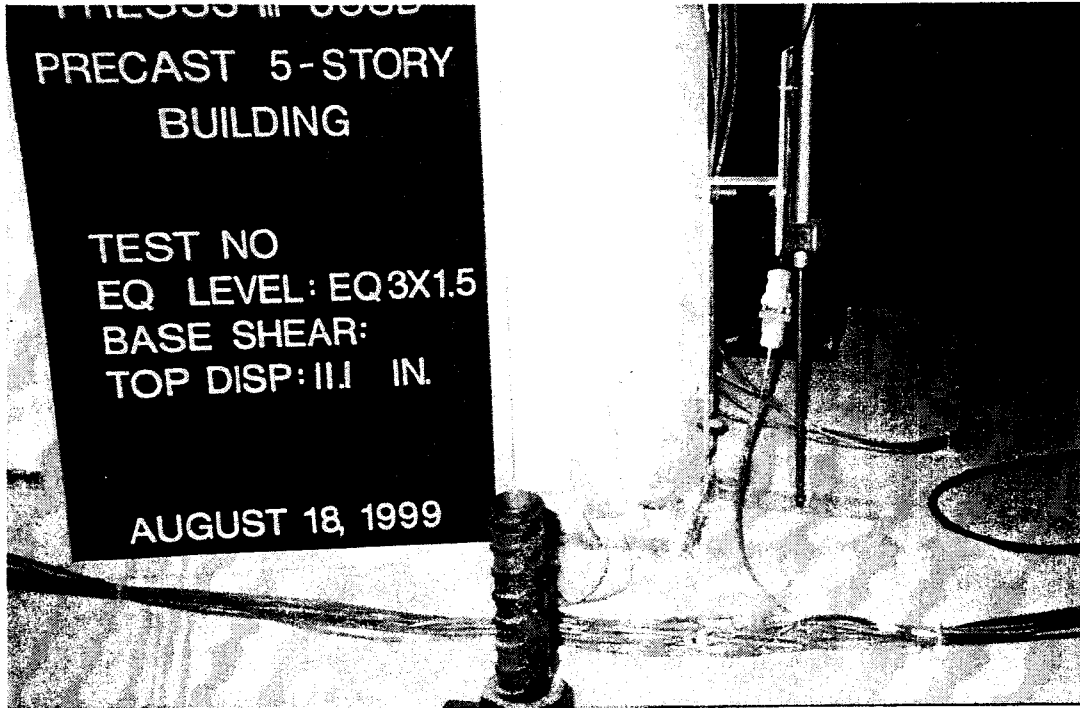
Wall Base Exterior (1.5 EQ-3)
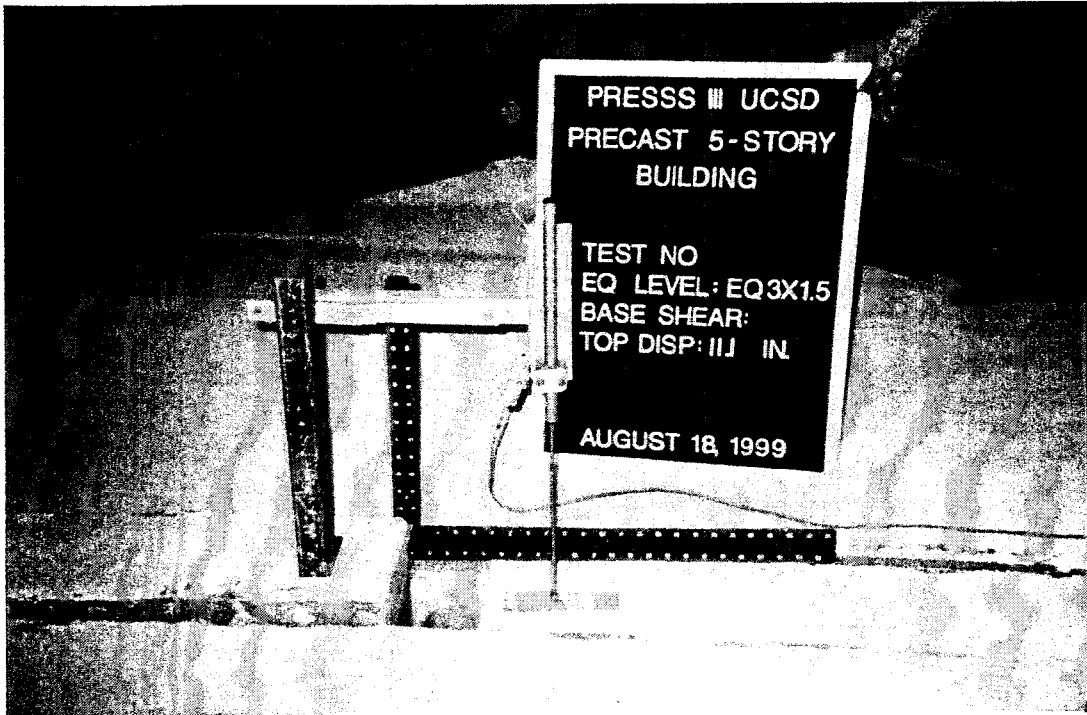
Wall Top Vertical Joint Offset (1.5 EQ-3)

REFERENCES

Carr, A. J., "Ruaumoko Program for Inelastic Dynamic Analysis – Users Manual," Department of Civil Engineering, University of Canterbury, Christchurch, New Zealand, 1998.

Conley, J. R., Priestley, M. J N., and Sritharan, S., *Precast Seismic Structural Systems PRESSS-3: The Five-Story Precast Test Building, Vol. 3-1: Wall Direction Response*, in press.

Earth Mechanics, Computer Program: SHAPE, Fountain Valley, CA, 1998.

Gregorian, C. E., Yang, T.-S., and Popov, E. P., "Slotted Bolted Connection Energy Dissipators," Report No. UCB/EERC-92-10, Earthquake Engineering Research Center, University of California, Berkeley, July, 1992.

Iragashi, A., Seible, F., Hegemier, G., and Priestley, M. J. N., *The U.S.-TCCMAR Full-Scale Five-Story Masonry Research Building Test, Part III – Seismic Load Simulation,* Report SSRP 94/03, University of California, San Diego, CA, 1994.

Kelly, J. M., Skinner, R. I., and Heine, A. J., "Mechanisms of Energy Absorption in Special Devices for use in Earthquake Resistant Structures," *Bulletin of the New Zealand Society for Earthquake Engineering*, Vol. 5, No. 3, September, 1972, pp. 63-88.

Kurama, Y., Pessiki, S., Sause, R., Lu L.-W., and El-Sheikh, M., "Analytical Modeling and Lateral Load Behavior of Unbonded Post-Tensioned Precast Concrete Walls," Report No. EQ-96-02, Lehigh University, Bethlehem, PA, 1996.

Muller, P., "Seismic Behavior of Precast Walls," *Proceedings*, Third U.S. National Confrence on Earthquake Engineering, Charleston, SC, 1986, Vol. II, pp.1239-1249.

Nakaki, S. D., and Englekirk, R. E., "PRESSS Industry Seismic Workshops: Concept Development," *PCI Journal*, Vol. 36, No. 5, September-October 1991, pp. 54-61.

Nakaki, S. D., Stanton, J. F., and Sritharan S., "An Overview of the PRESSS Five-Story Precast Test Building," *PCI Journal*, Vol. 44, No. 2, March-April 1999, pp. 26-39.

Nakaki, S. D., and Sritharan, S., *Precast Seismic Structural Systems PRESSS-3: The Five-Story Precast Test Building, Vol. 3-2: Construction*, in press.

PBSE Ad-Hoc Committee of Structural Engineers Association of California, APPENDIX G – Tentative Performance Based Seismic Engineering Guidelines, SEAOC Blue Book, December 1998.

Paulay, T., and Priestley, M. J. N., *Seismic Design of Reinforced Concrete and Masonry Buildings*, John Wiley and Sons, New York, NY, 1992.

Pall, A. S., Marsh C., and Fazio, P., "Friction Joints for Seismic Control of Large Panel Structures," *PCI Journal*, Vol. 25, No. 6, November-December 1980, pp. 38-61.

Pampanin, S., Priestley, M. J N., and Sritharan, S., *Precast Seismic Structural Systems PRESSS-3: The Five-Story Precast Test Building, Vol. 3-1: Frame Direction Response*, in press.

Priestley, M. J. N., "Overview of PRESSS Research Program," *PCI Journal*, Vol. 36, No. 4, July-August 1991, pp. 50-57.

Priestley, M. J. N., "The PRESSS Program -- Current Status and Proposed Plans for Phase III," *PCI Journal*, Vol. 41, No. 2, March-April 1996, pp. 22-40.

Priestley, M. J. N., "Displacement-Based Approaches to Rational Limit States Design of New Structures," Keynote Address, 11th European Conference on Earthquake Engineering, Paris, September 1998.

Sause, R., Zhao, C., and Pessiki, S., "Seismic Analysis of Unbonded Post-Tensioned Wall in PRESSS Five-Story Test Building," ATLSS Report No. 00-XX, Center for Advanced Technology for Large Structural Systems, Lehigh University, Bethlehem, PA (in preparation) 2001.

Schultz, A. E., "Seismic Resistance of Horizontal Connections for Precast Concrete Panels," Department of Civil Engineering, North Carolina State University, Raleigh, NC, July, 1992.

Schultz, A. E., and Magaña, R. A., "Seismic Behavior of Connections in Precast Concrete Walls," Paper No. SP 162-12, Mete A. Sozen Symposium, ACI SP 162, American Concrete Institute, Farmington Hills, MI, 1996, pp. 273-311.

Stanton, J. F., and Nakaki, S. D., *Precast Seismic Structural Systems PRESSS-3: The Five-Story Precast Test Building, Vol. 3-1: Seismic Design*, in press.

Stanton, J. F., and Nakaki, S. D., *Precast Seismic Structural Systems PRESSS-3: The Five-Story Precast Test Building, Vol. 3-9: Design Guidlines*, in press.

Sritharan S., Igarashi, A., Priestley M. J. N., Seible F., "Test Design of the PRESSS Five-Story Precast Concrete Building," Proceedings, 68th Annual Convention, Structural Engineers Association of California, Santa Barbara, CA, 1999, pp. 255-261.